GENERAL ATOMIC
DIVISION OF GENERAL DYNAMICS

GA-4391

INVESTIGATIONS OF CARBIDES AS CATHODES FOR THERMIONIC SPACE REACTORS

QUARTERLY PROGRESS REPORT
FOR THE PERIOD ENDING MAY 31, 1963

Contract NAS 3-2532
National Aeronautics and Space Administration

September 25, 1963

DISCLAIMER

GENERAL ATOMIC

DIVISION OF

GENERAL DYNAMICS

JOHN JAY HOPKINS LABORATORY FOR PURE AND APPLIED SCIENCE

P.O. BOX 608. SAN DIEGO 12. CALIFORNIA

GA-4391

INVESTIGATIONS OF CARBIDES AS CATHODES FOR THERMIONIC SPACE REACTORS

QUARTERLY PROGRESS REPORT FOR THE PERIOD ENDING MAY 31, 1963

Contract NAS 3-2532

National Aeronautics and Space Administration

Work done by:

D. L. Bosseau
F. D. Carpenter
J. A. Chaplain
B. A. Czech
N. Elsner
D. G. Guggisberg
M. H. Horner
R. G. Hudson
D. E. Johnson
J. R. Lindgren
C. C. Morris
D. Peat
G. Reeve
C. W. Savery
D. Smith
T. Tagami
R. C. Weed
A. F. Weinberg
K. Worth
L. Yang

Report written by:

L. Yang
A. F. Weinberg
F. D. Carpenter
M. H. Horner
R. G. Hudson
J. R. Lindgren

Technical Management
NASA-Lewis Research Center
Space Electric Power Office
J. W. R. Creagh

September 25, 1963

PREVIOUS REPORTS IN THIS SERIES

Contract NAS 5-1253

GA-2548 Quarterly Progress Report for the Period Ending August 31, 1961

GA-2670 Quarterly Progress Report for the Period Ending November 30, 1961

GA-3007 Quarterly Progress Report for the Period Ending February 28, 1962

GA-3245 Quarterly Progress Report for the Period Ending May 31, 1962

GA-3523 Final Report for the Period Ending August 31, 1962

Contract NAS 3-2310

GA-3093 Quarterly Progress Report for the Period Ending March 31, 1962

GA-3337 Quarterly Progress Report for the Period Ending June 30, 1962

GA-3642 Final Report for the Period Ending January 30, 1963

Contract NAS 3-2532

GA-3866 Quarterly Progress Report for the Period Ending November 30, 1962

GA-4173 Quarterly Progress Report for the Period Ending February 28, 1963

SUMMARY

The work accomplished during the third quarter, ending May 31, 1963, of Contract NAS 3-2532 is summarized below.

1. LONG-TERM STUDIES (>1000 hr) OF THE VAPORIZATION AND ELECTRON EMISSION OF UC-ZrC AND W-CLAD UC IN Cs VAPOR

The two long-term test cells have been fabricated and tested. One has been loaded with a 30 UC—70 ZrC sample and the other with a 90 UC—10 ZrC sample. The rates of vaporization of these samples in vacuum have been determined both in the absence and in the presence of a nickel anode maintained at 983°K with an electrode spacing of 20 mils, in order to set the baseline values. Measurement of the rates of vaporization of these samples under these conditions in the presence of cesium vapor at a pressure of about 1.8 torr are in preparation and will be continued for 1000 hr.

Operation of the first test cell, containing the 90 UC—10 ZrC emitter, was terminated after 510 hr because of leakage through a faulty metal gasket sealing the electron-gun compartment.

The second test cell, containing a vapor-deposited tungsten-clad UC emitter, has been assembled and operated for a period of 111 hr. The test was terminated because a leak developed between the cell compartment and the electron-gun compartment. A control cell containing a solid tungsten emitter is being assembled to check the modifications made in the design of the electron-gun chamber and the filament in order to overcome such difficulties. Components for four other test cells have been received. Fabrication of the emitters for these cells has been partially completed.

2. STUDIES OF THE HIGH-TEMPERATURE PROPERTIES OF UC-ZrC

Measurements have been completed on the vacuum vaporization rates of two cold-pressed and sintered 30 UC—70 ZrC samples (B_1-9 and B_1-9a) in the temperature range 2073° to 2273°K, and of a cold-pressed and sintered 90 UC—10 ZrC sample (B_1-10) in the temperature range 2013° to 2085°K. The vacuum emission of B_1-9 in the temperature range 1700° to 2000°K and its open-pore fraction have also been determined. The results are compared with those obtained on other UC-ZrC samples.

Physical redeposition studies have been made in the following cases:

UC (2015°-2083°K) with nickel anode at 558° to 983°K,
90 UC–10 ZrC (2027° to 2038°K) with nickel anode at 983°K,
30 UC–70 ZrC (2082° to 2123°K) with nickel anode at 983°K.

The activation, poisoning, and regeneration of the vacuum emission of a hyperstoichiometric uranium carbide sample have been studied in the temperature range 1670° to 2000°K.

The high-temperature furnace, with the sample loading and testing fixtures in position, has been tested at 2073°K. Minor mechanical difficulties encountered have been corrected. The bearing guiding the loading rod has been shifted to a cooler region of the furnace to avoid freezing of the rod by the bearing when the furnace is at a high temperature.

3. IRRADIATION STUDIES

The unclad-carbide capsule has been successfully irradiated in the General Electric Test Reactor (GETR) for two cycles; all of the high-temperature W–W26Re thermocouples have been functioning satisfactorily. The irradiated capsule has been returned to the General Atomic Hot Cell Facility for postirradiation examinations.

The clad capsule has been assembled and shipped to the GETR for irradiation beginning the second week of June, 1963.

4. STUDIES OF NEW CATHODE MATERIALS

The vacuum emission of the stoichiometric $UMoC_2$ sample (D_1-2) has been measured in the temperature range 1750° to 2000°K. The rate of vacuum vaporization of a cold-pressed and sintered 30 UC–70 NbC sample (D_1-3) has been determined in the temperature range 2050° to 2198°K.

The compatibility between 98 wt-% W–2 wt-% Mo alloy and UC-ZrC (90 UC–10 ZrC and 30 UC–70 ZrC) has been studied at 2073°K for a period of 24 hr (Run D_2-4). The diffusion samples after Runs D_2-1 (Ir, Re, and W-26Re versus UC), D_2-2 (85 wt-% W–15 wt-% Mo versus UC), and D_2-3 (98 wt-% W–2 wt-% Mo versus UC) have been examined by electron-microprobe techniques.

Electron-microprobe studies have been made on the vapor-deposited tungsten-clad hyperstoichiometric UC (5.02 wt-% C, sample D_3-1) after it

was subjected to diffusion-emission studies at 2073°K for a period of 838 hr. Two carbide samples, one hypostoichiometric UC (4.70 wt-% C, sample D_3-2) and the other 30 UC–70 ZrC (sample D_3-3) have been clad with vapor-deposited tungsten and will be subjected to similar studies.

5. FABRICATION DEVELOPMENT

The main effort during this quarter has been in the fabrication of the samples for the clad irradiation capsule.

BLANK

CONTENTS

INTRODUCTION

This report covers the work accomplished during the third quarter of Contract NAS 3-2532, which is a continuation of the work under Contracts NAS 5-1253[1] and NAS 3-2310,[2] to investigate thermionic cathode materials for the direct conversion of fission heat to electrical energy for space applications. Measurements of the vaporization, electron emission, and diffusion properties of various candidate materials under Contract NAS 5-1253 showed that both UC-ZrC and W-clad UC (or UC-ZrC) were promising thermionic cathode materials which may provide useful life (e.g., one year or longer) and performance (e.g., several w/cm^2). The purpose of the present contract is to make further studies of these materials in order to establish their feasibility for long-term thermionic applications in a reactor environment and to develop new cathode materials. The investigation is divided into five major areas:

1. Long-term (>1000 hr) studies of the vaporization and electron emission of UC-ZrC and W-clad UC (or UC-ZrC) in Cs vapor.

2. Further investigation of the high-temperature properties of UC-ZrC, including the effect of sample density and pore structure on the vaporization and electron-emission characteristics in vacuum, the effect of anode temperatures and chemical additives on the vaporization characteristics, the controlling factors of the electron-emission properties, and the high-temperature mechanical properties.

3. Studies of the dimensional stability and fission-gas release properties of UC-ZrC and W- and W-Mo-alloy-clad UC, UC-ZrC, W-UC cermet, and W-UO_2 cermet fuels after irradiation at high temperatures.

4. Studies of the vaporization, electron emission, and compatibility characteristics of new cathode materials.

5. Fabrication development in the preparation of UC-ZrC and W- and W-alloy-clad uranium-containing refractory nuclear fuels with controlled structures and compositions.

The cells used in these studies and the sample coding system were described in Table 1 of GA-3866.[3]

EXPERIMENTAL PROGRAM

1. LONG-TERM STUDIES ON THE VAPORIZATION AND ELECTRON EMISSION OF UC-ZrC AND W-CLAD UC (OR UC-ZrC) IN Cs VAPOR

1.1. Rate of Vaporization of UC-ZrC in Cs Vapor

During the second quarter of this contract, it was shown that the presence of cesium vapor at a pressure of 1.8 torr reduced the rate of vaporization of a cast 90 UC–10 ZrC sample (A_1-1a, density 93.4%) at 2093°K by a factor of six during a 100-hr run. To check the accuracy of this figure, another 100-hr run was made during the present quarter under similar conditions at 2083°K with another cast 90 UC–10 ZrC sample (B_1-3, density 95.5%). The vacuum vaporization characteristic of this sample was studied during the first quarter of this contract. Prior to the cesium run, the rate of vaporization of B_1-3 in vacuum was remeasured at 2083°K and found to agree with the first quarter result. The data obtained in the presence of cesium, however, indicated that the vaporization loss was reduced by a factor of only 1.4. One possible explanation for such a discrepancy could be the difference in the convection conditions in the cesium vapor adjacent to the carbide surface during these two runs and the dependence of the vaporization loss on such convection conditions. The cell used in these tests has no anode (as shown in GA-4173, Fig. 1). In a cesium cell, with the carbide cathode situated in the vicinity of an anode surface, the convection condition would certainly be different from that in the absence of the anode. More meaningful results can be obtained only if an anode at an interelectrode spacing comparable to that in a cesium cell is incorporated in the test cell.

Two cells were therefore built for this purpose. They are similar to the redeposition cell shown in Figs. 13 and 14 of GA-4173.[4] The anode, however, is cooled by water, through a metal thermal barrier, instead of by compressed air. By varying the thermal conductance of the barrier, the anode temperature can be adjusted from 553° to 1123°K. (Figure 1 is a schematic drawing of this cell.) One of the cells has been loaded with a cold-pressed and sintered 30 UC–70 ZrC sample (B_1-9a) and the other with a cold-pressed and sintered 90 UC–10 ZrC sample (B_1-10). To set the baseline values, the vacuum vaporization rates have been determined in the Langmuir vaporization apparatus and the anode effect on the vacuum vaporization rates has been determined in the test cells in the presence of a nickel anode at 983°K and with an interelectrode spacing of 20 mils. The vacuum-vaporization results are described in Section 2.1.1, and the anode effect on the

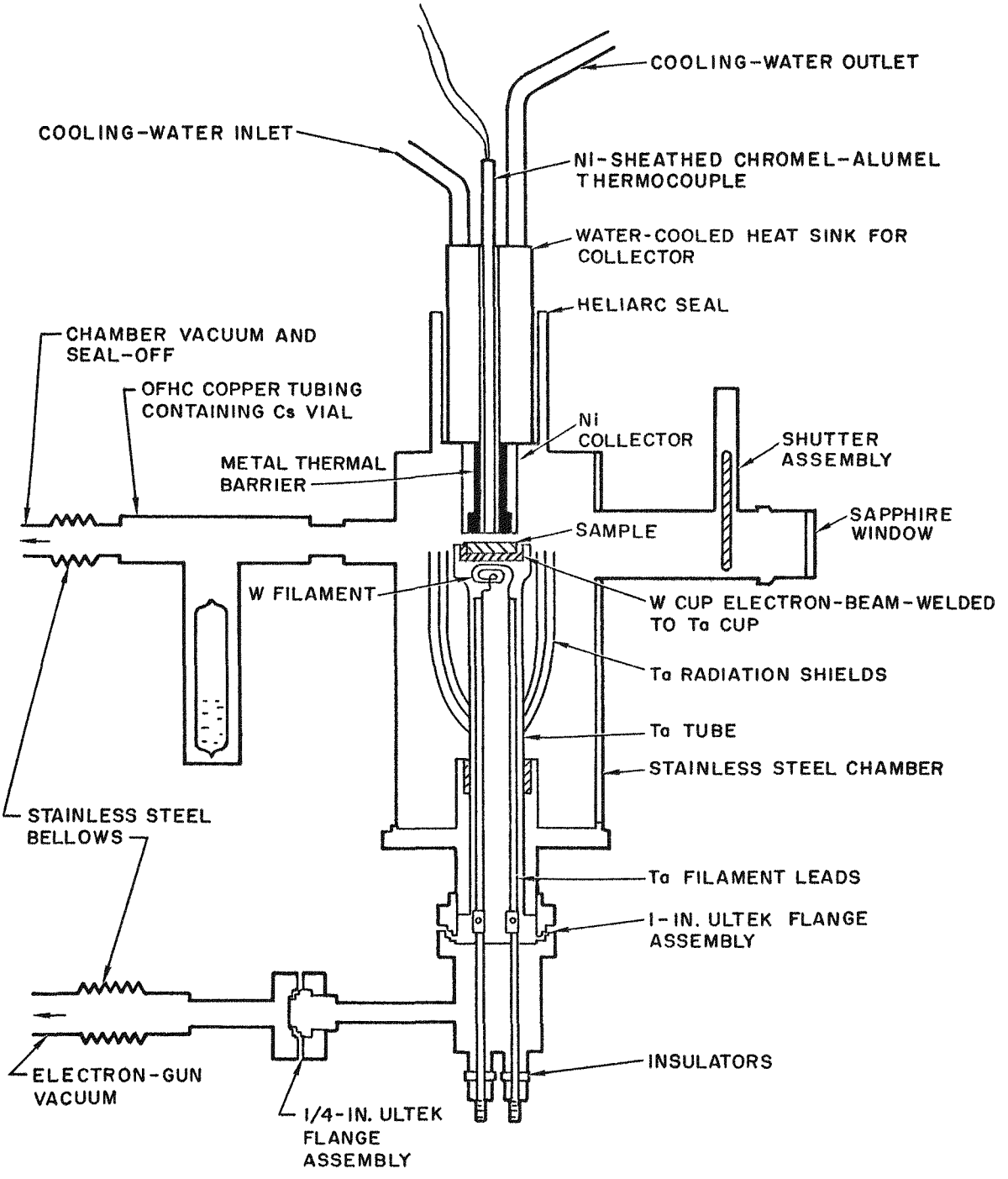

Fig. 1--Schematic drawing of test-cell arrangement for studying the effect of cesium vapor on vaporization loss of UC-ZrC

rates of vaporization is presented in Section 2.2. Preparation is under way for the initiation of the cesium runs.

1.2. Emission Stability of UC-ZrC and W-clad UC (or UC-ZrC) in Cs Vapor

The first test cell containing a 90 UC–10 ZrC emitter had been in operation for about 300 hr by the end of February, 1963. The decrease in cell output indicated that the emitter was poisoned. At the beginning of this quarter, the emitter was thermally treated to regenerate its emission, but the test had to be terminated after a total operating time of 510 hr because leaks developed in the cell components. Postoperational examination indicated that a metal gasket used to seal the electron-gun compartment had sprung a leak when the tantalum tube separating the electron-gun compartment and the cell was hot. This resulted in the embrittlement of the tantalum holding the tungsten cup and emitter and the tantalum sheath of the thermocouple, which caused leaking.

The operation of the second test cell commenced during the latter part of April, 1963. This cell contained a vapor-deposited tungsten-clad uranium carbide emitter with the configuration shown in Fig. 2. Prior to the sealing of the cell, the vacuum saturation emission of the emitter was measured and was found to agree with previously published data[5]--4.0 ma/cm^2 at 2073°K.

The cell operated for approximately five days for a total of 111 hr. For 60 hr of the last 70 hr of operation, the cell produced a maximum power output of about 2 w/cm^2 at an emitter temperature of about 2073°K. Figure 3 presents the performance data for several operating conditions. Figure 4 is a profile of the power density for the period during which the cell was operating.

Before the operating conditions of the cell could be optimized, the test was terminated because the pressure in the electron-gun compartment had exceeded 1×10^{-5} torr, which tripped the ion-gauge relay and thus cut off the cell. Postoperational examinations revealed that although the unit was leak-tight to the ambient atmosphere, a large leak developed internally between the emitter compartment and the electron-gun compartment.

It appears that there may be a definite problem in the filament design of the electron-gun system. The flat pancake filament introduces considerable thermal stress on the base of the tantalum emitter holder by concentrating most of the bombardment current in the center of the filament. Thermal etching and grain growth in this central portion are quite evident from visual examination of the tantalum holder. Corrective measures are being taken. First, the filament will be made slightly conical, so that

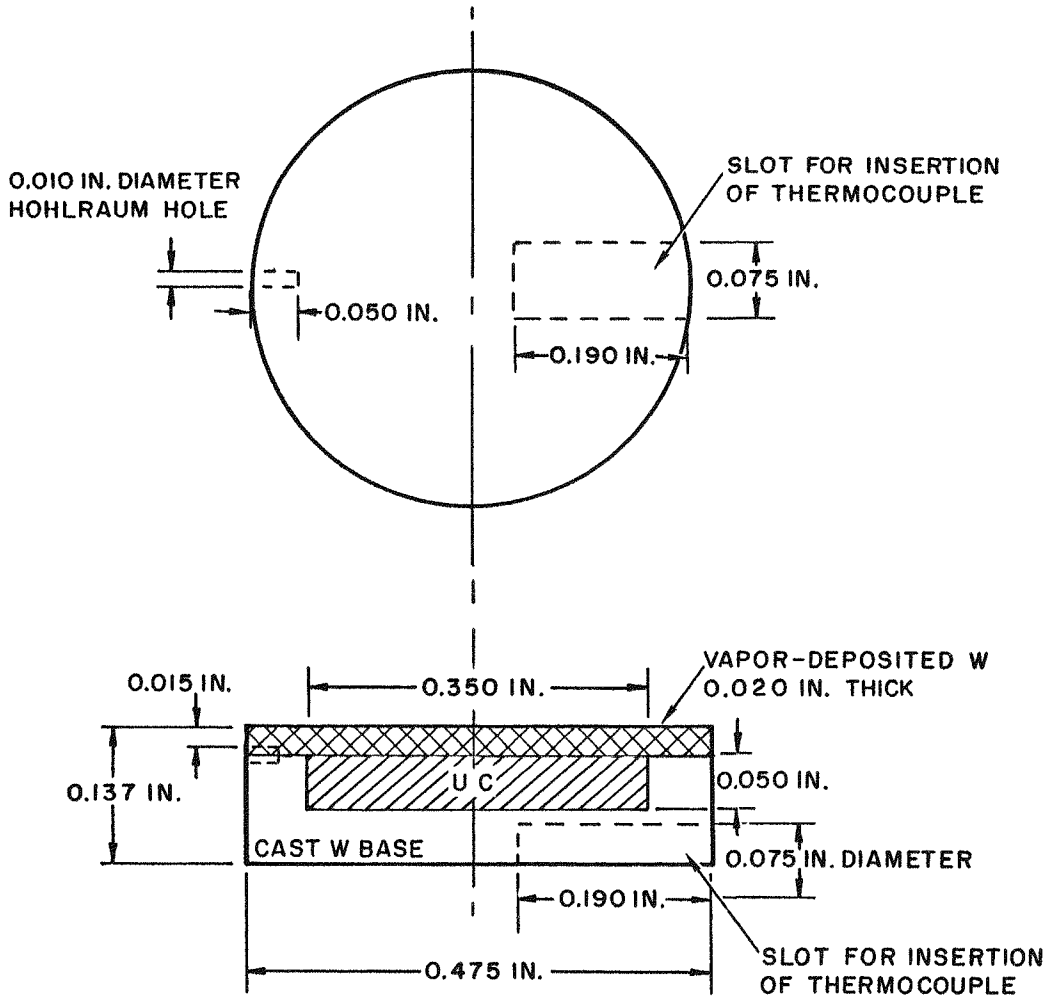

Fig. 2--Vapor-deposited tungsten-clad uranium carbide emitter for emission life-test cell

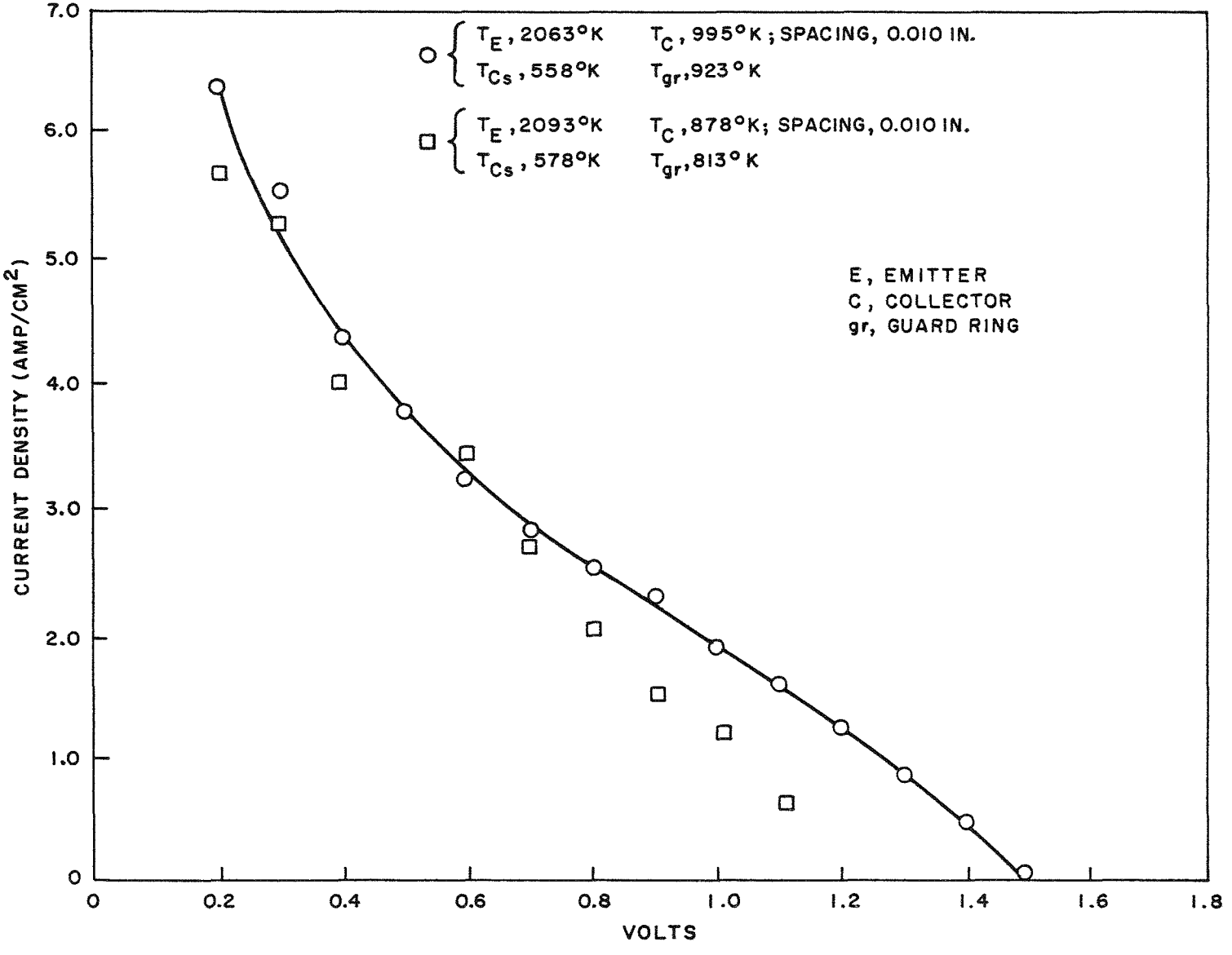

Fig. 3--Some performance data of the second emission life-test cell

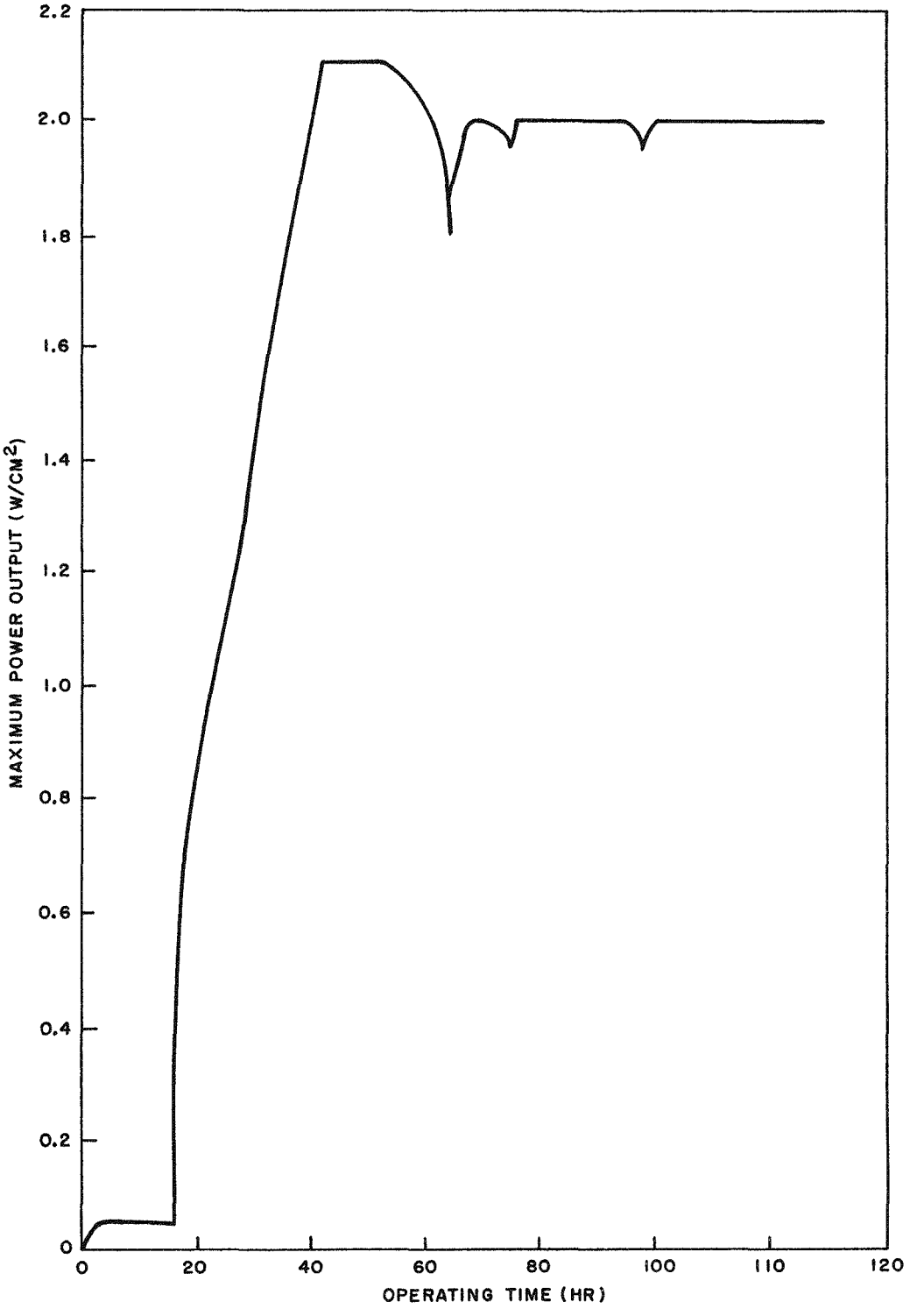

Fig. 4--Maximum power output of the second emission life-test cell as a function of hours of operation

its central portion will be farther from the tantalum surface than its circumference. This will allow the bombardment power to be more uniformly distributed over a large surface area. Second, the power input for maintaining the emitter at a given temperature can be reduced by diffusion bonding the tungsten cup to the tantalum holder to provide a better heat conduction path. Third, during this diffusion bonding, a thin disk of tungsten can also be bonded to the surface of the tantalum holder facing the electron gun, for thermal protection. In addition, the possibility of providing a complete tungsten holder for the emitter will not be overlooked.

Several other observations were made during the assembly and operation of this second cell which may help to improve the cleanliness and performance of future cells. During the assembly of the cell, the emitter assembly must be heated to operating conditions without the collector and guard-ring assembly in the system. This will eliminate the deposition of impurities from the tantalum holders, the tantalum radiation shields, and the titanium getter on the collector surface. If any of these impurities were to form an oxide coating on the collector surface, an electrical resistance could be introduced in the cell circuit. Another area where a small electrical resistance could exist, which might affect the cell output, is in the contacts between the emitter and the emitter holders. These problem areas can be checked and the problems resolved by studying the output of a control cell that contains a solid cast-tungsten emitter diffusion-bonded to the tantalum support tube. The emitter assembly and the collector-guard-ring assembly would be outgassed separately and the diffusion bonding should help to eliminate any internal electrical resistance. Such a cell is being assembled. Components for the other four emission life-test cells have been received. Two vapor-deposited tungsten-clad 30 UC–70 ZrC emitters have been prepared, and one vapor-deposited tungsten-clad uranium carbide emitter is being fabricated. Two 90 UC–10 ZrC unclad carbide emitters are waiting for final outgassing, and two 30 UC–70 ZrC unclad carbide emitters are being prepared.

2. STUDIES OF HIGH-TEMPERATURE PROPERTIES OF UC-ZrC

2.1. Effect of Porosity on the Vacuum Vaporization and Emission of UC-ZrC

To facilitate fission-gas release and to prevent fuel swelling, UC-ZrC containing a large number of open pores may have to be used, either as unclad emitters or as fuel for the clad emitters. It is therefore necessary to know how pore structures affect the vacuum emission and vaporization characteristics of these materials.

Previously, a new sample was first studied for its vacuum emission properties before measurement of its vacuum vaporization characteristics.

However, it was soon learned that new samples prepared by the cold-pressing and sintering technique were always metal-rich and that the excess metal content was removed by the thermal treatments in the vaporization runs, mostly during the outgassing period. The emission results obtained before the vaporization runs therefore represent the metal-rich "transient" state and have no significance in thermionic applications. For this reason the vacuum emissions of these samples had to be remeasured after the vaporization runs.

During this quarter, a new procedure was adopted in which the samples were studied for their vacuum vaporization rates before measurement of their vacuum emissions. Since the change in the composition and density of the samples occurred primarily during the outgassing period prior to the vaporization runs, both the vaporization and the emission results obtained with this procedure can be considered as accurate for samples of essentially constant composition and density.

2.1.1. Vacuum Vaporization

During this quarter, measurements were completed on two cold-pressed and sintered 30 UC–70 ZrC samples (B_1-9 and B_1-9a) which were cut from the same carbide piece, and on a cold-pressed and sintered 90 UC–10 ZrC sample (B_1-10). The results are shown in Tables 1, 2, and 3 and are plotted as a function of temperature in Fig. 5. Also included in this figure are the vaporization results for the cold-pressed and sintered 88 UC–12 ZrC sample (B_1-2), determined during the first quarter.[3] It is apparent that good agreement exists between the results for B_1-9 and B_1-9a and between the results for B_1-10 and B_1-2. B_1-9 has a density of 86.7% based on the theoretical density of its final composition, 28.3 UC–71.7 ZrC, and 89% of its void consists of open pores. Sample B_1-2 has a density of 88.5% based on the theoretical density of its final composition, 88 UC–12 ZrC, and also 89% of its void consists of open pores. Both B_1-9a and B_1-10 are being used to study the effect of cesium vapor on the rate of vaporization of UC-ZrC. Their exact compositions, densities, and pore structures will be determined after the cesium runs.

The results in Fig. 5, when compared with those for the less porous UC-ZrC samples of similar compositions, again illustrate the enhancement of vacuum-vaporization loss from more porous samples.

2.1.2. Vacuum Emission

The vacuum emission of sample B_1-9 was measured after the completion of the vaporization studies. The results are shown in Fig. 6, together with those for the hot-pressed sample B_1-7. It can be seen that in spite of the presence of a much higher open-pore fraction of the void in

Table 1

VAPOR-LOSS INVESTIGATION OF 30 UC–70 ZrC SAMPLE B_1-9[a]
(Cold-pressed and sintered)

Run No.	Temp. (°K)	Exposure Time (sec × 10^4)	Rate of Weight Loss [(mg/cm^2/sec) × 10^{-5}]	Counting Rate (alpha counts/min/cm^2)		UC Surface Concentration Based on Counting Rate (mol-%)	Density (g/cm^3)
				Side 1	Side 2		
Original	----	----	----	964	973	15.5	7.56
Degas	2193	9.54	9.99	536	544	8.5	7.69
1	2273	2.52	6.45	493	508	8.0	7.71
2	2163	4.38	2.55	446	466	7.5	7.71
3	2245	2.88	4.43	454	464	7.5	7.73
4	2128	2.88	1.85	450	467	7.5	7.72
5	2073	3.42	1.34	453	447	7.0	7.71

[a] X-ray diffraction analysis performed prior to vapor-loss determinations indicated a composition of about 30 UC–70 ZrC, single phase. Original composition, $U_{0.151}Zr_{0.367}C_{0.482}$; final composition, 28.3 UC–71.7 ZrC. Sample had a density of 86.7% based on the final composition following the vaporization runs.

Table 2

VAPOR-LOSS INVESTIGATION OF 30 UC–70 ZrC SAMPLE B_1-9a[a]
(Cold-pressed and sintered)

Run No.	Temp. (°K)	Exposure Time (sec × 10^4)	Rate of Weight Loss [(mg/cm^2/sec) × 10^{-5}]	Counting Rate (alpha counts/min/cm^2)		UC Surface Concentration Based on Counting Rate (mol-%)	Density (g/cm^3)
				Side 1	Side 2		
Original	----	-----	----	1017	1009	16	7.67
Degas	2236	16.2	8.71	506	521	8	7.89
1	2230	6.48	4.01	370	512	8	7.91
2	2093	5.40	1.83	464	511	8	7.92
3	2138	3.96	2.13	439	473	7.5	7.92

[a]X-ray diffraction analysis performed prior to vapor-loss determinations indicated a composition of approximately 30 UC–70 ZrC, single phase. Original composition, $U_{0.151}Zr_{0.367}C_{0.482}$. Based on 30 UC–70 ZrC, the specimen had a density of 87.5% after vapor-loss investigations. Final composition will be determined after life-test in a cesium environment.

Table 3

VAPOR-LOSS INVESTIGATION OF 90 UC–10 ZrC SAMPLE B_1-10[a]
(Cold-pressed and sintered)

Run No.	Temp. (°K)	Exposure Time (sec × 10^4)	Rate of Weight Loss [(mg/cm^2/sec) × 10^{-5}]	Density (g/cm^3)
Original	----	-----	-----	11.42
Degas	2085	12.06	14.8	11.35
1	2085	4.68	8.73	11.32
2	2013	5.94	3.94	11.29

[a] No counting rate was taken owing to the 3% enriched UC in sample. Original composition, $U_{0.463}Zr_{0.058}C_{0.479}$. Based on 90 UC–10 ZrC, the specimen had a density of 86.9% after vapor-loss investigations. Final composition will be determined after life-test in a cesium environment.

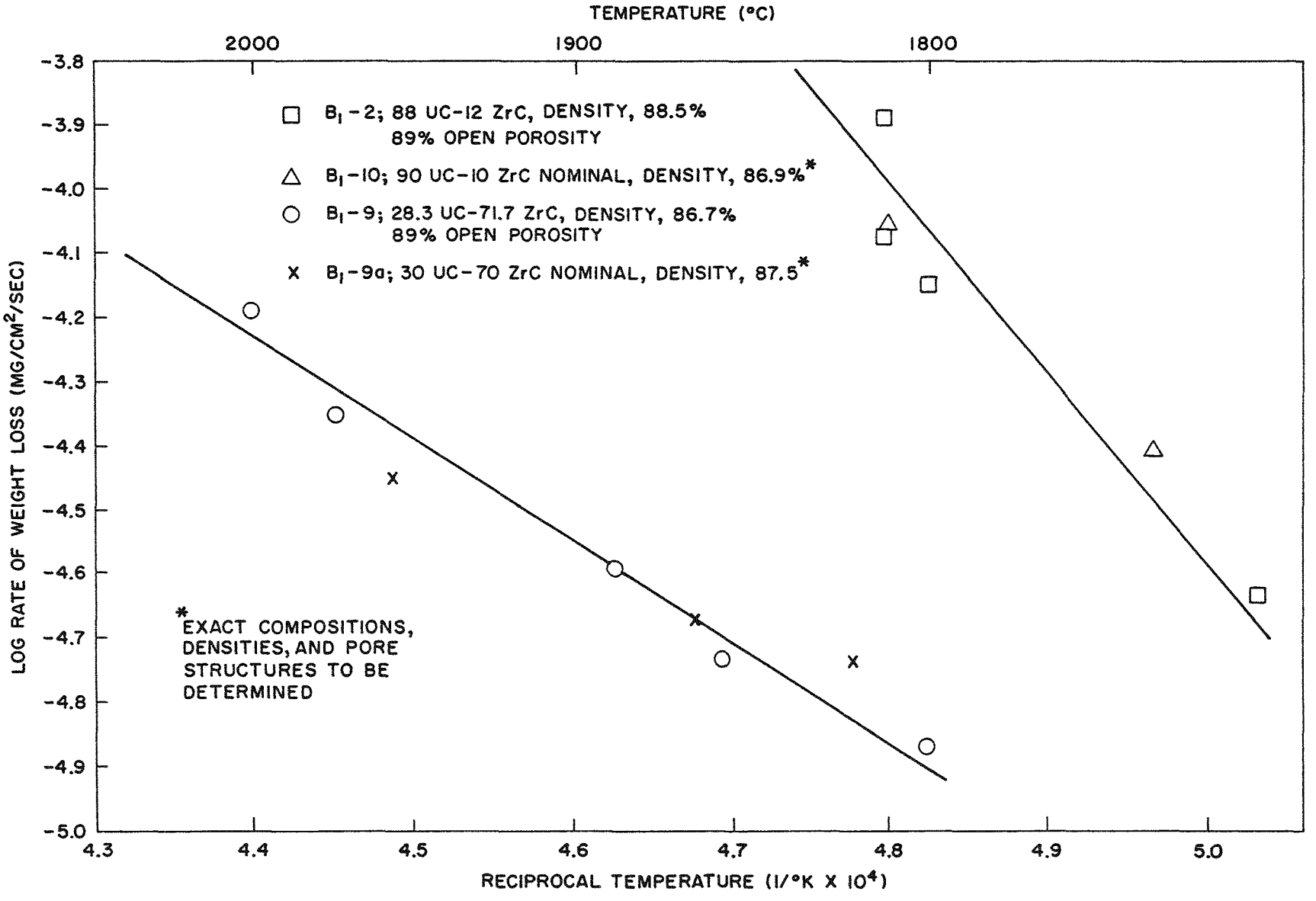

Fig. 5--Vacuum rate of vaporization for 90 UC–10 ZrC and 30 UC–70 ZrC samples, cold-pressed and sintered

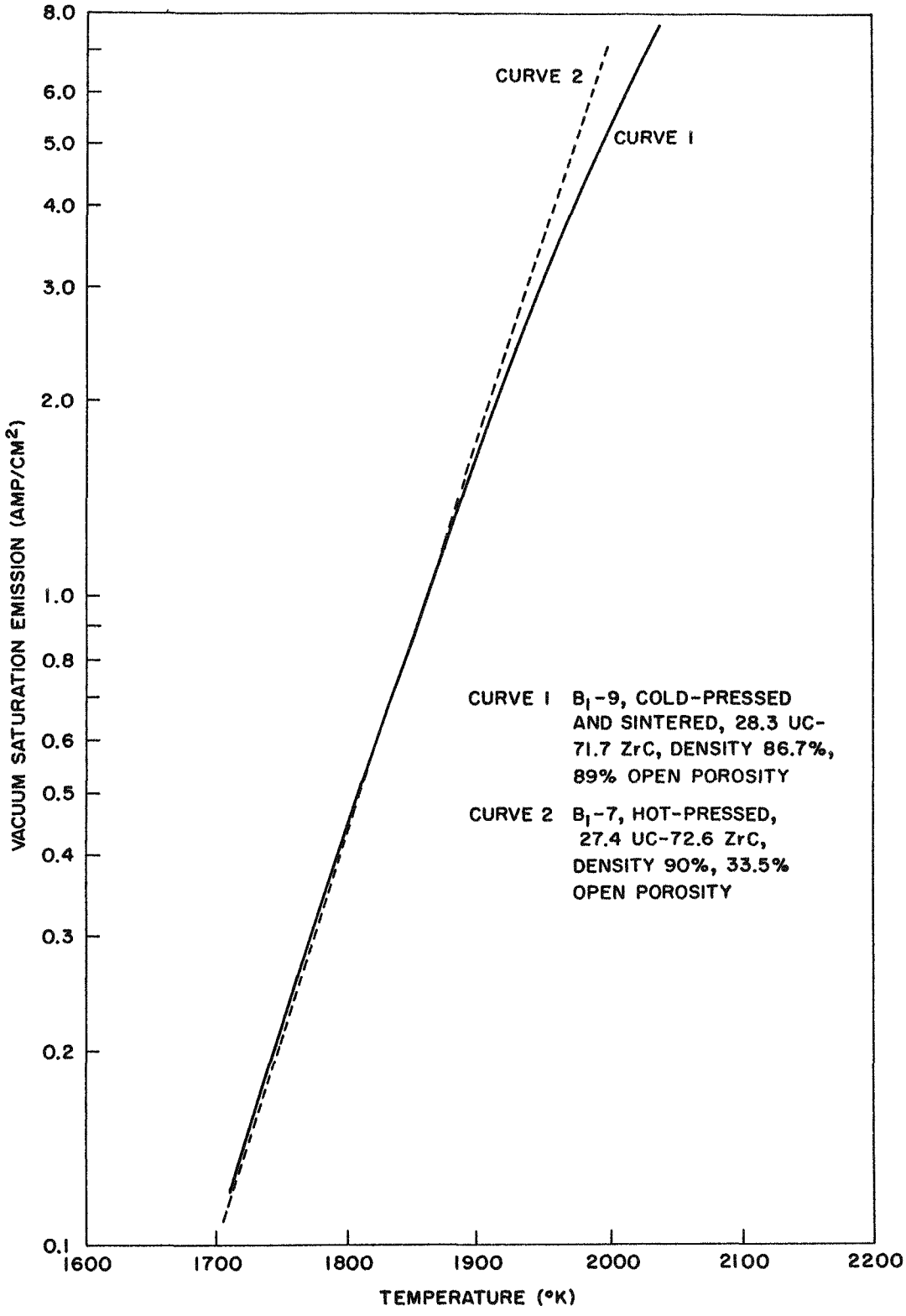

Fig. 6--Comparison of vacuum saturation emission of sample B_1-9 with sample B_1-7 (data taken after vaporization studies)

B_1-9 than in B_1-7 (89% versus 33.5%), the emission data for these two samples show good agreement.

The open-pore fraction in B_1-9 was determined by the mercury porosimeter technique after the vacuum emission measurements. The results shown in Fig. 7 indicate that about 89% of its void consists of open pores.

2.2. Redeposition Studies

To test the redeposition cell (see GA-4173, Figs. 13 and 14), a physical redeposition run was made with a uranium carbide cathode at 2003°K and a nickel anode at 1053°K, with an interelectrode spacing of 20 mils. The anode, which was cooled with a stream of compressed air, after 72 hr developed a leak at the point where the nickel-sheathed Chromel-Alumel thermocouple was welded to it and where the compressed air impinged on it. The arrangement was therefore modified to allow the anode to be cooled with water flowing through a metal thermal barrier. The anode temperature was varied by changing the nature of the material and the thermal conductance of the barrier. The cell with the modified anode-cooling arrangement is shown in Fig. 1. The exposed cathode surface is 1/2 in. in diameter and the nickel anode is 5/8 in. in diameter.

The effect of the anode surface on vaporization loss was studied for the following cases:

1. UC (sample B_2-1) with nickel anode at 558°, 683°, and 983°K.
2. 30 UC–70 ZrC (sample B_1-9a) with nickel anode at 983°K.
3. 90 UC–10 ZrC (sample B_1-10) with nickel anode at 983°K.

The results are shown in Table 4. The vacuum rates of vaporization of B_1-9a and B_1-10 were reported in Section 2.1.1. The vacuum rates of vaporization of B_2-1 (cold-pressed and sintered, initial composition $UC_{1.05}$), measured in the redeposition cell, are included in Table 4 and plotted in Fig. 8.

The results given in Table 4 indicate that (1) for UC and 90 UC–10 ZrC, the vaporization loss of the cathode was reduced by the presence of a high-temperature anode, (2) for UC, the vaporization loss decreased with the increase of the anode temperature, and (3) for 30 UC–70 ZrC, the vaporization loss was not affected by the presence of a high-temperature anode at 983°K. The reduction in vaporization loss is presumably due to the back-scattering of the vaporized atoms by the anode surface. The vapor species from UC and 90 UC–10 ZrC consists mostly of uranium and carbon atoms,[1][6] whereas that from 30 UC–70 ZrC should include a considerable amount of zirconium. The difference between the results for

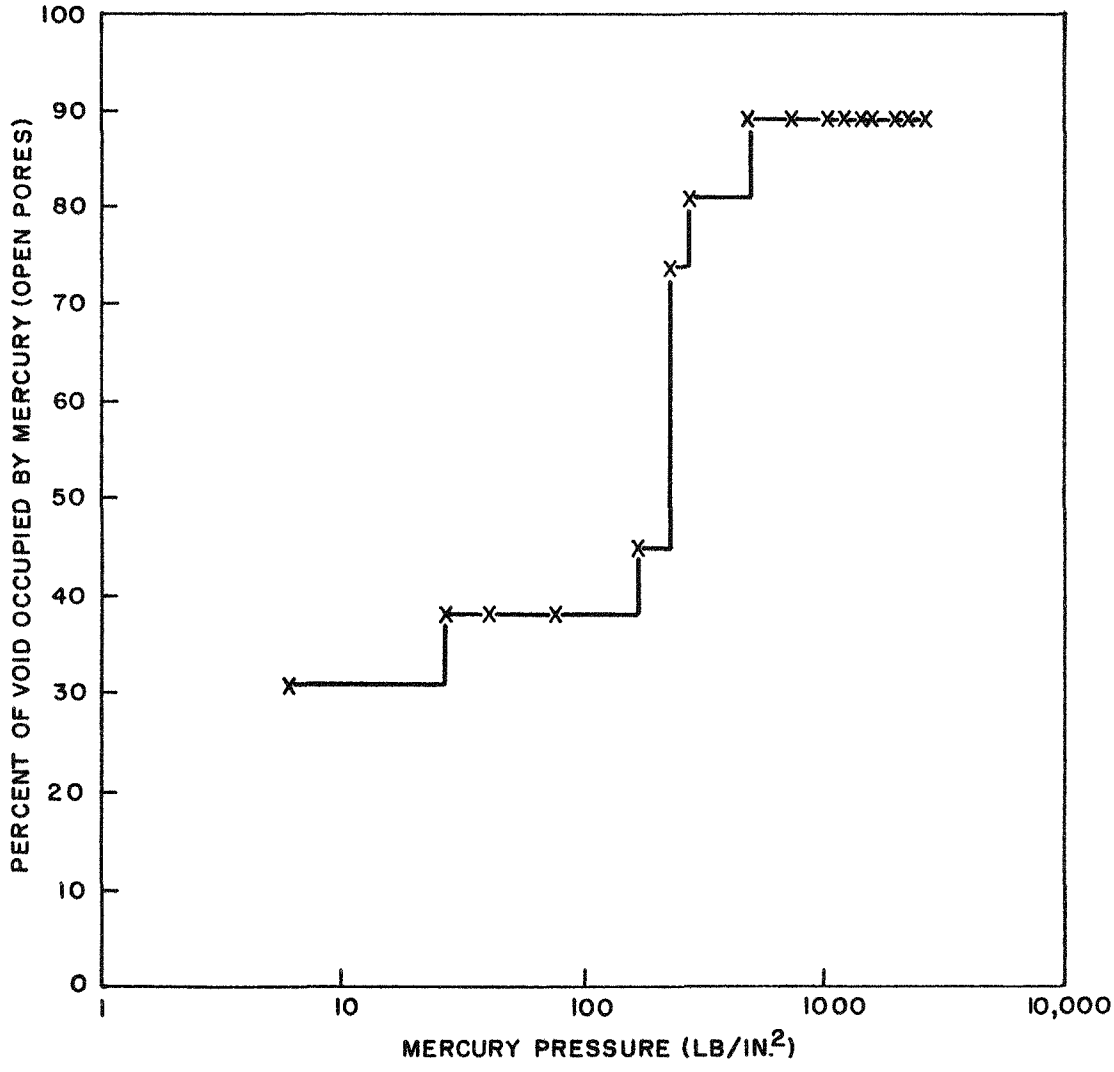

Fig. 7--Mercury porosimetric plot for sample B_1-9 (28.3 UC–71.7 ZrC, density 86.7%) showing that ~89% of the void consists of open pores

Table 4

ANODE EFFECT ON VAPORIZATION LOSS OF UC AND UC-ZrC

Sample No.[a]	Run No.	Temp. of Sample (°K)	Temp. of Collector (°K)	Exposure Time (sec × 10^5)	Rate of Weight Loss [(mg/cm^2/sec) × 10^{-5}]	Rate in Absence of Anode[b] / Rate in Presence of Anode
B_2-1	1	2013	558	3.852	8.16	~1
(UC)	2	2083	983	3.636	16.3	2.0
	3	1983	No anode	2.106	6.56	--
	4	1963	No anode	3.060	4.01	--
	5	1948	683	3.060	1.93	1.5
	6	2008	983	3.102	3.77	2.3
	7	2010	No anode	1.296	7.45	--
	8	2063	No anode	0.936	24.40	--
B_1-9a	4	2123	983	3.384	2.38	~1
(30 UC–70 ZrC)	5	2082	983	3.456	1.66	~1
B_1-10	3	2038	983	3.564	2.10	2.2
(90 UC–10 ZrC)	4	2027	983	3.456	1.69	2.3

[a]All of these samples were prepared by cold-pressing and sintering. The initial composition of B_2-1 was $UC_{1.05}$ with a density of about 86% based on the theoretical density of UC. Details on B_1-9a and B_1-10 are given in Fig. 5.

[b]The data for B_2-1 were obtained from Fig. 8; the data for B_1-9a and B_1-10 were obtained from Fig. 5.

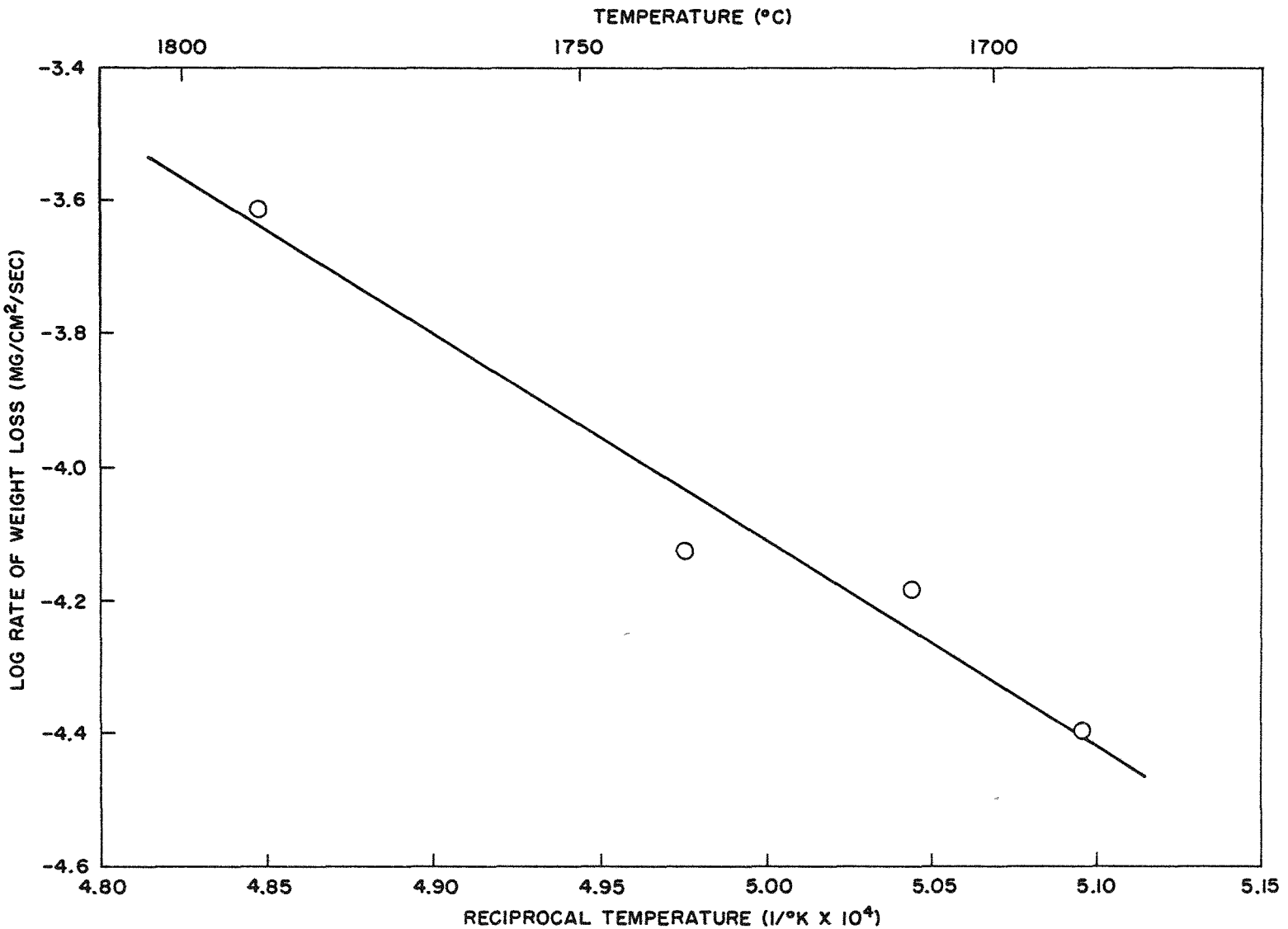

Fig. 8--Vacuum rate of vaporization versus temperature for uranium carbide, cold-pressed and sintered, 86% theoretical density, initial composition $UC_{1.05}$

UC and 90 UC–10 ZrC and that for 30 UC–70 ZrC could be due to the difference in the condensation and back-scattering behavior of uranium and zirconium from the nickel anode surface. Since zirconium has a much lower vapor pressure than uranium, it would be expected that zirconium will condense much more easily on the anode surface than uranium. The presence of zirconium condensate on the anode surface may help to increase the anode capture of carbon and uranium by alloying and by chemical combination. The back-scattering of the vaporized atoms thus may become negligible and the anode effect on the vaporization loss of the carbide may be considerably reduced or even nullified. The nature and amount of condensate on the anode surface are being analyzed for the samples listed in Table 4. The results should help to determine whether the above explanation is plausible.

2.3. Thermionic Emission Microscopy

During this quarter, the activation, poisoning, and regeneration of the emission from a uranium carbide surface were studied with the thermionic-emission microscope. The sample was made by casting and was hyperstoichiometric (exact carbon content to be determined). X-ray examinations of the sample after outgassing in vacuum (10^{-6} torr) at 1700°C for a period of 8 hr indicated that the sample consisted of a mixture of UC and U_2C_3. The sample was then polished with fine emery paper and placed in the sample holder of the microscope. Emission patterns were taken of the polished surface at 1670°K and then at 1670° and 1770°K after various thermal treatments in a vacuum of 10^{-6} to 3×10^{-7} torr. The results, as shown in Fig. 9, indicate that increasing amounts of the surface became activated as the temperature of the thermal treatment was increased. However, the emission pattern still appeared patchy even after thermal treatment at 2000°K. The pattern observed at 2000°K (not shown in Fig. 9) had essentially the same features as shown at the lower right in Fig. 9, although the intensity was much higher. Inside the poorly emitting region, there seemed to be a second phase of much better emission. The correlation between the emission pattern and the structural features is now being studied.

In the course of studying the activation of the emission by thermal treatment, it was observed that each time the sample was cooled down from a higher temperature, T_1, to a lower temperature, T_2, dark patches appeared on the emission pattern but when aged at T_2 the pattern will gradually revert to the features characteristic of the sample at temperature T_2 (see Fig. 10). The degradation of the emission is interpreted as being caused by the depletion of uranium on the surface by heating at a high temperature and by the adsorption of gases on the surface at certain sites when cooled. When the sample was aged at T_2, the uranium concentration on the surface was replenished by diffusion, the adsorbed gas atoms were removed by pumping, and the emission at the surface became regenerated.

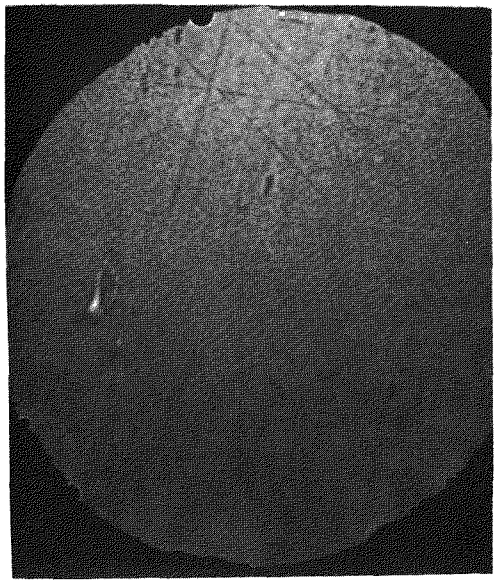

Initial polished surface at 1670°K

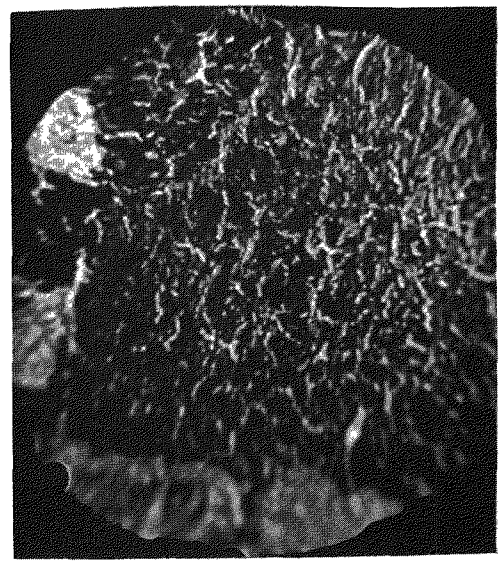

Partial activation after 18 hr at 1670°K

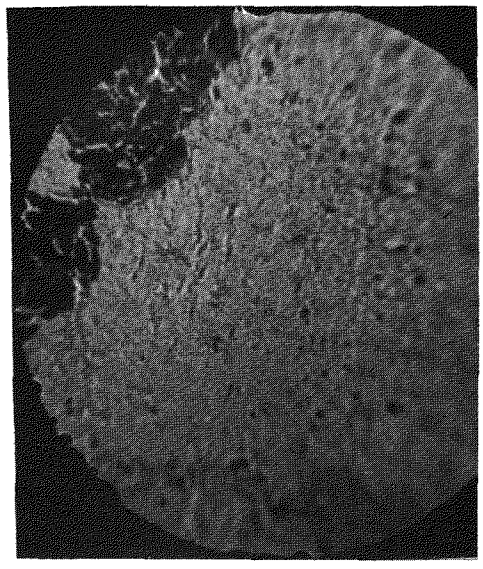

Further activation after 12 hr at 1900°K, pattern taken at 1770°K

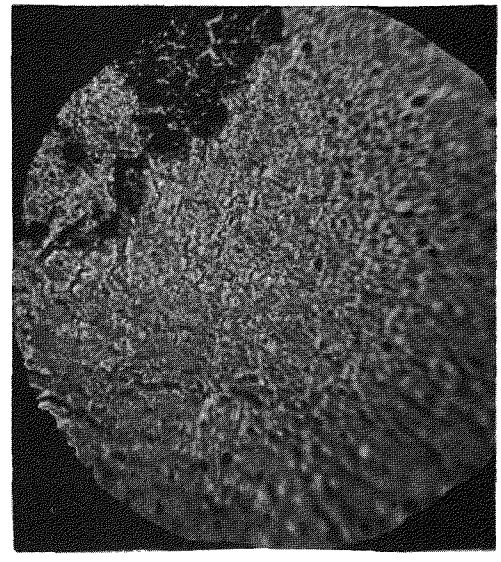

More activation after 3 hr at 2000°K, pattern taken at 1770°K

Fig. 9--Electron emission patterns from a uranium carbide surface showing the successive activation of the emission from a polished surface after thermal treatment at various temperatures (NOTE: bright regions are better emitting areas. The pattern for the initial polished surface was taken at twice the exposure times of the other patterns)

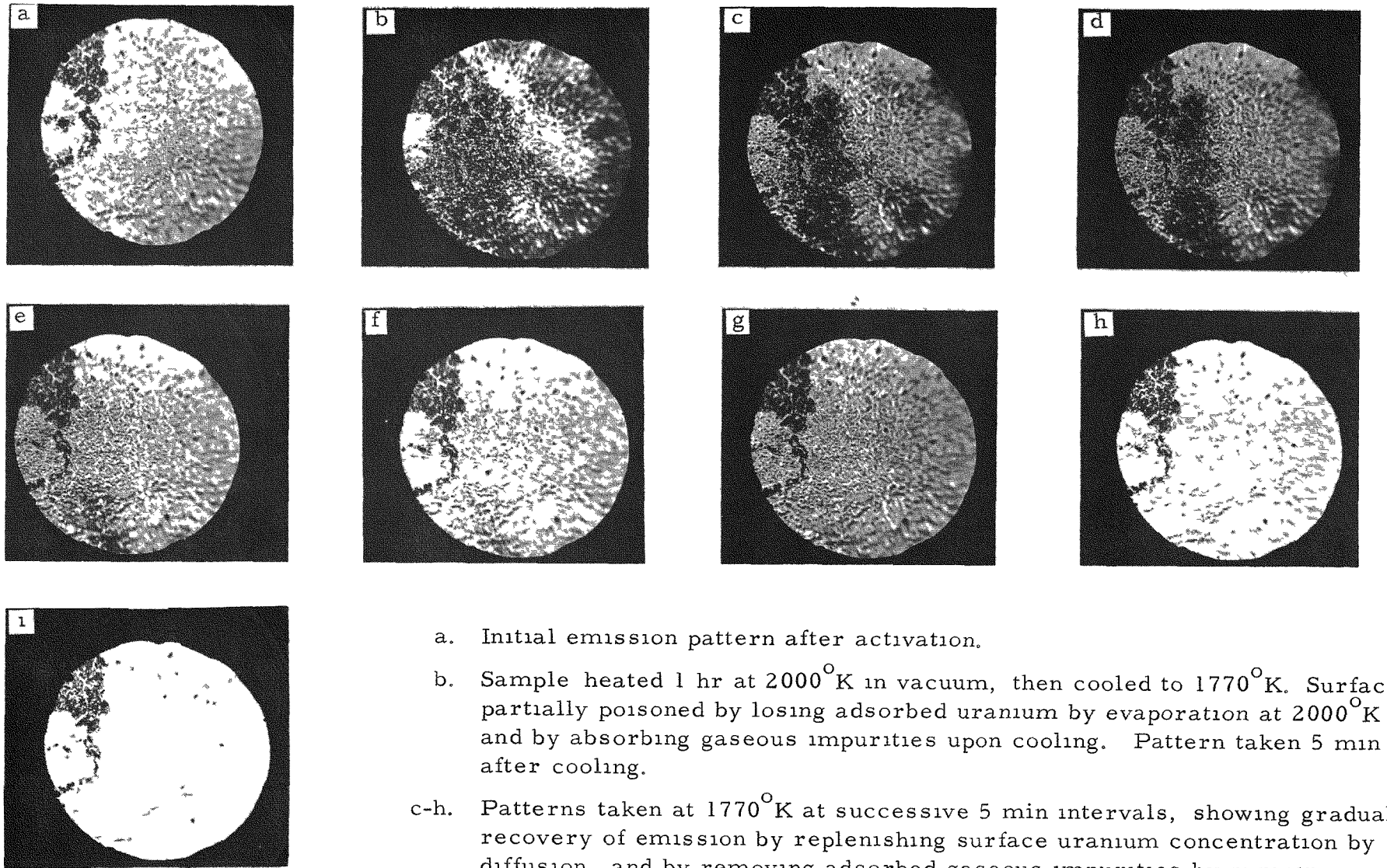

a. Initial emission pattern after activation.

b. Sample heated 1 hr at 2000°K in vacuum, then cooled to 1770°K. Surface partially poisoned by losing adsorbed uranium by evaporation at 2000°K and by absorbing gaseous impurities upon cooling. Pattern taken 5 min after cooling.

c-h. Patterns taken at 1770°K at successive 5 min intervals, showing gradual recovery of emission by replenishing surface uranium concentration by diffusion, and by removing adsorbed gaseous impurities by pumping.

i. Fully recovered emitting surface.

Fig. 10--Electron emission patterns from a uranium carbide surface showing the poisoning and regeneration of the emitting surface

The poisoning of the emission of this sample in a poor vacuum has also been studied. When the activated sample was exposed at room temperature to a vacuum of 10^{-2} to 10^{-3} torr for a period of 12 hr, or to the atmosphere for a period of a few hours, poisoning of the surface occurred, as indicated by the appearance of large dark patches in the emission patterns. When the sample was brought to a higher temperature (e. g., 1670° to 1770°K), the emission recovered in all cases within 8 hr at 1670°K and within 1 hr at 1770°K in a vacuum of 10^{-6} torr.

Other uranium carbide samples and 90 UC–10 ZrC samples are being prepared to continue these studies. An effort will be made to correlate the emission patterns with the microstructures and a study will be made of the activation, poisoning, and regeneration of UC-ZrC with various amounts of uranium carbide.

2. 4. High-temperature Mechanical Properties

The purpose of the mechanical-properties evaluation is to determine what effect the U/Zr ratio of UC-ZrC has on strength and to obtain data with which to predict the swelling behavior during irradiation.

The sample-testing fixtures have been incorporated into the furnace and heated to 1800°C for "shake-down" evaluation of the equipment. Minor mechanical difficulties were observed, such as loosening of the bottom testing fixture and swelling of the sample-loading tube in its guide. In addition, the bottom of the furnace was found to be uneven so that the stability of the alignment of the whole furnace was affected. Necessary corrections and refittings were made to overcome these difficulties.

During a subsequent heating operation, it was noted that the sample-loading push rod expanded thermally and froze against the water-cooled guide bushing. This guide bushing was to provide for the alignment of the push rod in contacting the specimen. Thus it became apparent that a much better system was needed to provide for push-rod alignment. A decision was made to enlarge the water-cooled guide sleeve so that it acted only as a thermal shield. In addition, an alignment bearing integral with the push rod was added to the top plate of the furnace (see Fig. 11). The features of the alignment bearing are described as follows:

1. The center of the bearing was aligned with the centerlines of the push rod and the furnace top plate.
2. The top portion of the bearing was threaded internally to fit the Instron Universal Tester load cell to assure alignment of the load cell with the push rod.
3. A water-cooled heat barrier was placed between the push-rod connection and the alignment bearing to keep the bearing surfaces cool.

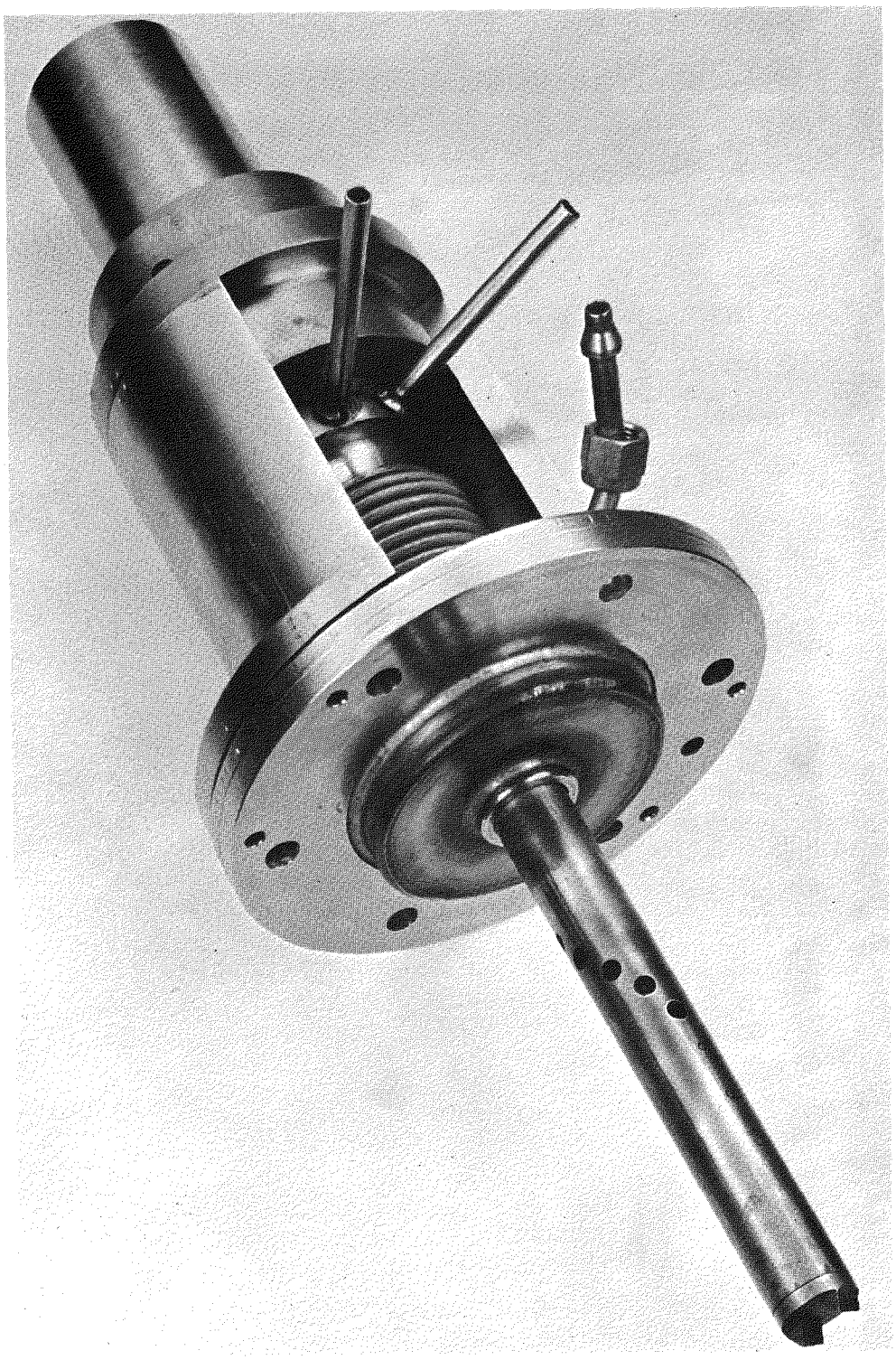

Fig. 11--Top of furnace for measuring mechanical properties, showing push rod for loading sample and guiding-alignment bearing. Note water-cooling arrangement for interface

Testing of machined, outgassed 10 UC–90 ZrC bars will be initiated shortly. The composition and number of bars to be used in the test program are as follows:

Composition	No. of Test Specimens Planned
ZrC	12
10 UC–90 ZrC	7
30 UC–70 ZrC	12
50 UC–50 ZrC	12
80 UC–20 ZrC	20
UC	12

Techniques for electrical-discharge machining flats on the 1/4-in.-diameter and 1-1/4-in.-long test bars have been developed. Six bars can be machined concurrently to an end-to-end and side-to-side tolerance of 0.0002 in.

3. IRRADIATION STUDIES

3.1. Unclad-carbide Capsule

The unclad-carbide capsule has been irradiated in the General Electric Test Reactor (GETR) for two cycles. All the thermocouples have been functioning well. The readings for the four high-temperature thermocouples during the two irradiation cycles are shown in Fig. 12. The capsule is now back at the General Atomic hot cell. Post-irradiation examination of the contents of the capsule should be started early in the next quarter.

3.2. Clad Capsule

The clad capsule has been assembled and shipped to the GETR. A description of this capsule is given in the following sections.

3.2.1. Nature of Samples in Capsule

Because of compatibility limitations, samples consisting of UC and 90 UC–10 ZrC clad with a 98 wt-% W–2 wt-% Mo alloy were eliminated from the list shown in Table 10 of GA-4173.[4] The nature of the fuel samples included in the clad capsule is summarized in Table 5.

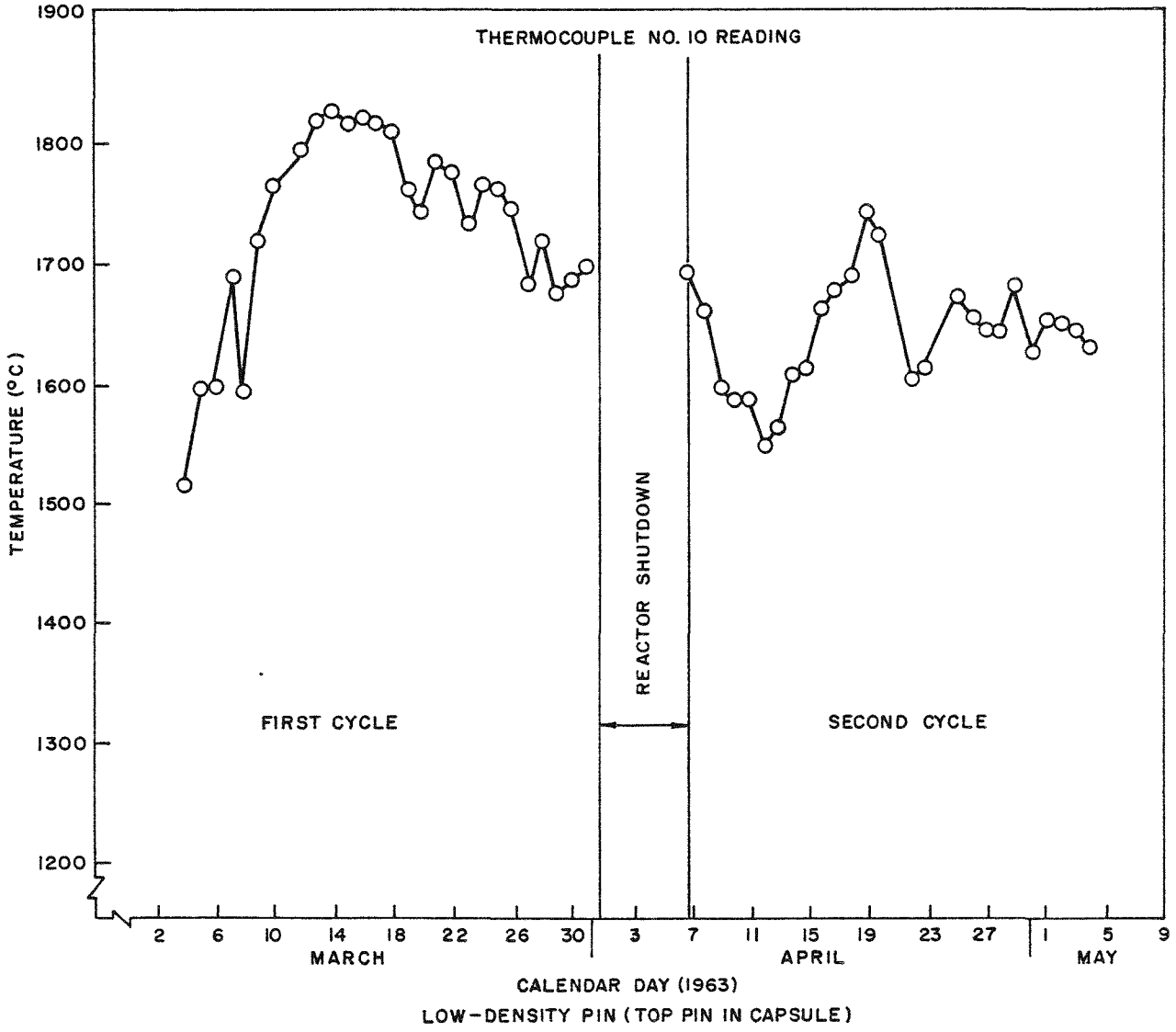

Fig. 12--Temperature of pins in unclad capsule GA2-306-1F1

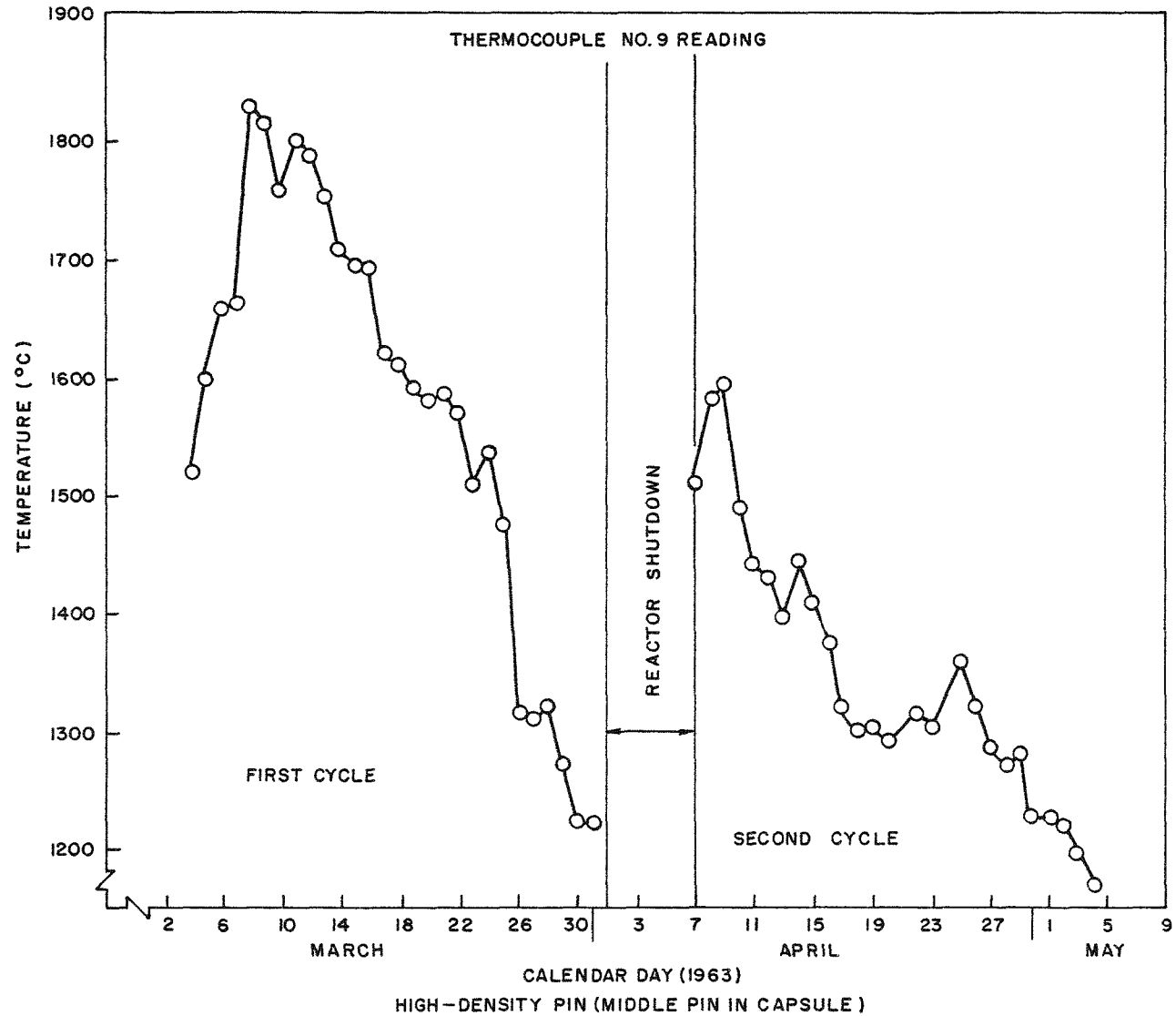

Fig. 12 (continued)

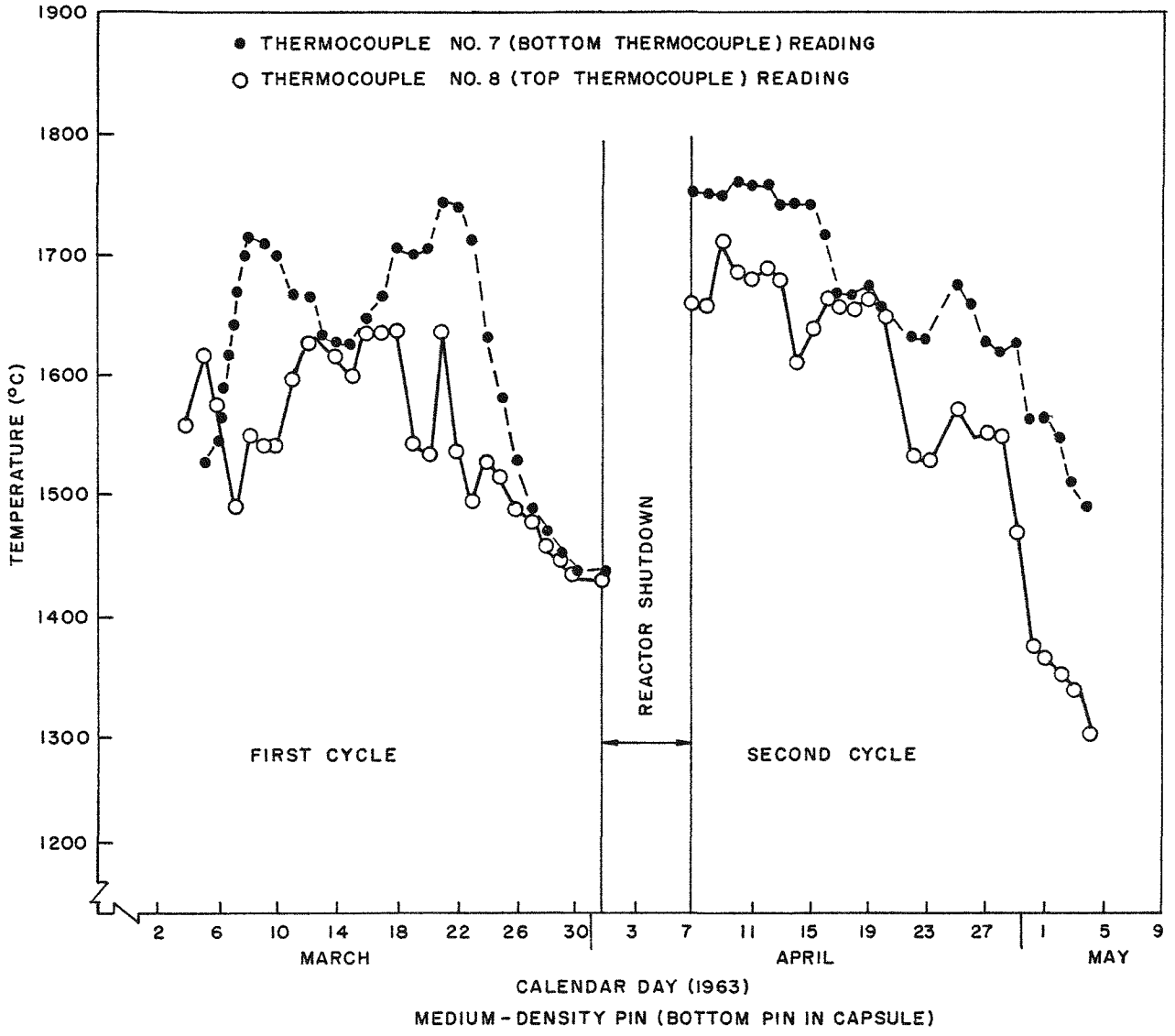

Fig. 12 (continued)

Table 5

FUEL SAMPLES INCLUDED IN THE CLAD CAPSULE

Cladding	Fuel	Fuel Density[a]	Number of Samples
W (vapor-deposited)	UC	High	2
		Low	2
	90 UC–10 ZrC	High	2
		Low	2
	30 UC–70 ZrC	High	2
		Low	2
	W-UO_2 cermet	~60 vol-% fuel	2
	W-UC cermet	~60 vol-% fuel	2
98 wt-% W–2 wt-% Mo alloy (cast, hot-swaged, and machined)	30 UC–70 ZrC	High	2
		Low	2
	W-UO_2 cermet	~60 vol-% fuel	2
	W-UC cermet	~60 vol-% fuel	2

[a] High density,>90% theoretical value; low density, 85% to 90% theoretical value.

In addition to the 24 fuel specimens, the capsule also contained 9 vapor-deposited tungsten-clad, enriched 90 UC–10 ZrC samples as thermal shields for temperature-gradient control and 2 vapor-deposited tungsten-clad, depleted 90 UC–10 ZrC as control samples. The capsule contained a total of 35 samples.

3.2.2. Sample Configurations

The configurations of the finished vapor-deposited tungsten-clad samples and the 98 W–2 Mo-clad samples are shown in Figs. 13a and 13b, respectively. The void was included inside the cladding to collect the fission gases released from the fuel; it has a volume approximately equal to that of the fuel. The axial hole was for the insertion of the tungsten-thermocouple well. All samples have nominal dimensions of 3/8 in. OD, 1/8 in. ID, and 5/16 in. high. The nominal cladding thickness around the fuel is 20 mils.

3.2.3. Sample Fabrication

3.2.3.1. Fuel Fabrication

Carbide Fuels. The UC and the 90 UC–10 ZrC carbide fuel samples

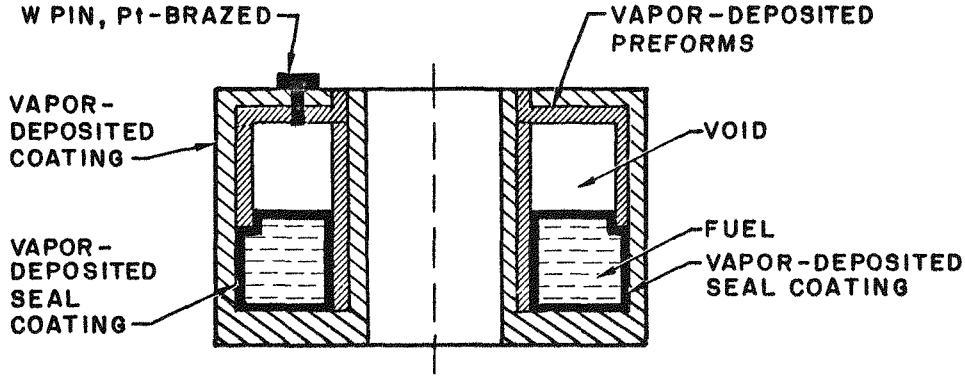

(a) Vapor-deposited tungsten cladding

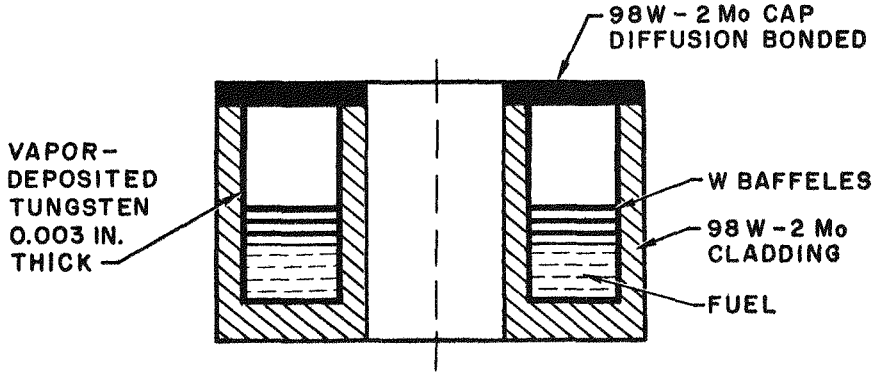

(b) 98 wt-% W—2 wt-% Mo cladding

Fig. 13--Configurations of finished irradiation samples to be included in clad capsule

were fabricated by cold-pressing and sintering, according to the procedures described in GA-4173.[4] The 30 UC–70 ZrC fuel samples were prepared by vacuum hot-pressing under conditions similar to those for fabricating the 20 UC–80 ZrC fuel samples for the unclad-carbide capsule.[4] The outgassing, machining, and characterization (structures, dimensions, densities, and compositions) of these fuel samples were carried out according to procedures similar to those used for the carbide samples in the unclad capsule.[4] The finished samples were sealed in glass ampoules before the cladding operation. The enrichment of these samples was adjusted so that the U^{235} density was approximately 29.4×10^{20} atoms/cm^3 of the fuel. Metallographic and X-ray examinations of duplicates of these samples showed that all were single-phase materials containing no UC_2 or free metal. The compositions of the samples are shown in Table 6.

Table 6

COMPOSITION OF CARBIDE FUEL SAMPLES FOR CLAD CAPSULE

Nominal Composition	Final Composition after Outgassing (mol-%)		
	C	U	Zr
90 UC–10 ZrC (depleted)	48.8	45.8	5.7
90 UC–10 ZrC (enriched)	48.7	45.9	5.3
UC (enriched)	50.0	50.0	----
30 UC–70 ZrC (enriched)	49.0	15.7	35.4

Cermet Fuels. The W–60 vol-% UC cermet samples were prepared in the following manner. Uranium carbide powder (-325 mesh), obtained by grinding arc-melted uranium carbide buttons, was cold-pressed at 90,000 psi, sintered in vacuum at 1600°C, and annealed in vacuum at 1800°C for 20 hr to homogenize the alloy. Chemical analysis indicated that the material was homogenized after this treatment and had a carbon content of 4.70 wt-%. The compact was then crushed and the -100/+200 mesh fraction was mixed with the required amount of -325 mesh tungsten powder and 0.03 wt-% of -325 mesh nickel powder as a sintering aid. The mixture was blended by hand tumbling in a glass vial for about 1/2 hr and then was vacuum hot-pressed in a graphite die at 1800°C and 8000 psi to produce cylinders 0.4 in. in diameter and 5/16 in. in height. The product had a density of 96% to 98% of the theoretical value. Metallographic examination revealed that the dispersion was uniform and single-phase (see Fig. 14).

The W–60 vol-% UO_2 cermet samples were prepared according to the following procedures. Spherical UO_2 particles about 100 μ in diameter,

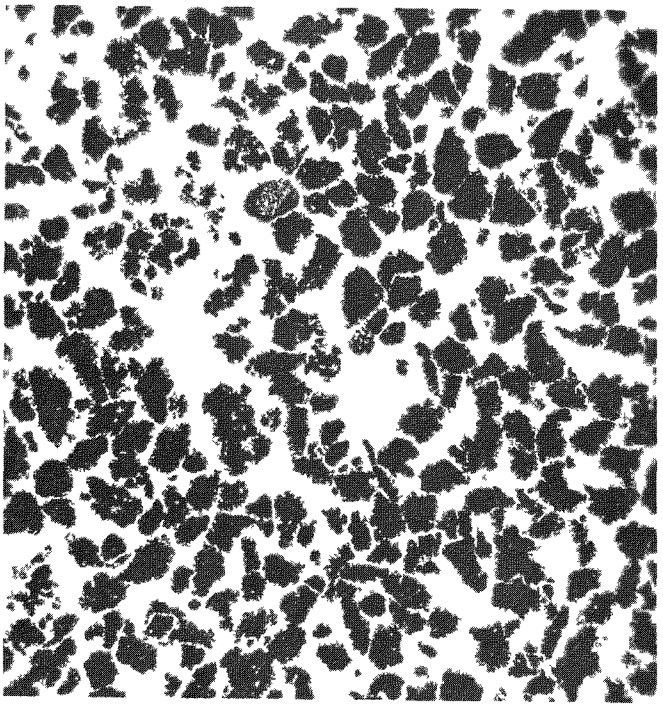

3091-1-1 ×50

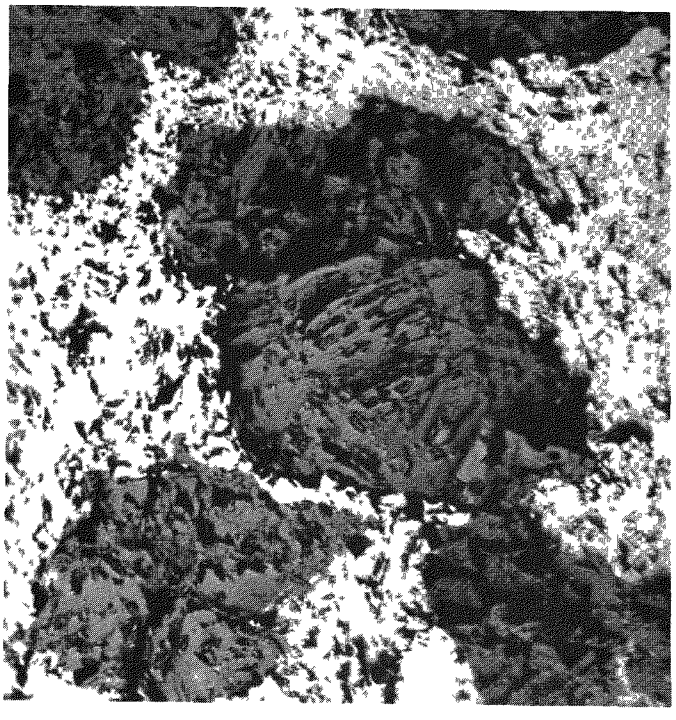

3090-1-1 ×250

Fig. 14--Hot-pressed W–60 vol-% UC cermet, 98% theoretical density

both depleted and fully enriched (obtained from United Nuclear Corporation), were blended to the degree of enrichment required. The UO_2 powder was then mixed with the required amount of -325 mesh tungsten powder and 0.03 wt-% of -325 mesh nickel powder, as a sintering aid, and was vacuum hot-pressed in a graphite die at 1750°C and 7000 psi into cylinders of about the same size as the W-UC cermet compacts. The density of the product was 93% to 95% of the theoretical value. Figure 15 shows photomicrographs of a W-UO_2 cermet sample prepared in this way.

A blended mixture of depleted and fully enriched UO_2 particles was used to achieve the required fuel enrichment because partially enriched UO_2 particles were not available at the time. A blended mixture of UO_2 and tungsten powder instead of tungsten-coated UO_2 particles was used to prepare the cermet because the coating process was not sufficiently developed to ensure a satisfactory product.

The enrichment of the cermet fuels was adjusted to give a U^{235} density of approximately 34.6×10^{20} atoms/cm^3.

3.2.4. Cladding Operation

3.2.4.1. Cladding of Fuels with Vapor-deposited Tungsten

When the carbide fuels were coated with tungsten by the WF_6+H_2 reaction, according to the configuration shown in Fig. 13a, at San Fernando Laboratory, difficulties were encountered because of corrosion of the fuel by the gaseous mixture surrounding the fuel. (No such problem existed when the carbide fuel was coated previously, according to the configuration shown in Fig. 30a of GA-4173.) This problem was solved by first depositing a thin coating of tungsten on the carbide fuels under conditions where the attack on the carbide fuels by the ambient gas mixture was minimized. The cladding thickness was then built up in accordance with the configuration shown in Fig. 13a. Figure 16 is a photomicrograph of a 90 UC–10 ZrC sample coated with 0.002 in. of tungsten by the modified vapor-deposition method, illustrating the absence of attack on the carbide by the ambient gases during the coating operation.

After the cladding operation was completed, the outside diameter and the ends of the sample were finished to specified dimensions by grinding, and the inside diameter was machined to size by electrical-discharge machining. To remove any gas trapped inside the cladding can, a hole was drilled with a carbide tool on one of the end surfaces and the sample was outgassed in vacuum at 1750°C for a period of 24 hr. Before and after the outgassing, the sample was checked for leaks using a helium leak detector.

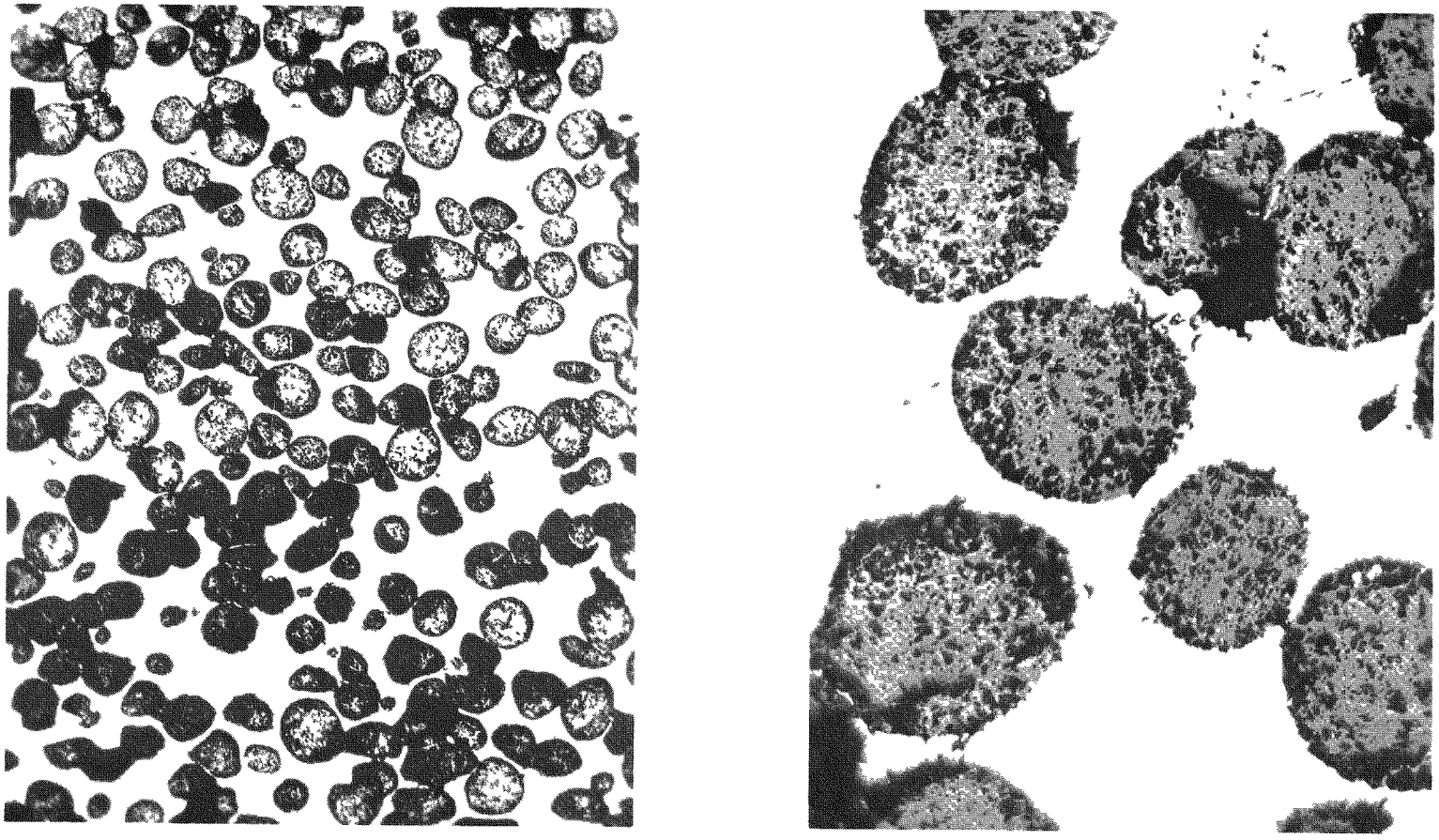

Fig. 15--Hot-pressed W–60 vol-% UO_2 cermet, 94% theoretical density

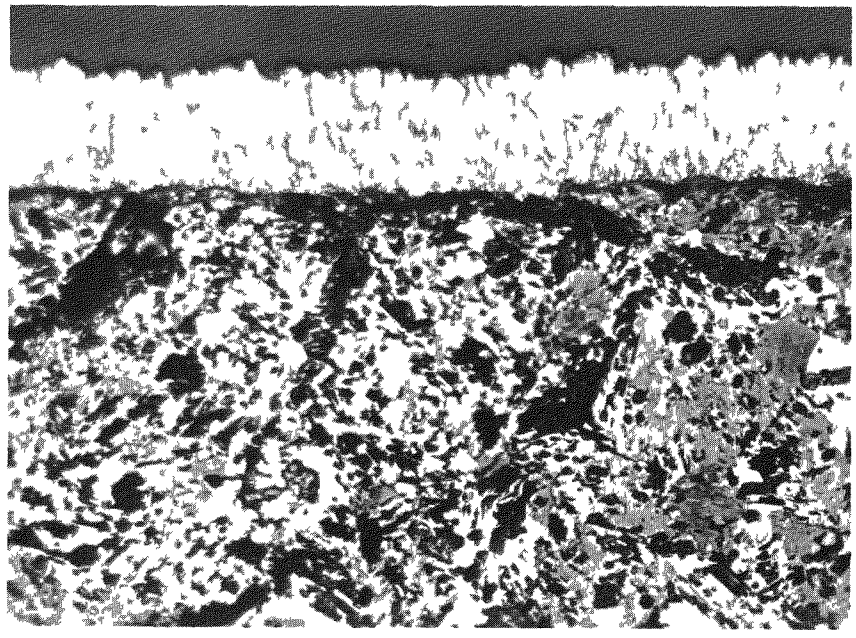

3288-1-1 ×250

Fig. 16--90 UC–10 ZrC clad with 0.002 in. vapor-deposited tungsten. Note there is no visible attack of the carbide by the ambient gas mixture during the deposition

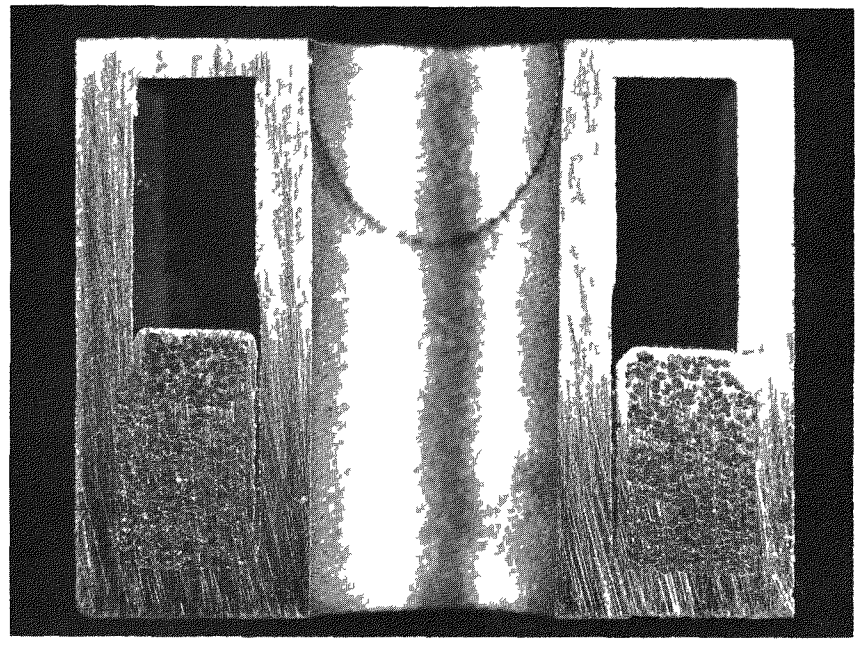

3749-1-2 ×10

Fig. 17--Cross section of vapor-deposited tungsten-clad $W–UO_2$ cermet sample

A tungsten pin was then vacuum-brazed into the hole with platinum, according to the procedures established during last quarter.[4] After brazing, the sample was again checked for leaks using helium pressurization followed by immersion in alcohol. The finished samples, having a configuration such as that shown in Fig. 13a, were stored in sealed glass ampoules before being assembled into the irradiation capsule. Figure 17 shows a cross section of a tungsten-clad W-UO_2 cermet sample, with the thin seal coating clearly visible. Figures 18a and b show the end view and the side view of a tungsten-clad depleted 90 UC–10 ZrC sample.

3.2.4.2. Cladding of Fuels With 98 wt-% W–2 wt-% Mo Alloy

Cups of the W-Mo alloy in the shape shown in Fig. 33b of GA-4173[4] were prepared by machining. To minimize the chance of fuel-cladding interaction (see Section 2.4.2), the inside surfaces of the cups were coated with a layer of vapor-deposited tungsten 0.003 in. thick prior to the loading of the fuel. After the outgassed fuel and the tungsten baffles* were loaded into the cup, a 98 wt-% W–2 wt-% Mo cap was diffusion-bonded in vacuum to the cup by using 0.01-in.-thick W–26Re alloy sheet as an intermediate layer.[4] The sample was then checked for leaks using pressurization in helium followed by immersion in alcohol. The outside diameter and the ends of the sample were then ground and the inside diameter was machined by electrical-discharge machining to the dimensions required. The sample was again checked for leaks and outgassed at 1700°C for 2 hr. The finished samples with the configuration shown in Fig. 13b were stored in sealed glass ampoules before being assembled into the irradiation capsule.

3.2.5. Arrangement of Samples in Pins

The clad samples listed in Table 6 are grouped into four pins: (1) the first cermet pin, (2) the low-density pin, (3) the high-density pin, and (4) the second cermet pin. Figure 19 shows the schematic arrangement of a fuel pin, which is similar to that in the unclad capsule[3] except that the ZrC thermal shields at each end were replaced by three sheets of 0.005-in. tungsten foil. In each pin, in addition to the tungsten-foil thermal shields, there were two pieces of tungsten-clad enriched 90 UC–10 ZrC thermal shields, one at each end of the pin. Since the presence of a depleted control sample causes perturbation of the temperature of its neighboring sample, a control sample was incorporated only in the first cermet pin and in the high-density pin. In addition, an extra tungsten-clad enriched 90 UC–10 ZrC piece was inserted between the fuel samples and the control sample in the high-density pin, to minimize the temperature perturbation effect. Separating the cermet samples into two groups was primarily to avoid having all of

*Provided to minimize fuel redistribution by vaporization. These baffles are not needed for the tungsten-clad samples because of the presence of the seal coating.

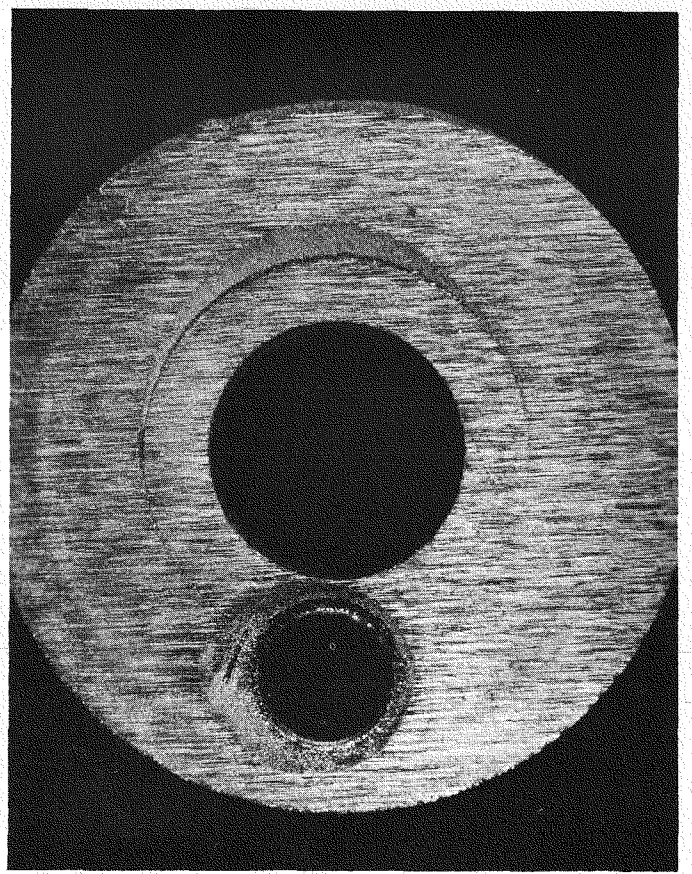

3757-1-1 (a) ×10

3757-1-2 (b) ×10

Fig. 18--Vapor-deposited tungsten-clad depleted 90 UC–10 ZrC sample: (a) top view, hole for outgassing also shown; (b) side view

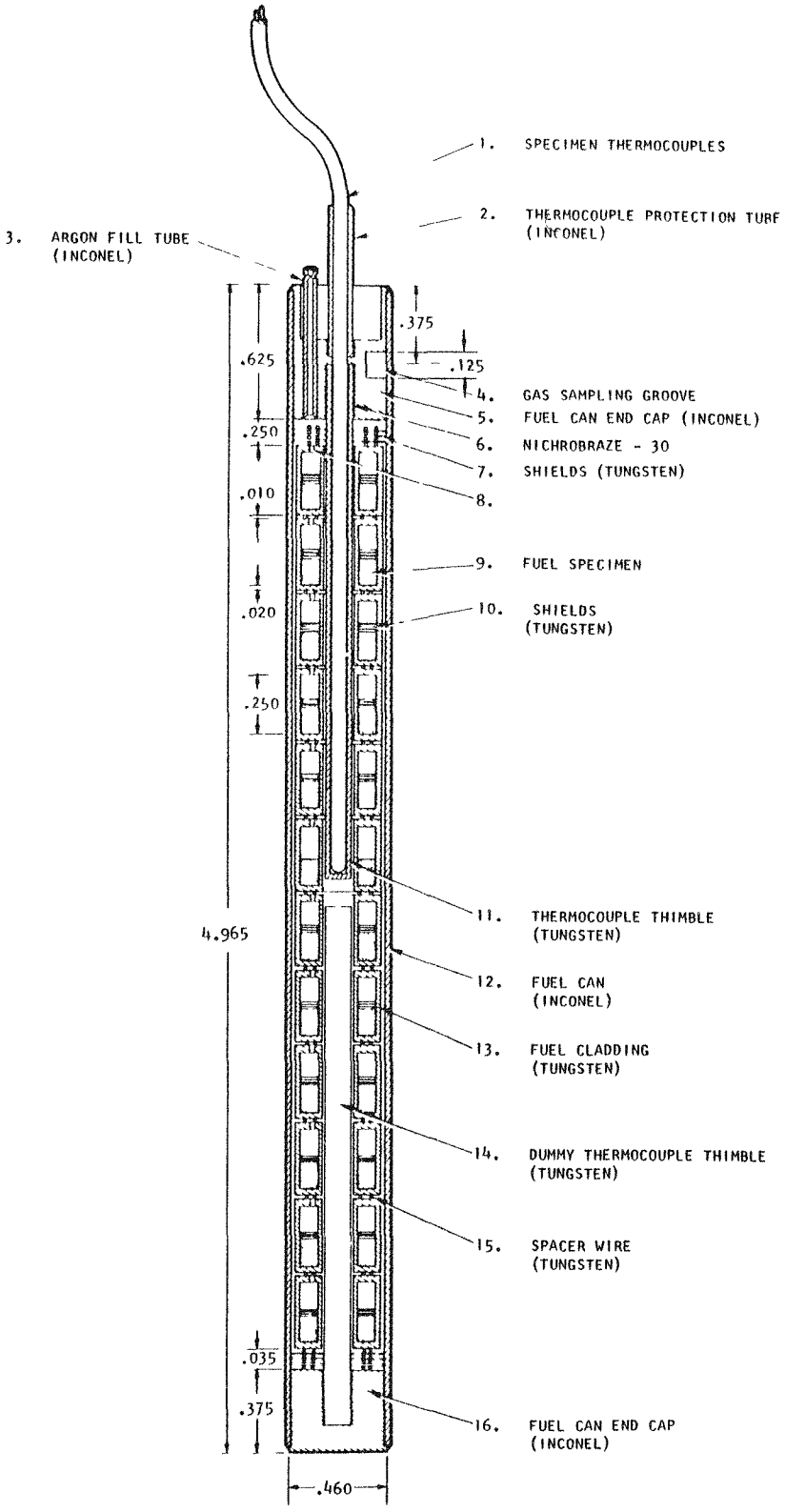

Fig. 19--Longitudinal cross section of fuel pin in clad irradiation capsule GA2-306-2F2

the cermet samples located at the bottom of the capsule where the average neutron flux, during the reactor cycle, is the lowest.

The arrangement of the samples in the four pins is shown in Figs. 20a, b, c, and d. The high-temperature W—W26Re (Ta-sheathed) thermocouple inserted in each pin was located at a point where the temperature was expected to be the highest along the axis of the pin. Each pin was filled with purified argon at a pressure of approximately 10 cm Hg, which would rise to about 1 atm at the irradiation temperature (1700° to 1750°C). In all cases, a gap of about 0.005 in. was maintained between adjacent samples with tungsten wires. The radial gas gap between the samples and the Inconel container was maintained by 15-mil tungsten wires.

3.2.6. Arrangement of Pins in the Capsule

The arrangement of the pins in the capsule is shown in Fig. 21; Fig. 22 shows the transverse cross section of the capsule. In addition to the four W—W26Re high-temperature thermocouples, there were six Chromel-Alumel thermocouples for monitoring the outer Inconel-can temperature and for controlling the composition of the He + N_2 mixture in the variable-thermal-conductance gas gap. The locations of these thermocouples and the length of each pin are shown in Fig. 23. Figure 24 shows the calculated radial temperature distribution in the capsule, and Fig. 25 gives the calculated axial temperature distribution through a typical tungsten-coated fuel sample. Figure 26 is a radiograph of the assembled capsule and Fig. 27 shows the dimensions of the capsule and lead-tube assembly.

3.2.7. Irradiation Schedule

The clad capsule will be irradiated in the GETR for one cycle. It is expected that the irradiation will be completed by the middle of July, 1963. Hot-cell examinations of the irradiated capsule should start at the beginning of August, 1963. Because of the higher burnup rate made possible by the presence of a void and thus a large heat-radiating area for each clad sample, it is expected that the total burnup achievable in one cycle will be approximately equivalent to that for the unclad-carbide capsule in two cycles.

4. STUDIES OF NEW CATHODE MATERIALS

The development of new materials with better high-temperature stability, emission performance, and compatibility properties than the UC-ZrC and simple tungsten-clad fuel systems is covered in this section. This development involves studies of the vacuum vaporization and emission

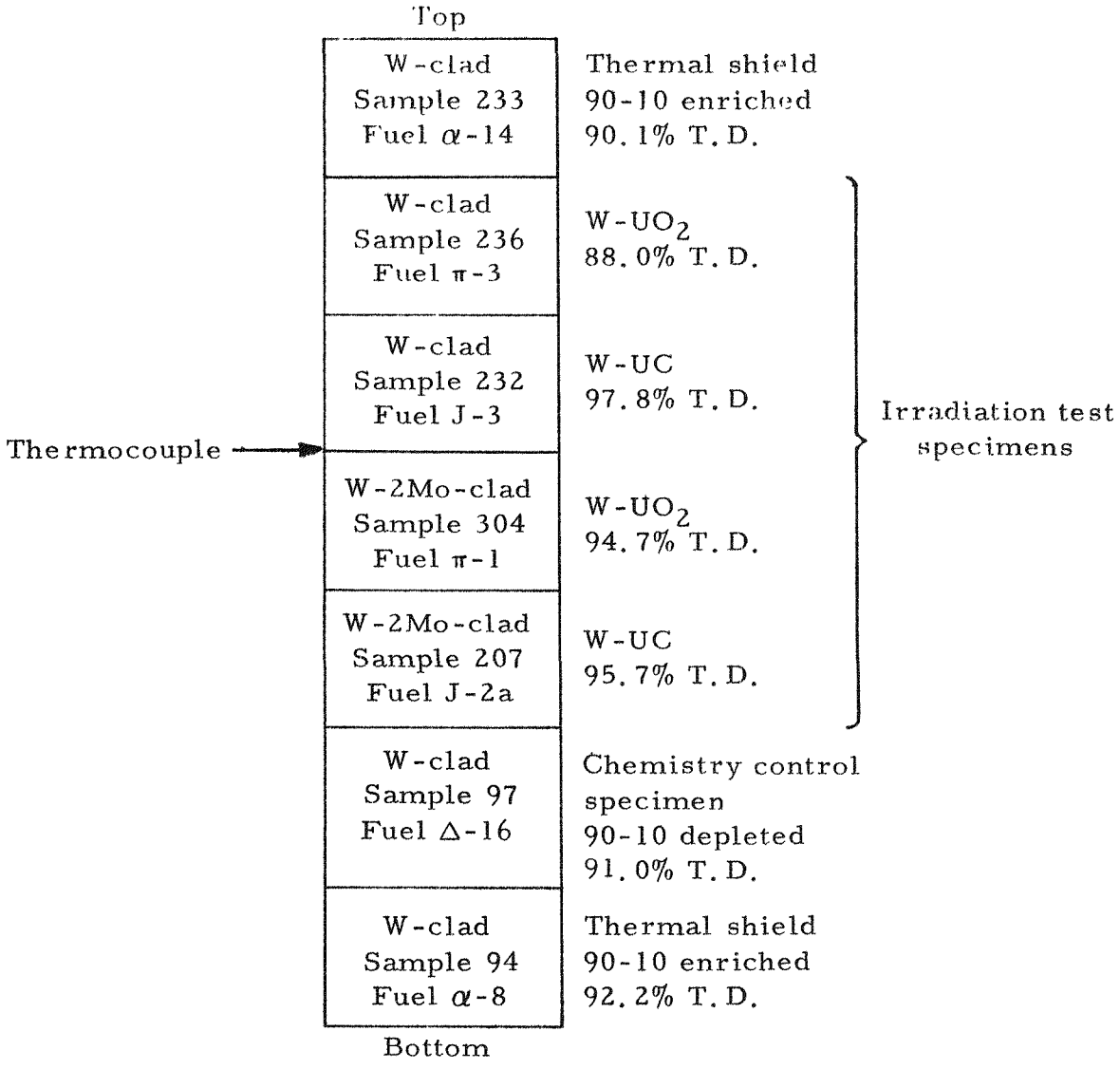

Fig. 20--Arrangement of samples in clad irradiation capsule GA2-306-2F2
(a) First cermet pin, top of capsule (pin No. 4 in Fig. 21)

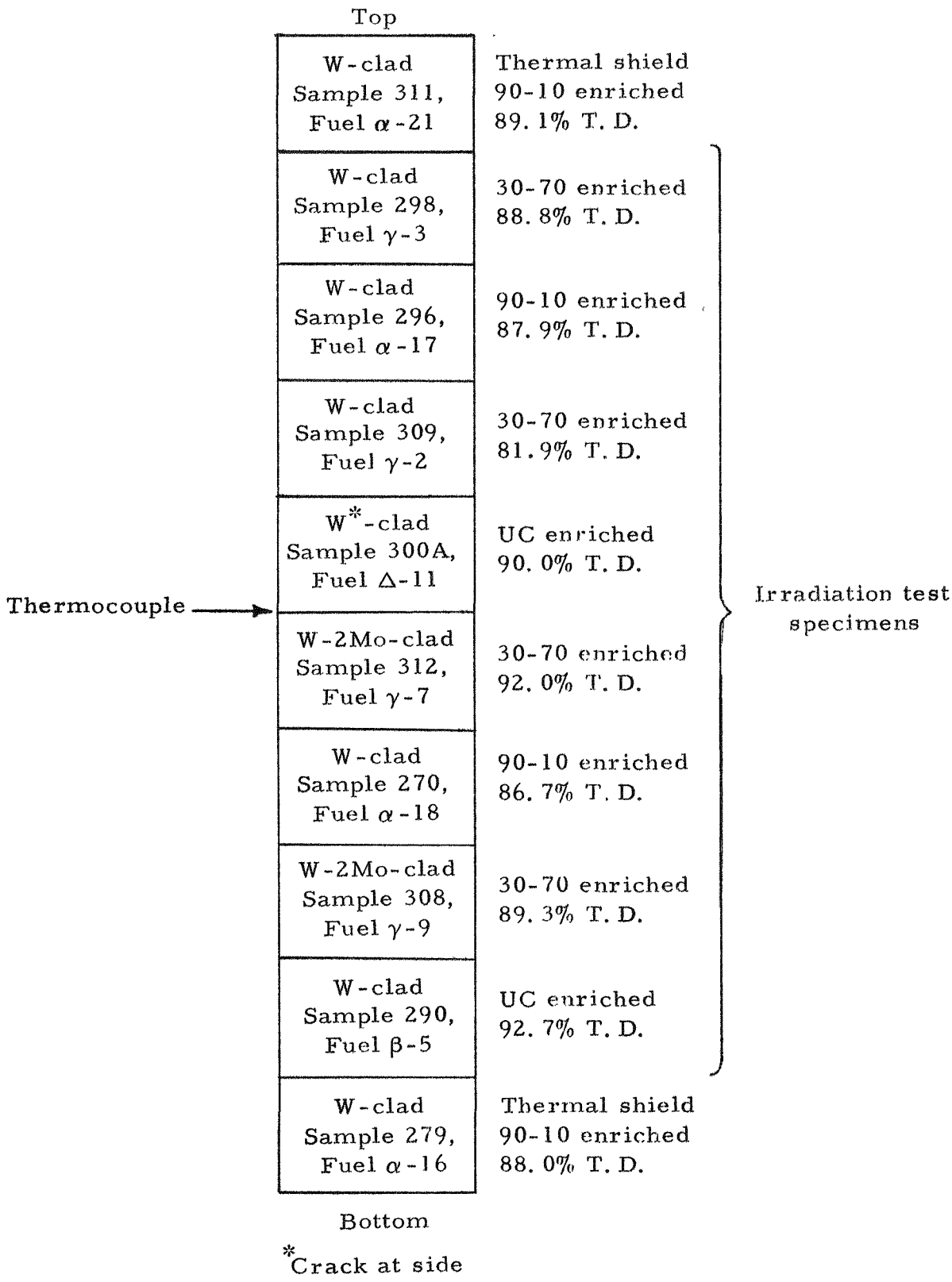

Fig. 20--(b) Low-density pin, second from top of capsule (pin No. 3 in Fig. 21)

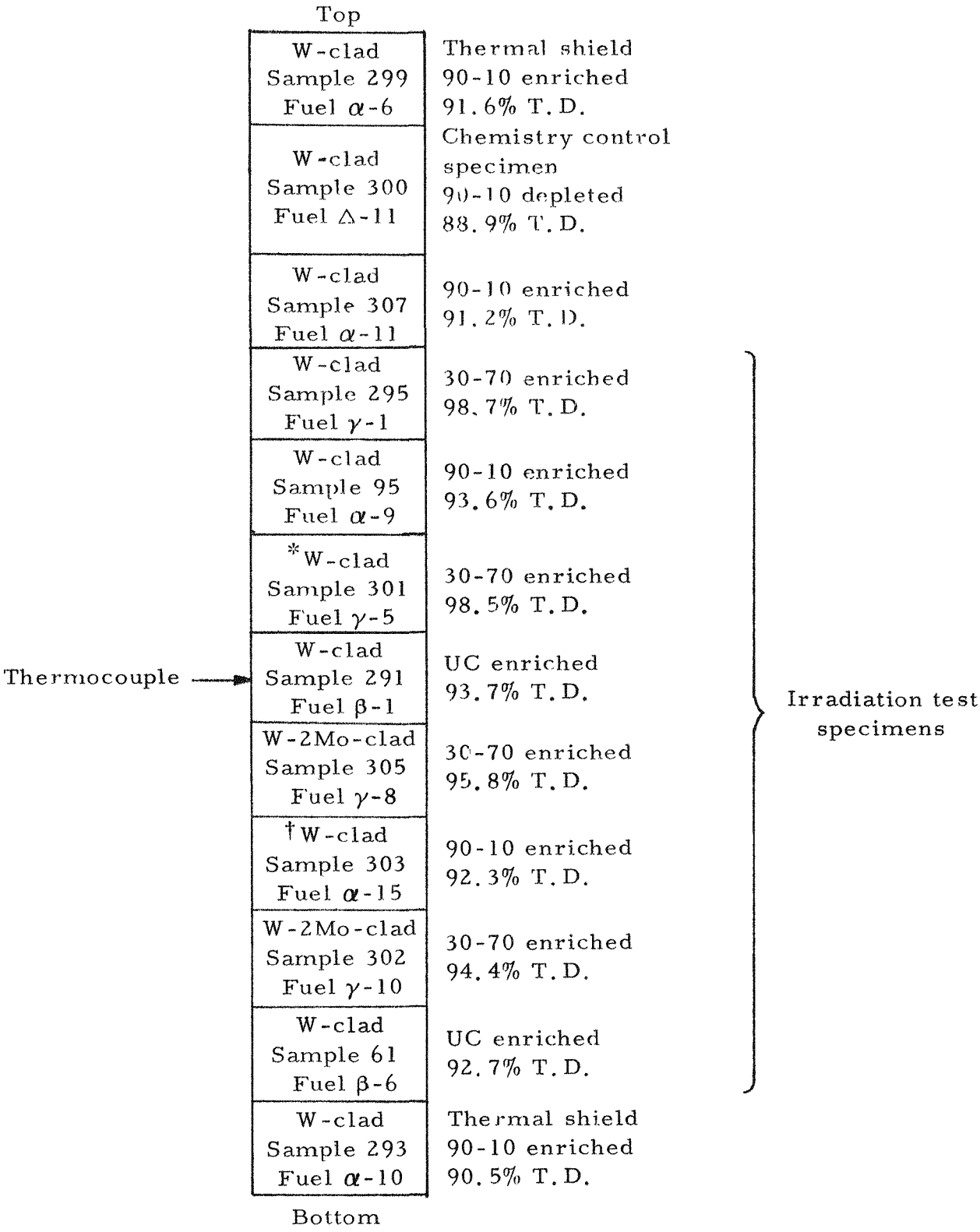

*One blister observed at side
†Leaks at inside cylindrical surface

Fig. 20--(c) High-density pin, third from top of capsule (pin No. 2 in Fig. 21)

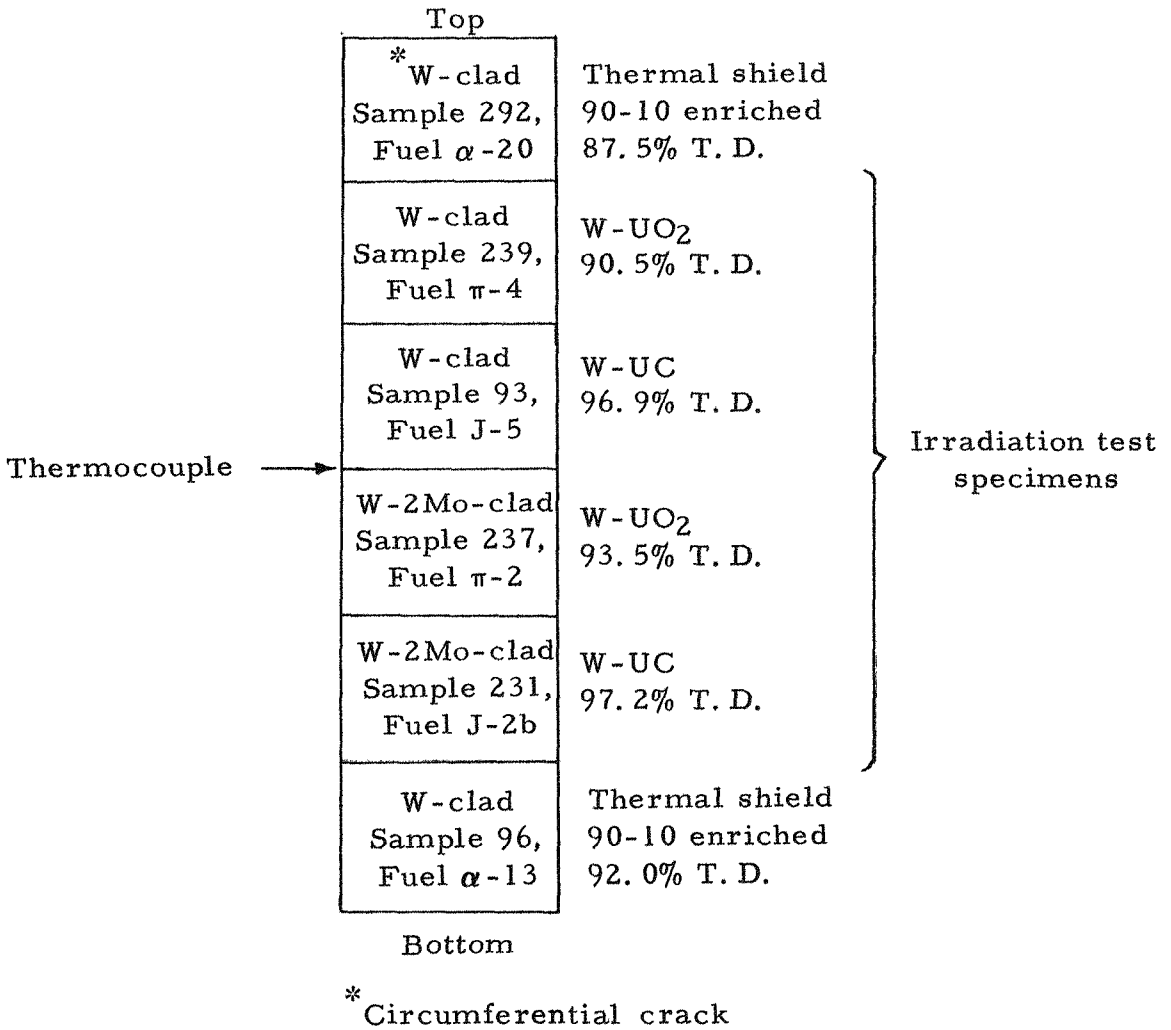

Fig. 20--(d) Second cermet pin, bottom of capsule (pin No. 1 in Fig. 21)

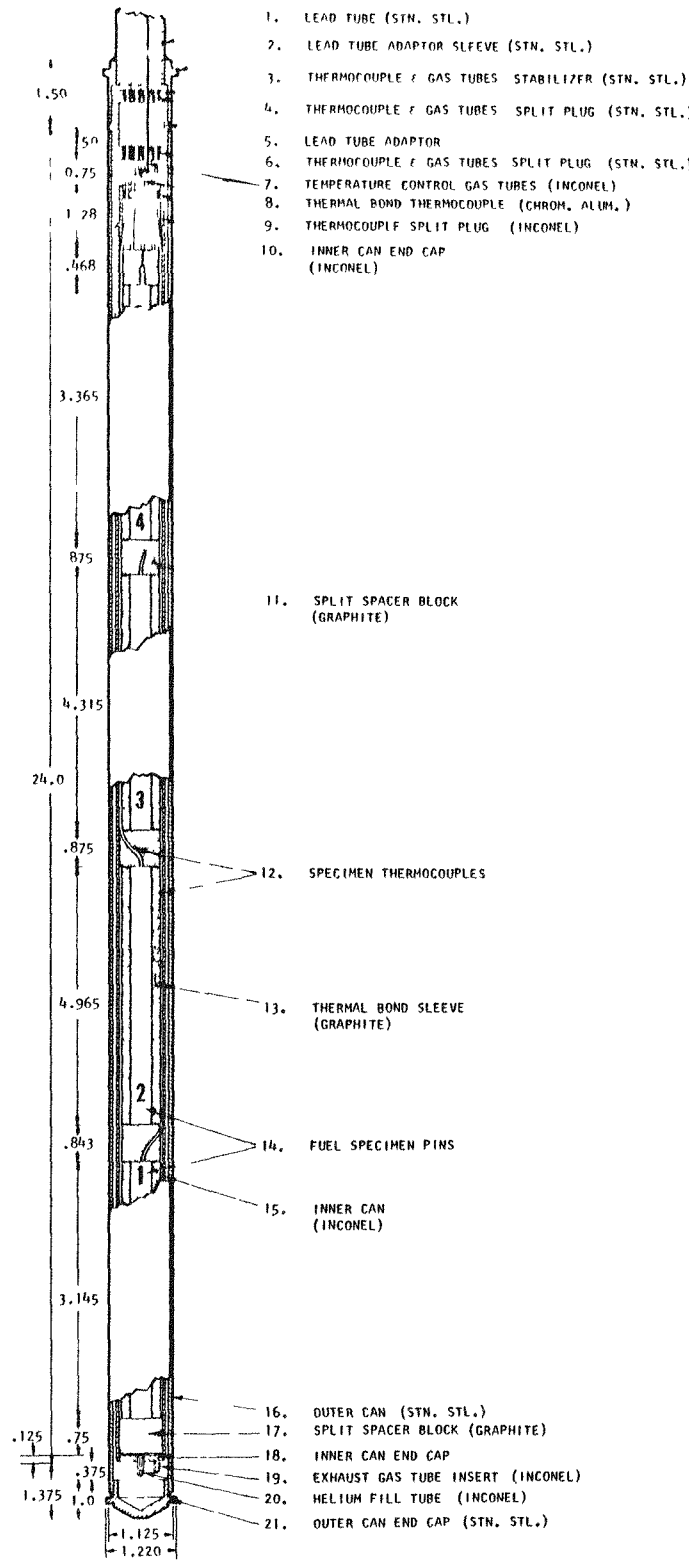

Fig. 21--Longitudinal cross section of capsule
GA2-306-2F2

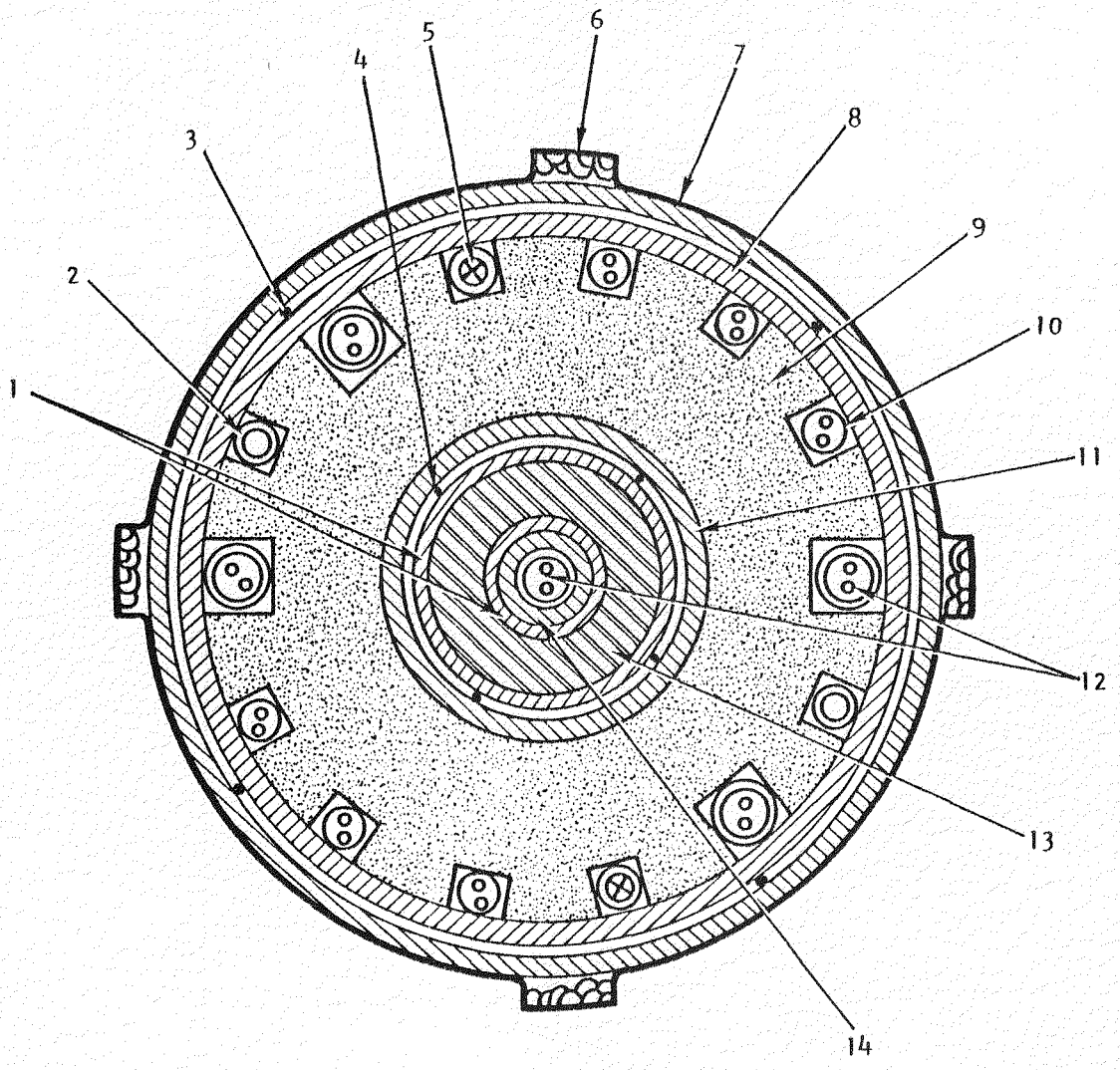

1. FUEL CLADDING (TUNGSTEN)
2. GAS SUPPLY TUBE (INCONEL)
3. SPACER WIRE (NICHROME)
4. SPACER WIRE (TUNGSTEN)
5. DOSIMETER
6. SPACER STUD (STN. STL.)
7. OUTER CAP (STN. STL.)
8. INNER CAN (INCONEL)
9. THERMAL BOND SLEEVE (GRAPHITE)
10. THERMAL BOND THERMOCOUPLE (CHROM - ALUM.)
11. FUEL CAN (INCONEL)
12. SPECIMEN THERMOCOUPLES
13. FUEL SPECIMEN
14. THERMOCOUPLE THIMBLE (TUNGSTEN)

Fig. 22--Transverse cross section of capsule GA2-306-2F2

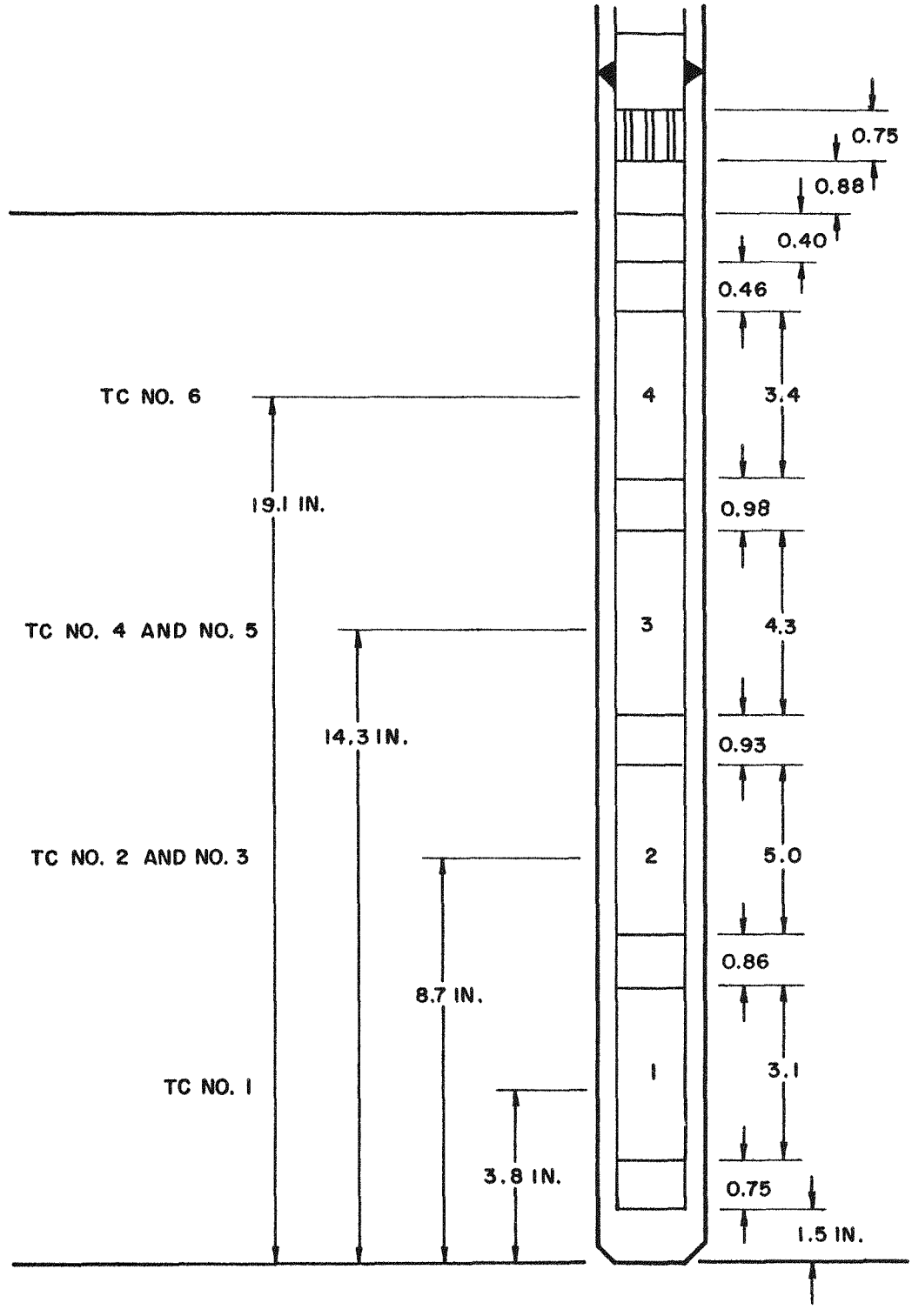

Fig. 23--Schematic illustration of fuel pin and thermocouple locations in capsule GA2-306-2F2

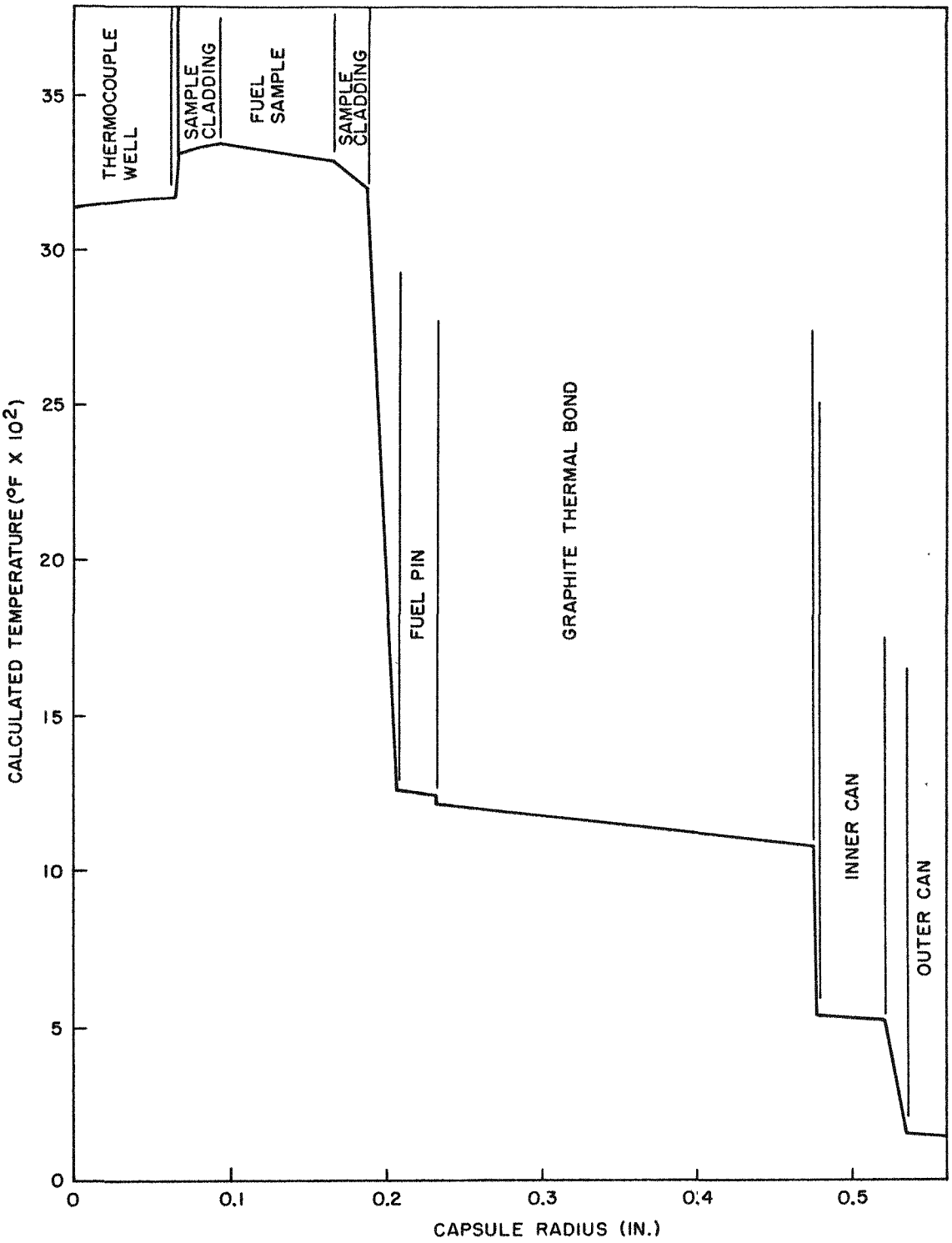

Fig. 24--Calculated radial temperature distribution in capsule GA2-306-2F2

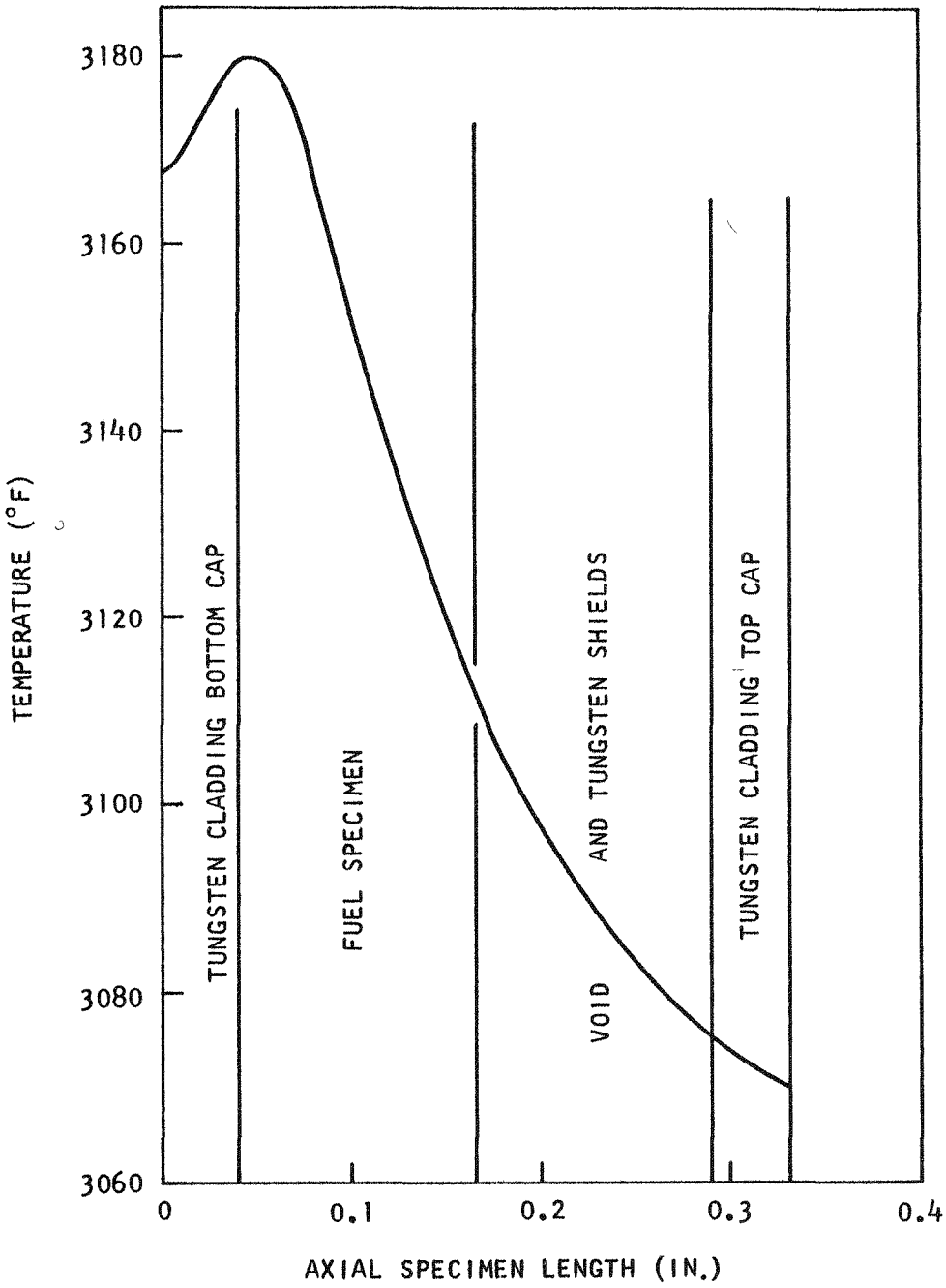

Fig. 25--Calculated axial temperature distribution through a typical tungsten-clad fuel specimen in capsule GA2-306-2F2

Fig. 26--Radiograph of capsule GA2-306-2F2

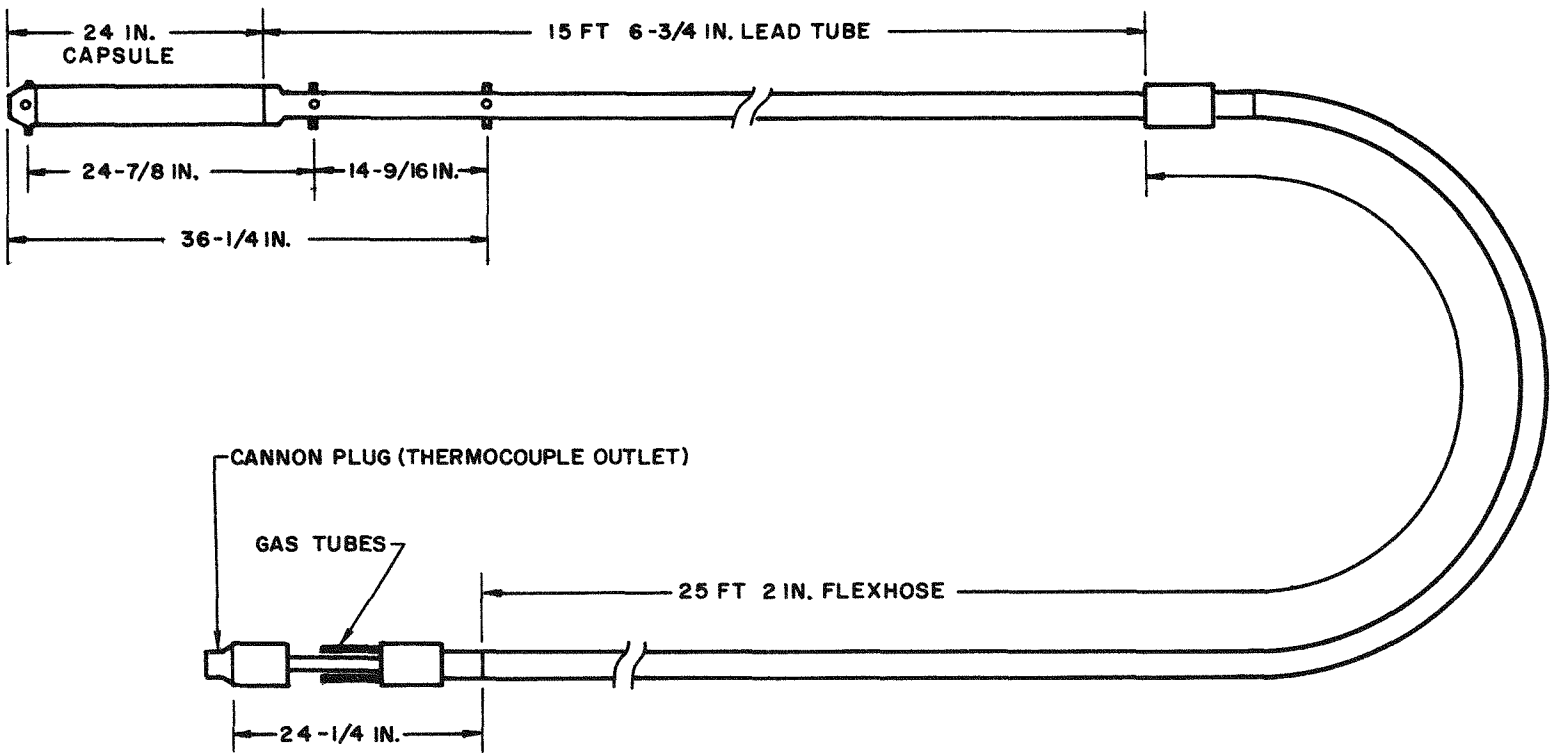

Fig. 27--Diagram of capsule GA2-306-2F2 and lead-tube assembly

characteristics of uranium-containing carbides other than UC-ZrC; the diffusion between uranium-containing fuels and refractory metals other than tungsten; and the effect of ZrC barriers on the compatibility between refractory metals and uranium-containing fuels.

4.1. Vacuum Emission and Vaporization

4.1.1. Vacuum Emission

During this quarter, measurements have been made on the vacuum emission of a hot-pressed stoichiometric $UMoC_2$ sample (D_1-2), the vacuum-vaporization rates of which were reported in GA-4173.[4] The results of the vacuum-emission measurements are shown in Fig. 28. Included in this figure are the emission data of B_1-7 (27.4 UC–72.6 ZrC, hot-pressed). The close agreement between the two sets of data seems to substantiate the theory that the emissions of uranium-containing carbides depend on the presence of a uranium layer on the surface and therefore should be the same if the physical and chemical conditions of the samples and their environments allow such a layer to be maintained. Measurements of the vacuum emission of other uranium-containing carbides will be made under this program for further confirmation of this theory.

On the basis of the vacuum-emission data in Fig. 28 and the vacuum-vaporization data shown in GA-4173, there seems to be no special advantage in using $UMoC_2$ as an unclad cathode, since both its emission and vaporization properties are approximately equivalent to that of UC-ZrC with comparable uranium content.

4.1.2. Vacuum Vaporization

The rate of vacuum vaporization of a cold-pressed and sintered 30 UC–70 NbC sample (D_1-3) has been measured. The results are shown in Table 7 and plotted in Fig. 29 as a function of temperature. The sample had a density of 74.5% on the basis of the theoretical density of 30 UC–70 NbC calculated from X-ray data.[7] The exact composition and pore structure will be determined after the measurement of its vacuum emission has been completed. Samples of 30 UC–70 NbC with higher densities are being prepared for studying their vaporization properties.

4.2. Diffusion

Diffusion studies have been undertaken to discover new cladding materials and to determine clad-fuel combinations that would be suitable for clad-emitter applications. Diffusion studies this year have been directed toward the study of cladding materials that would be easier to fabricate than arc-cast tungsten (of the four refractory metals, Nb, Mo, Ta, and W,

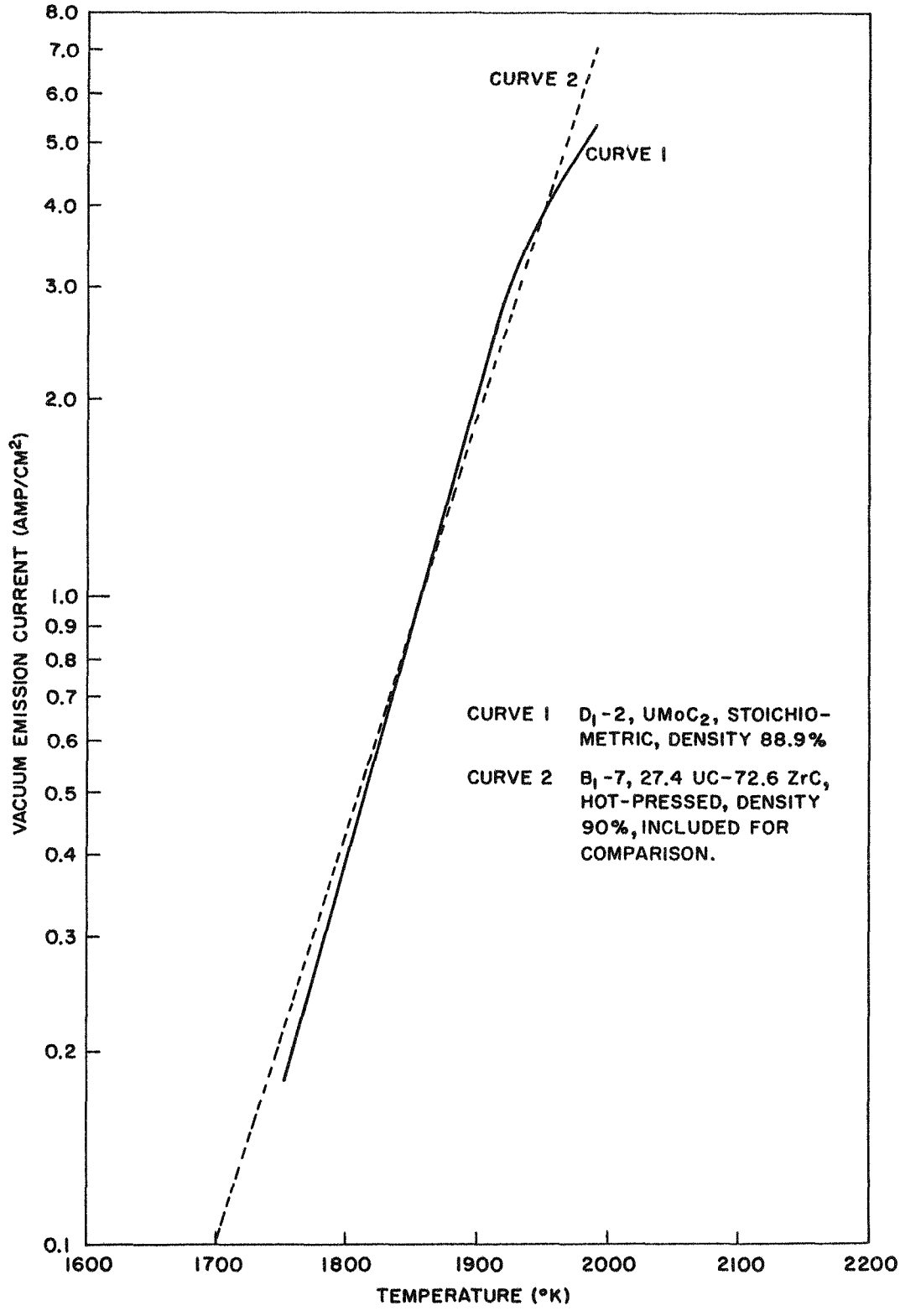

Fig. 28--Vacuum saturation emission of hot-pressed $UMoC_2$ sample D_1-2

Table 7

VAPOR-LOSS INVESTIGATION OF 30 UC–70 NbC SAMPLE D_1-3
(Theoretical density, 74.5% after Run No. 4)

Run No.	Temp. (°K)	Exposure Time (sec × 10^4)	Rate of Weight Loss [(mg/cm^2/sec) × 10^{-5}]	Counting Rate (Alpha counts/min/cm^2)		UC Surface Concentration Based on Counting Rate (mol-%)	Density (g/cm^2)
				Side 1	Side 2		
Original	----	-----	----	908	845	15	----
Degas	2083	172.8	----	---	---	---	7.40
1	2116	5.34	3.29	265	267	4.5	7.55
2	2088	3.24	3.67	252	252	4.0	7.56
3	2198	3.93	13.2	244	246	4.0	7.57
4	2050	7.56	1.42	201	200	3.0	7.56

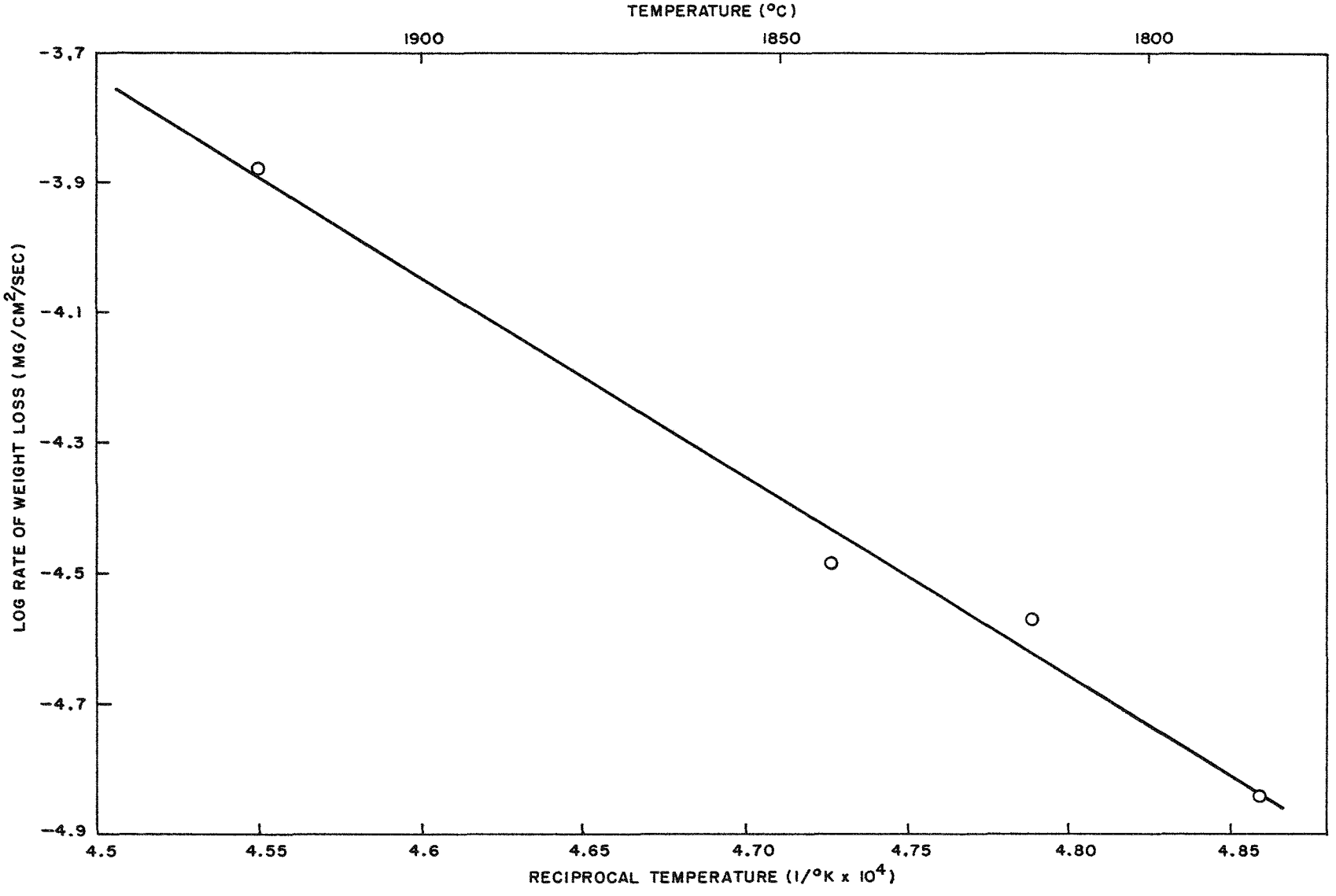

Fig. 29--Vacuum rate of vaporization of 30 UC–70 NbC nominal sample D_1-3, cold-pressed and sintered, density 74.5% based on theoretical density of nominal composition

tungsten has been shown to be the only suitable cladding for UC, UO_2, or UZrC with high uranium content at 1800°C.) Rhenium and iridium were studied because they have slightly better electron-emission characteristics in cesium than does tungsten. The tungsten alloys, W–26Re, 98 wt-% W–2 wt-% Mo, and 85 wt-% W–15 wt-% Mo, were evaluated because their small grain size would enhance fabricability and the alloy may reduce grain growth.

The examination procedures for diffusion specimens involves (1) determining metallographically the gross fuel-clad interaction or observable fuel penetration into the cladding, and (2) determining the concentration-penetration profiles by the electron-beam microprobe technique.

During the first and second quarters, the diffusion between UC and Ir, Re, 74 wt-% W–26 wt-% Re (Run D_2-1), 85 wt-% W–15 wt-% Mo (Run D_2-9), and 98 wt-% W–2 wt-% Mo (Run D_2-3) was studied at 1800°C for 24 hr, and the results are summarized below.

4.2.1. Recapitulation

4.2.1.1. Run D_2-1

Interaction occurred between all three suggested cladding materials and the hyperstoichiometric UC (5.02 wt-% C); the degree of interaction corresponded to the following: Ir > Re > 74 wt-% W–26 wt-% Re alloy. Iridium reacted with the uranium carbide so severely that it melted completely and could not be identified. The liquid phase that was formed penetrated the uranium carbide grain boundaries to considerable depth. A zone of interaction 6 to 10 μ thick was observed in pure rhenium and a layer of precipitate was seen in the 74 wt-% W–26 wt-% Re alloy.

4.2.1.2. Run D_2-2 and D_2-3

The results obtained on these samples may be summarized as follows:

1. UC (4.76 to 4.80 wt-% C), in contact with both 98 wt-% W–2 wt-% Mo and 85 wt-% W–15 wt-% Mo, developed an extensive grain-boundary liquid phase associated with radical grain growth.
2. Both 98 wt-% W–2 wt-% Mo and 85 wt-% W–15 wt-% Mo alloys were attacked by reaction with the uranium carbide and were penetrated throughout by a liquid phase thought to be a U-Mo alloy. This liquid phase was seen at a large percentage of the triple grain-boundary intersections.
3. Uranium carbide (4.76 to 4.80 wt-% C) in contact with pure tungsten showed liquid-phase formation in the carbide. The liquid did not penetrate the tungsten; however, the tungsten in contact with the carbide showed grain-growth inhibition.

The following hypotheses were formulated to explain the formation of a liquid phase in the uranium:

1. The single-phase structure of the metal-rich carbide used was due to a quenched-in high-temperature solubility for uranium; the excess metal precipitated during the thermal treatment of the diffusion couple.
2. Nitrogen and oxygen were present in the uranium carbide in sufficient quantities to hold the uranium in solution with uranium carbide to give a single-phase structure but were gettered by the test alloys to precipitate liquid uranium.
3. Carbon, because of an activity gradient, migrated from the carbide to the test alloys and pure tungsten, leaving the carbide so metal-rich as to precipitate uranium.

A hypothesis was also formulated to describe a mechanism for the penetration into 85 wt-% W–15 wt-% Mo and 98 wt-% W–2 wt-% Mo alloys by the liquid phase formed in the uranium carbide. This was that the alloys were made susceptible to liquid-uranium penetration by grain-boundary segregation of molybdenum, as the arc-cast materials were quenched from the liquidus to the solidus. A different type of segregation could have taken place owing to the differing mobilities of molybdenum and tungsten atoms during annealing of the material, as it was worked down to break up the cast structure.

During this quarter, thermal treatment procedures were established to check the first hypothesis. In addition, electron-beam microprobe analyses were used to check the segregation of Mo in the W-Mo alloys and to study the nature of diffusion species and new phase compositions in diffusion runs D_2-1, D_2-2, D_2-3, and the new compatibility ran D_2-4.

4.2.2. Electron-beam Microprobe Analysis

As stated above, the electron-beam microprobe or microanalysis was used to examine concentration profiles by step-scanning techniques.

The raw step-scanning data have not yet been evaluated to account for absorption, background, and other calibration effects, so accurate graphic presentation is not possible. However, some general conclusions have been drawn. These are presented and coordinated with examples of cathode-ray tube (CRT) display photographs, which show in a qualitative way the concentration gradients existing in the diffusion couples covered. Figure 30 shows, without detailing atomistic mechanisms, the radiations whose relative intensities are used in step scanning and in deriving CRT displays of concentration gradients. As shown, the energy of the primary electron beam (I,primary electron beam current) is disposed of by electron

scattering (I,back-scattered electrons), X-ray generation (I,characteristic X-rays), thermal radiation (I,heat), and sample current flow (I,sample current emanating).

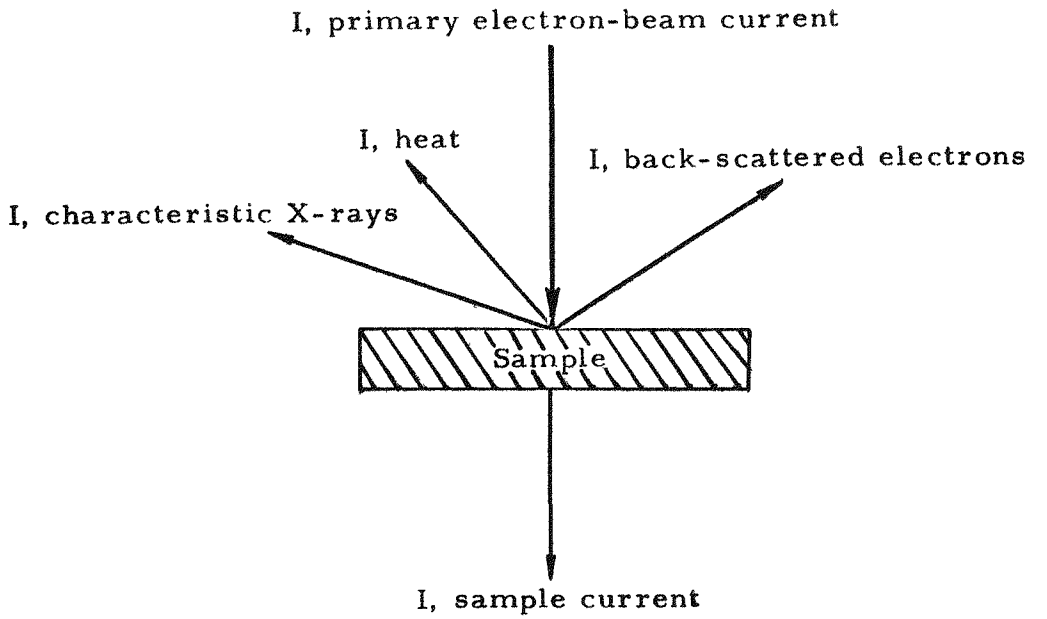

Fig. 30--Schematic diagram of electron-beam microprobe energy dissipation process

The radiation from the surface of the sample and the current intensity of the sample, generated by impingement of the primary electron beam, can be used in several ways to evolve a quantitative and/or qualitative representation of the compositional variation of the sample surface.

The variation in the intensity of back-scattered electrons measured over a scanned area is a qualitative measure of the compositional variation of the sample, since atoms of higher atomic number scatter electrons more effectively than those of a lower number. The intensity of back-scattered electrons can thus be stated to be a function of average atomic number. It is observed that sample current intensity and back-scattered electron intensity have an inversely proportional relationship.

Elements fluoresce with characteristic X-rays on impingement by the microanalysis electron beam. The characteristic X-rays are analyzed (with suitable crystals at Bragg angles) for intensity, to quantitatively determine the sample composition. To determine the compositional distribution across a specimen, a step-scanning process is used.

Both the intensity of back-scattered electrons and the intensity of characteristic X-rays may be displayed on a cathode-ray tube and photographed. During this process, the primary electron beam is swept rapidly over an area of the sample surface while the intensity of the back-scattered electrons or characteristic X-rays is monitored. Although magnifying the sweep area, the CRT electron-gun beam is coordinated with the motion of the primary electron beam of the microanalyzer, and the intensity of the monitored radiation is used to govern the accelerating potential of the CRT electrons and thus the image brightness.

4.2.2.1. Microprobe Results

Run D_2-2 (85 wt-% W–15 wt-% Mo Contacting UC). Microprobe analyses were desirable for this diffusion run (1) to determine the composition of the extensive grain-boundary liquid phase developed in the uranium carbide; (2) to confirm that the liquid phase, which penetrated through the 85 wt-% W–15 wt-% Mo alloy grain boundaries was actually U-Mo; and (3) to confirm that the 85 wt-% W–15 wt-% Mo alloy contained regions of high molybdenum content because of some segregation phonomenon.

The CRT display of back-scattered electron intensity from the liquid phase regions (see Fig. 31 for the microstructures) in the 85 wt-% W–15 wt-% Mo alloy after interaction with uranium carbide is shown in Fig. 32a. This figure shows that the liquid phase has a higher average atomic number than the surrounding 85 wt-% W–15 wt-% Mo and is probably predominantly uranium. Figure 32b, a CRT display of the characteristic X-ray intensity, $U_{M\beta}$, supports this view. Figures 32c and 32d, which show the characteristic X-ray intensity, $W_{L\alpha}$ and $Mo_{L\alpha}$, respectively, from the same sample, indicate that the liquid phase is depleted in tungsten and contains an amount of molybdenum similar in quantity to that of the surrounding 85 wt-% W–15 wt-% Mo alloy.

The CRT display of back-scattered electron intensity of the liquid phase formed in the uranium carbide is shown in Fig. 33a. The liquid phase is of higher average atomic number than the surrounding uranium carbide grains and is probably uranium. The corresponding CRT display of $U_{M\beta}$ X-ray intensity (Fig. 33b) substantiates this. Figure 33c, a CRT display of $W_{L\alpha}$ characteristic X-ray intensity, reveals that the liquid contains a small percentage of tungsten and that the bright spot is high in tungsten, probably a result of tungsten-electrode erosion into the melt during carbide formation from the elements. The intensity of the $Mo_{L\alpha}$ characteristic X-ray (see Fig. 33d) is inconclusive as to the distribution of molybdenum.

Back-scattered electron intensity from a sample of 85 wt-% W–15 wt-% Mo (see Fig. 34) in the pretest condition shows a variation in composition.

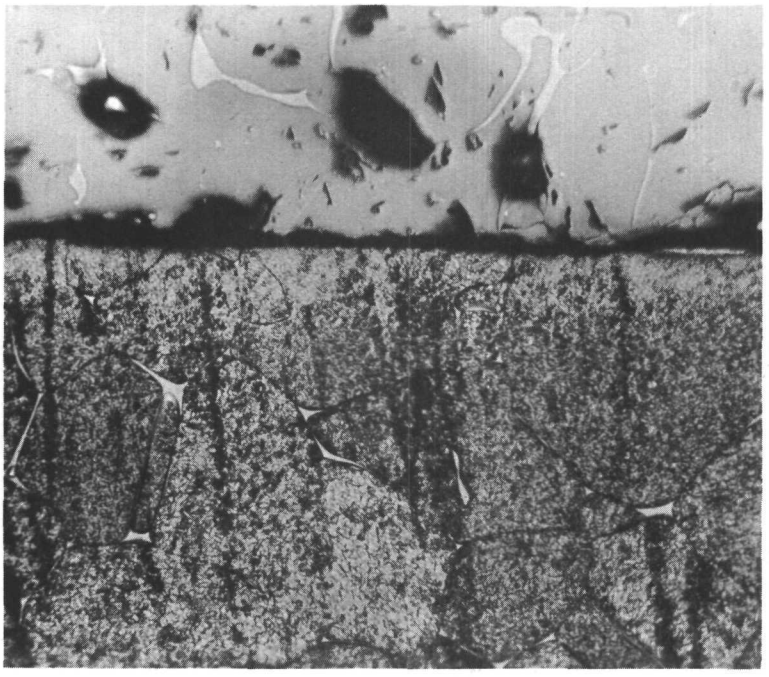

3055-1-2 ×200

Fig. 31--Liquid-phase formation in 85 wt-% W—15 wt-% Mo alloy and UC (Run D_2-2)

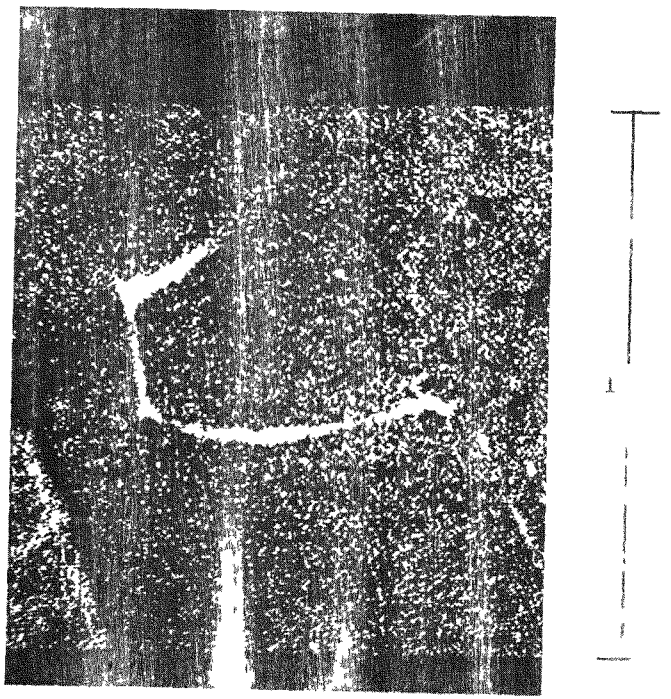

K-21462

(a) Back-scattered electrons

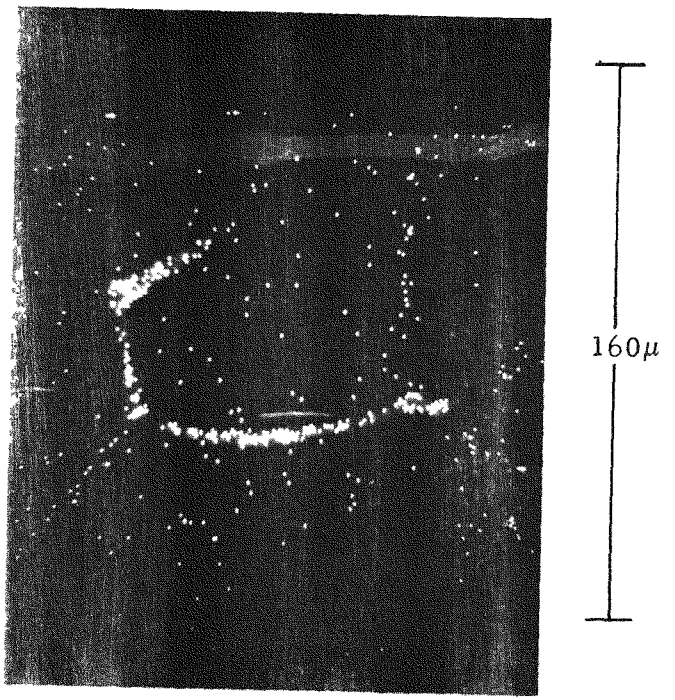

K-21456

(b) $U_{M\beta}$ characteristic X-ray intensity

Fig. 32--CRT displays showing liquid phase in 85 wt-% W–15 wt-% Mo in contact with uranium carbide at 1800°C for 24 hr (a, b, c, and d are from the same area)

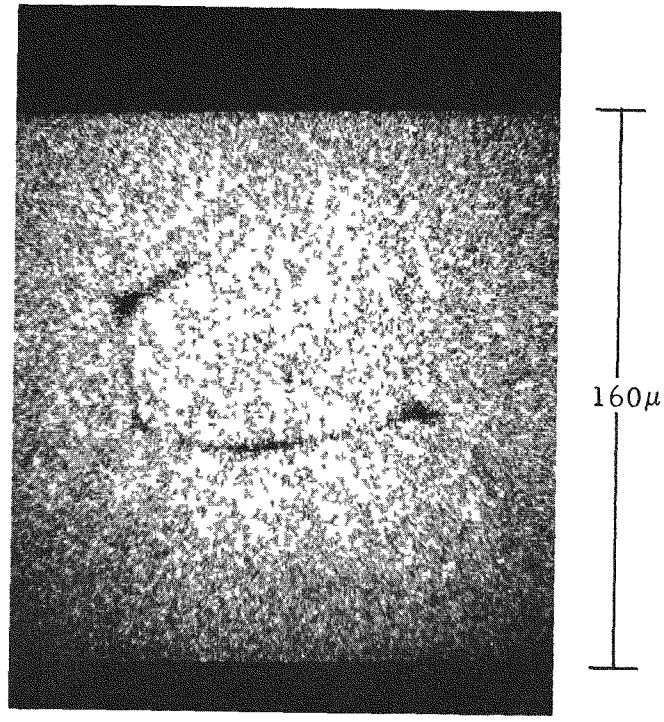

K-21469

(c) $W_{L\alpha}$ characteristic X-ray intensity

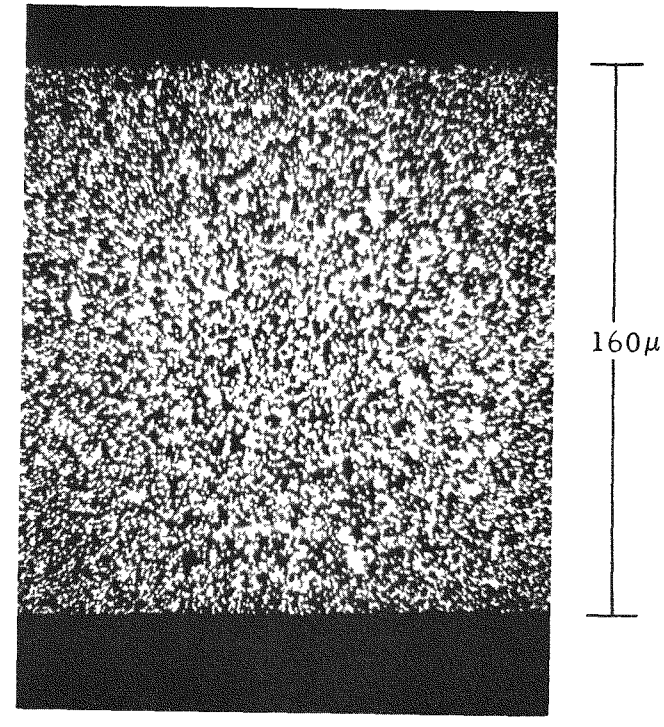

K-21465

(d) $Mo_{L\alpha}$ characteristic X-ray intensity

Fig. 32 (continued)

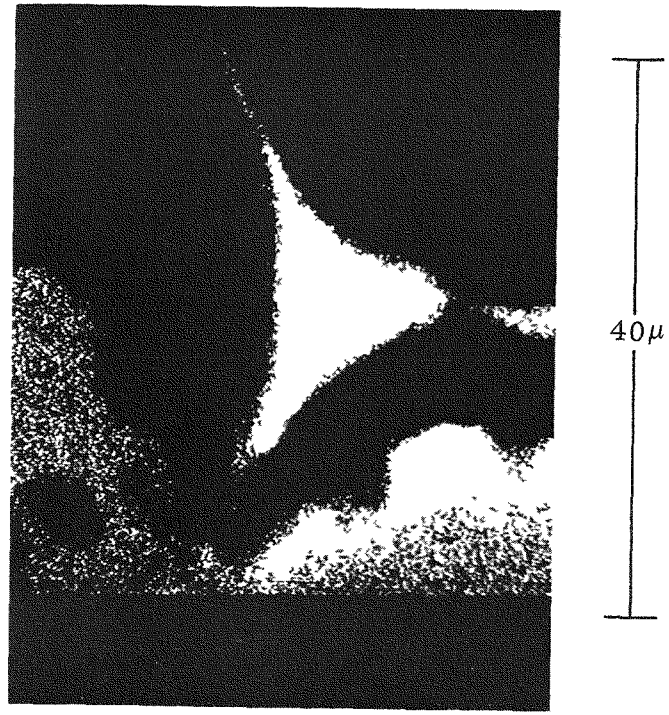

K-21460

(a) Back-scattered electrons

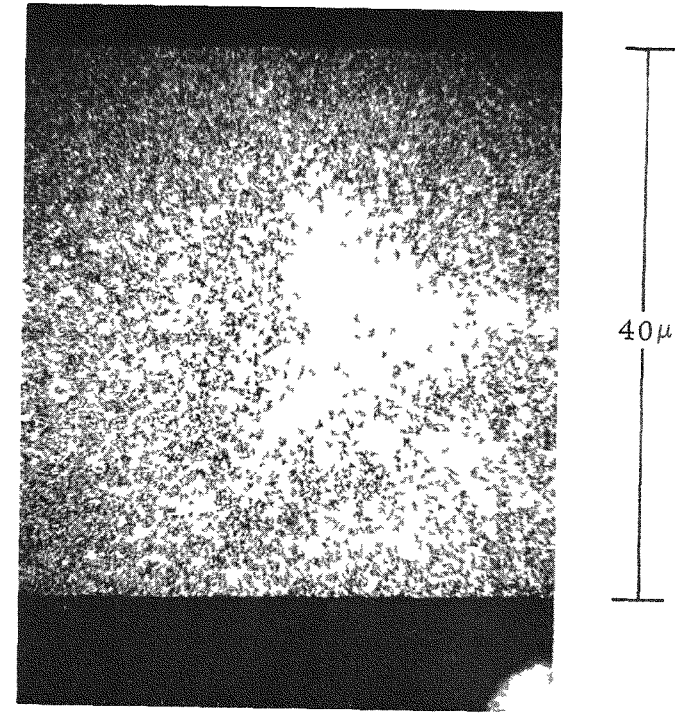

K-21466

(b) $U_{M\beta}$ characteristic X-ray intensity

Fig. 33--CRT displays showing liquid phase in uranium carbide in contact with 85 wt-% W–15 wt-% Mo at 1800°C for 24 hr (a, b, c, and d are from the same area)

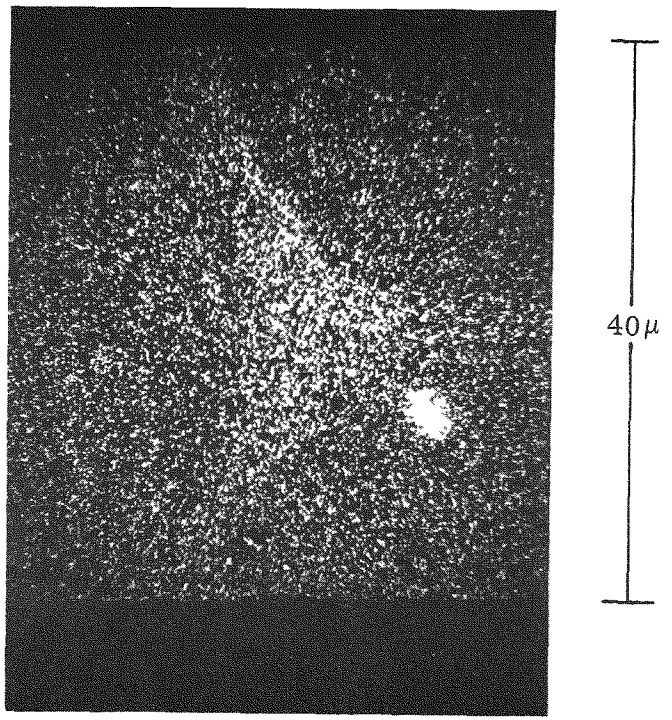

K-21459

(c) $W_{L\alpha}$ characteristic X-ray intensity

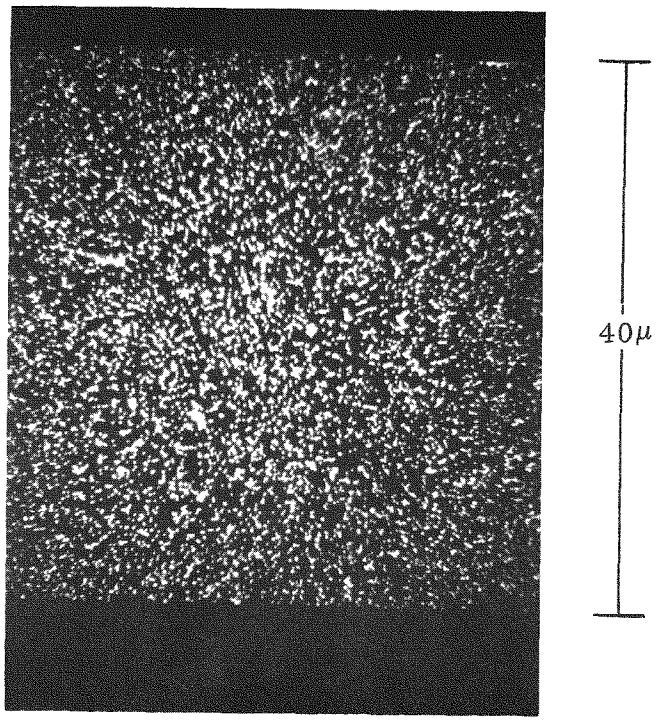

K-21461

(d) $Mo_{L\alpha}$ characteristic X-ray intensity

Fig. 33 (continued)

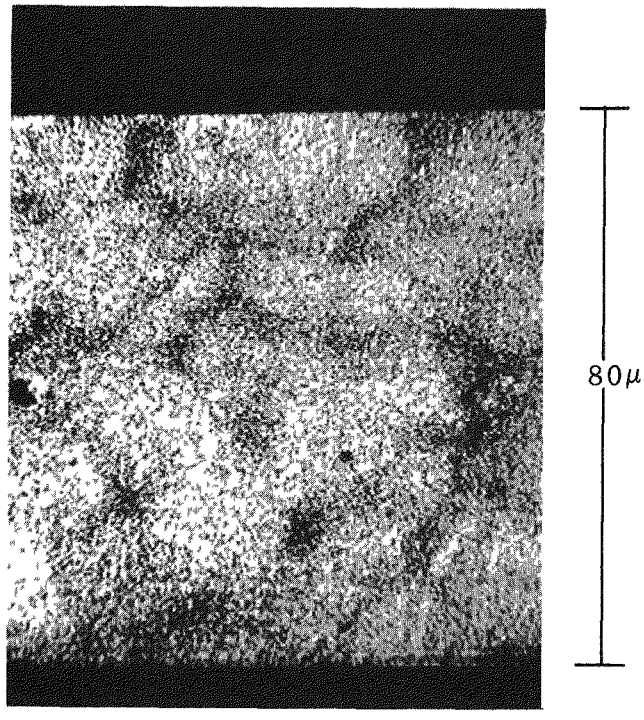

K-21458

Fig. 34--Back-scattered electron intensity by CRT display from a sample of 85 wt-% W–15 wt-% Mo in the pretest condition. Note evidence of segregation of alloy constituents; dark areas are molybdenum-rich regions

The dark areas are high in molybdenum and appear to be associated with the grain-boundary structure.

In conclusion, the following qualitative observations may be made:

1. The liquid phase formed in the 85 wt-% W—15 wt-% Mo is a U-Mo alloy which may contain a slight amount of tungsten.
2. The hypothesis that the 85 wt-% W—15 wt-% Mo alloy was susceptible to attack by the uranium-rich liquid phase formed in the uranium carbide, because of segregation effects, has been partially substantiated by the observation of concentration gradients in the pretest 85 wt-% W—15 wt-% Mo.

Results obtained on sample D_2-3 (98 wt-% W—2 wt-% Mo versus UC) are similar to those described above; the segregation of Mo in the alloy, however, is not as pronounced as in 85 wt-% W—15 wt-% Mo.

Run D_2-1, W—26Re Contacting UC. The angular precipitate particles observed near the W—26Re surface in contact with uranium carbide at 1800°C for 24 hr (see Fig. 35) are shown to have a low average atomic number by a CRT display of back-scattered electrons, Fig. 36a. The particles are thought to have a high carbon content and may be W_2C, the carbon being derived from the hyperstoichiometric uranium carbide used for the test. The CRT display of $W_{L\alpha}$ characteristic X-ray intensity, Fig. 36b, shows a decrease in tungsten concentration in the precipitate zone, as would be expected with W_2C precipitation. $Re_{L\alpha}$ characteristic X-ray intensity, Fig. 36c, shows an increase in the same area and the $U_{M\beta}$ characteristic X-ray intensity, Fig. 36d, shows a background count (step-scanning data show a uranium penetration of ~3 μ at a level of only a few hundreds of parts per million). If the precipitate is tungsten carbide, then it can be assumed that W—26Re may be suitable for use as cladding for stoichiometric or slightly hypostoichiometric UC or UZrC where carbon is not available for reaction with the alloy, since the small amount of precipitate formed might be harmful to the structural capabilities of the cladding. A diffusion run is planned using W—26Re in contact with hypostoichiometric 30 UC—70 ZrC at 1800°C for 24 hr.

Rhenium Contacting Uranium Carbide. CRT displays of the characteristic X-ray and back-scattered electron intensities are not available at present to illustrate the composition of the reaction layers shown in Fig. 37. Step-scanning data show that the reaction layers of Fig. 37 extend approximately 6 to 10 μ into the pure rhenium. The thicker reaction layer contains uranium, carbon, and rhenium at constant composition and appears to be a homogeneous phase. The uranium level is shown, by uncorrected step-scanning data, to be roughly equimolar with rhenium.

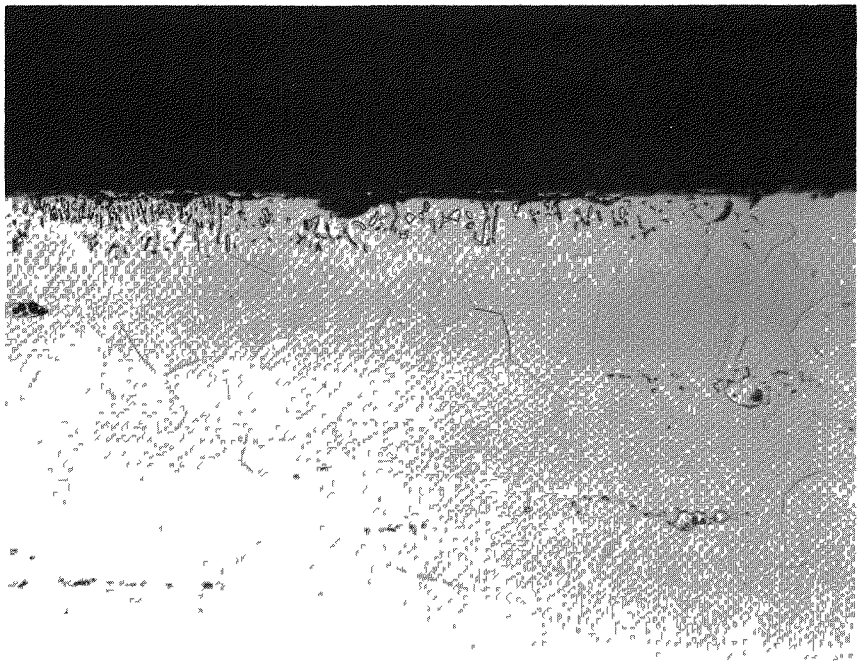

2521-2-1 ×250

Fig. 35--Specimen of W–26 wt-% Re in contact with uranium carbide at 1800° ±20°C for 24 hr. Note small precipitate particles near specimen surface; also that the matrix surrounding these particles is a different phase (lighter in appearance) from the W–26 wt-% Re in the center of the specimen

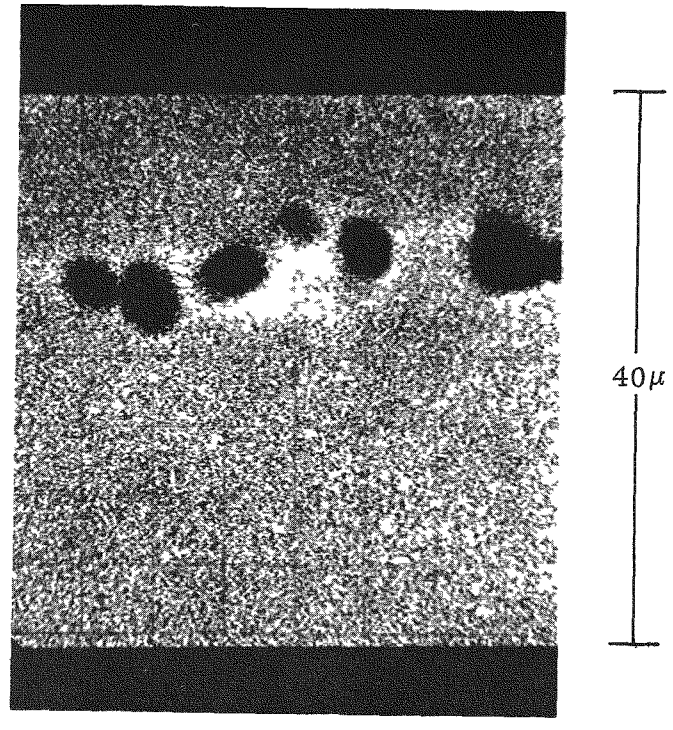

K-21464

(a) Back-scattered electron intensity

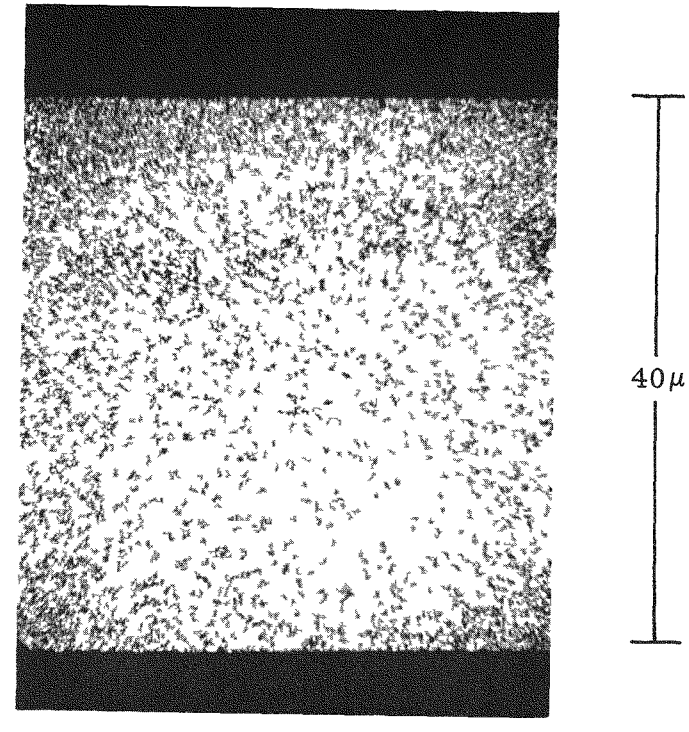

K-21468

(b) $W_{L\alpha}$ characteristic X-ray intensity

Fig. 36--CRT displays of W–26Re held in contact with hyperstoichiometric uranium carbide for 24 hr at 1800°C (a, b, c, and d are from the same area)

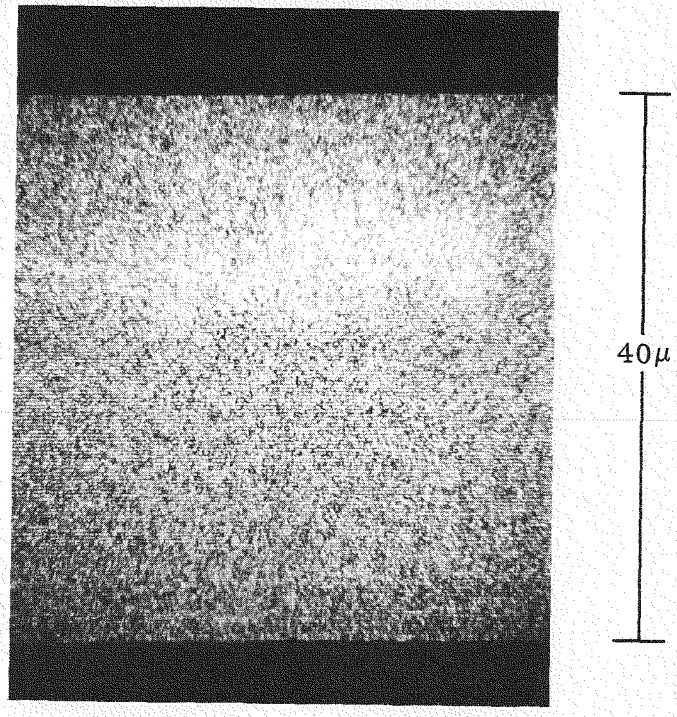

K-21467

(c) $Re_{L\alpha}$ characteristic X-ray intensity

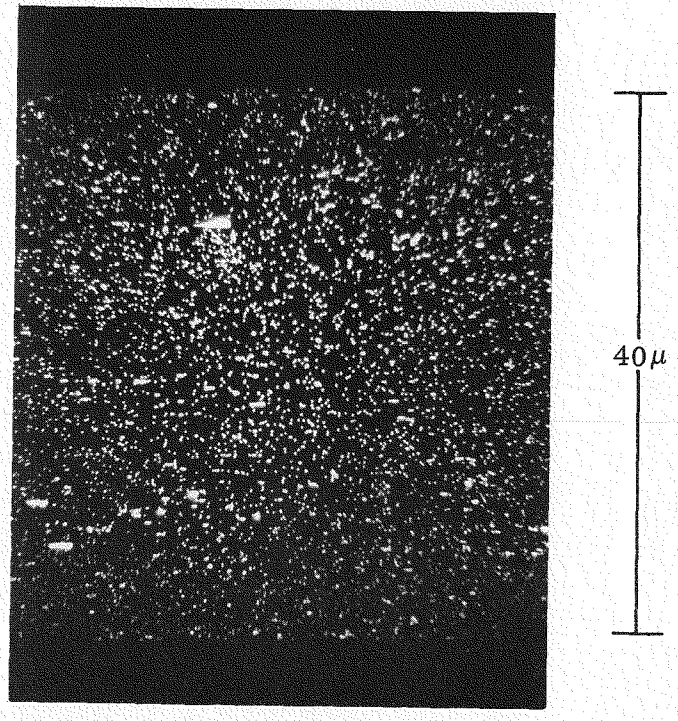

K-21457

(d) $U_{M\beta}$ characteristic X-ray intensity

Fig. 36 (continued)

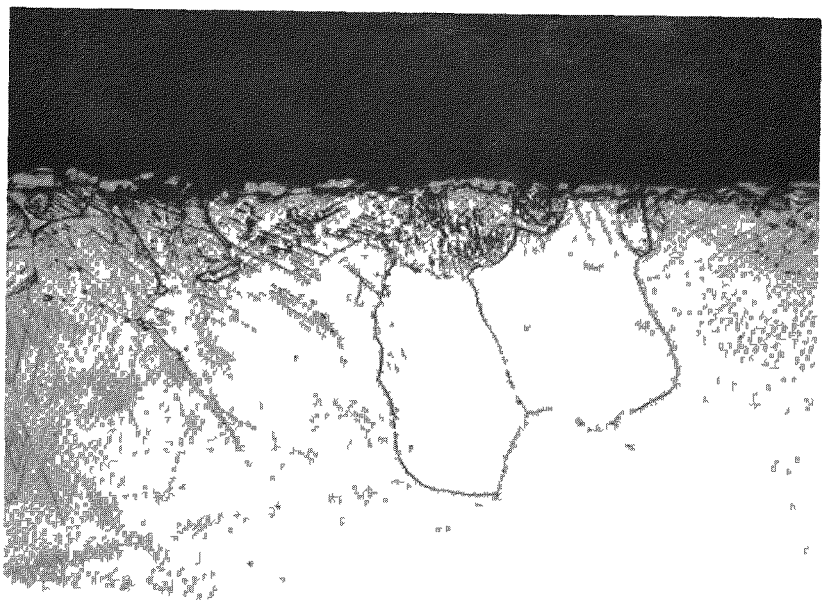

2521-1-3 (a) ×500

(a) Surface reaction layers. Note a reaction layer on the surface and a more extensive reaction layer beneath it; also note some evidence of grain-boundary attack

2521-1-4 (b) ×500

(b) Definition of surface reaction layers. Use of polarized light makes reaction layers more easily discernible. Note that this is not the same area of specimen as illustrated in (a)

Fig. 37--Rhenium in contact with uranium carbide at 1800° ±20°C for 24 hr

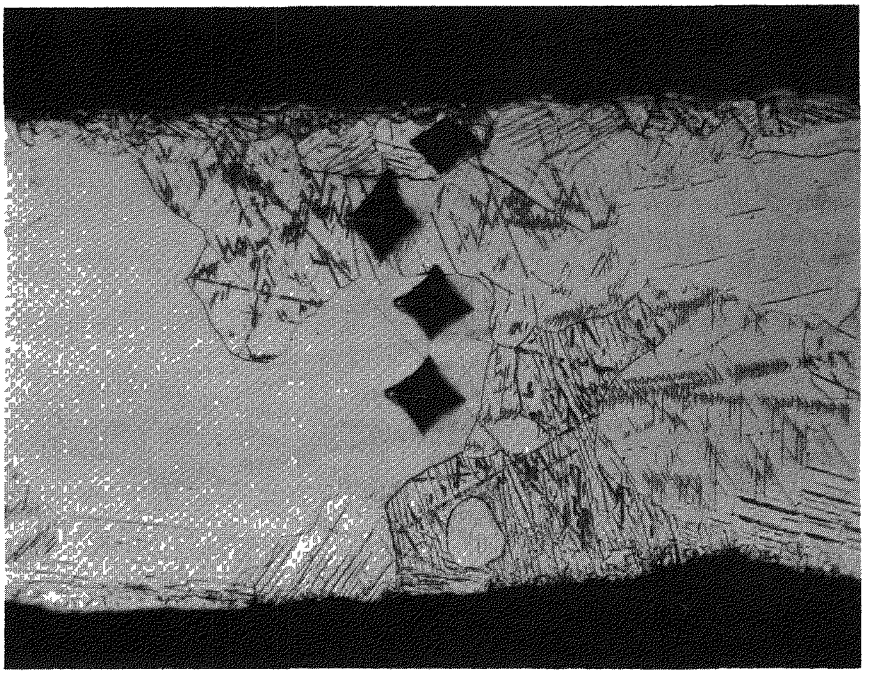

2521-1-1 ×250

(c) Hardness increase near specimen surface. Note smaller size of hardness indentation (diamond shapes) near the surface of the specimen in contact with uranium carbide

Fig. 37 (continued)

Since rhenium is susceptible to penetration by uranium when held for a short time (24 hr) at 1800°C in contact with hyperstoichiometric uranium carbide, it might be classified as an unsuitable cladding material for such a fuel. The criteria for such a classification are summarized as follows:

1. Even without considering fissioning, the mechanical properties of a cladding could be seriously impaired or at least placed in doubt by the presence of a phase containing rhenium, uranium, and carbon, since metallographic examination showed the phase to have higher hardness than the base material.
2. Fissioning of the diffusing uranium atoms, if it resulted in swelling of the diffusion zone, could cause serious deterioration of mechanical properties.
3. Development of a porous layer in the cladding by fission-product generation and concomitant swelling would impair fuel-to-cladding heat-transfer rates.
4. Thermal-spike formation, during fissioning, in the cladding and fuel might accelerate diffusion of uranium atoms in the cladding, making it less stable than observed without irradiation phenomena.

4.2.3. Thermal Treatment of Uranium Carbide

The hypothesis that the single-phase structure of the metal-rich uranium carbide (used for the compatibility determinations of UC versus 98 wt-% W–2 wt-% Mo and UC versus 85 wt-% W–15 wt-% Mo) was due to a quenched-in high-temperature solubility for uranium metal was checked by thermal treatment of the carbide.

A sample of the metal-rich uranium carbide (4.76% to 4.80% C), used for the compatibility runs referred to above, was supported on ZrC and heated to 1800°C for 2 hr, slowly cooled to 1100°C over a period of 2 hr, and then furnace-cooled to room temperature. The treatment was designed to remove a quenched-in structure and allow uranium to precipitate.

Metallographic examination of the heat-treated specimen revealed that a liquid phase was present at the edges of the specimen. Little grain growth was observed--Fig. 38 shows this structure. A. Accary[8] has referenced work by Magnier which shows the extent of uranium solubility in uranium carbide between 500° and 2300°C (see Fig. 39). Chemical analysis of arc-cast uranium carbide fuel slugs, prepared in large quantities for central power station use, [9] have shown consistantly that single-phase material may be slightly hypostoichiometric in carbon.

These results substantiate the hypothesis of a solubility of uranium in single-phase uranium carbide. Although the available metal-rich

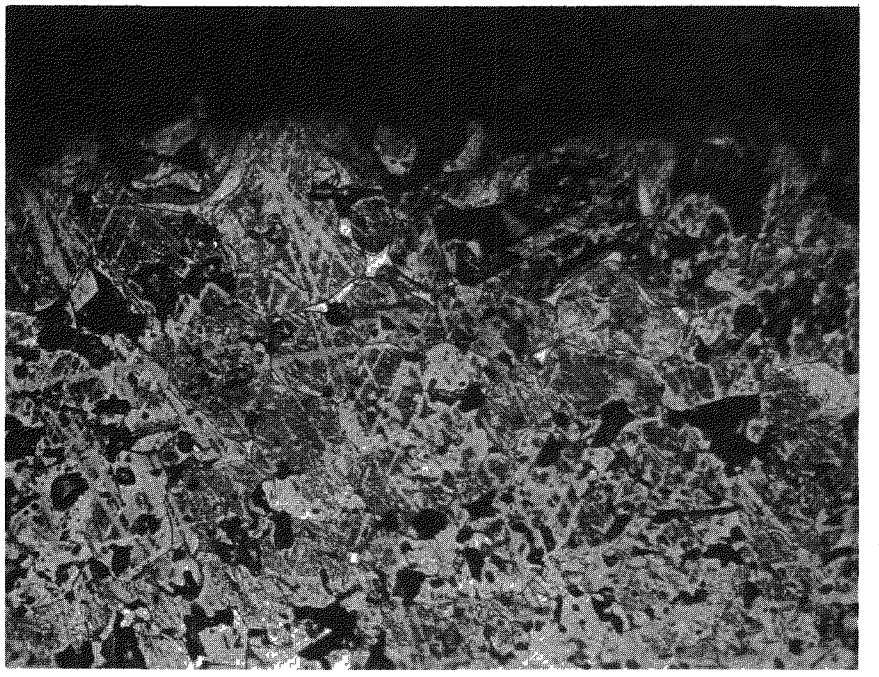

3188-1-2 ×250

Fig. 38--Metal-rich uranium carbide (4.76% to 4.80% C) supported on ZrC and heated to 1800°C for 2 hr, controlled cooled to 1100°C over a 2 hr period, then furnace cooled

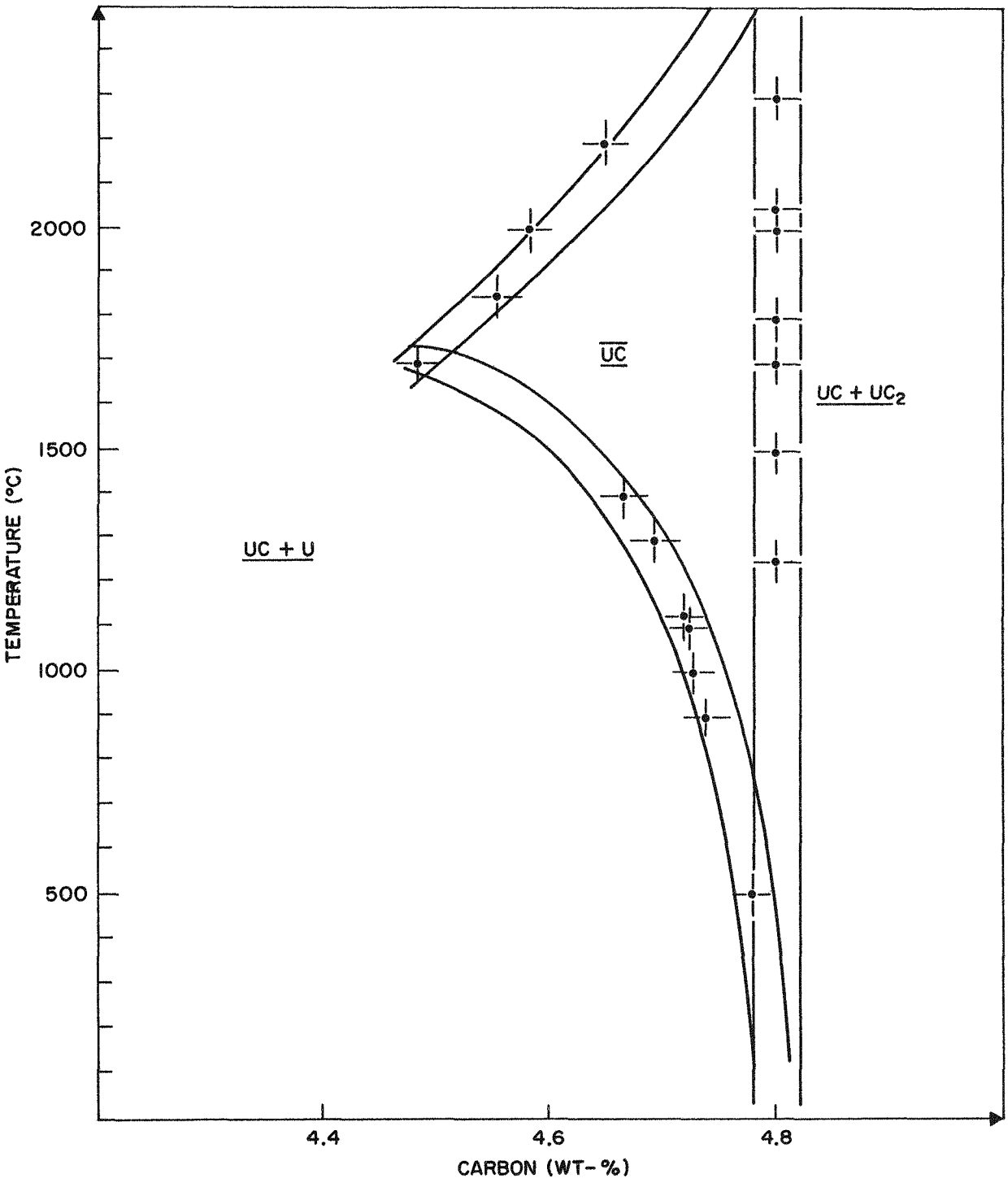

Fig. 39--Portion of UC binary system showing area of stability of single-phase hypostoichiometric uranium carbide (from Ref. 8)

carbide samples could be brought closer to stoichiometry by thermal treatment, Fig. 39 indicates difficulty in raising the uranium carbide carbon content higher than 4.75% to 4.76% by vaporization of uranium, unless one goes to temperatures where vaporization is too slow to be useful for this process (900° to 1100°C) or where de-densification effects might be harmful (>2100°C).

4.2.4. Thermal Treatment of 90 UC–10 ZrC

Several samples of 90 UC–10 ZrC were obtained to evaluate the compatibility of this fuel material with 98 wt-% W–2 wt-% Mo. The material was free from uranium inclusions and was metal-rich. It contained 4.79 to 4.80 wt-% C, whereas a stoichometric sample of this composition should contain 5.01 wt-% C.

In order to fully characterize the material prior to the compatibility run, the following tests were performed:

1. A sample with the above chemical composition, supported on clean ZrC, was heated to 1500°C for 1/2 hr, then cooled to 1270°C and held for 8 hr between 1270° and 1290°C to precipitate any quenched-in metal. Metallographic examination showed only trace amounts of precipitated metal at a few grain boundaries. Chemical analysis showed that the heat-treated material had essentially the same carbon content (4.72 to 4.76 wt-% C) as before the heat treatment. This lack of change in the carbon content indicates that the material was not affected by the evaporation of uranium from the sample during this treatment.
2. The 90 UC–10 ZrC used for the compatibility test with 98 wt-% W–2 wt-% Mo was subjected to a heat treatment designed to remove any free uranium from the structure by evaporation. The material was heated to 1800°C in a cold-wall vacuum chamber for 1 hr and then cooled for 1 hr at each of the following temperatures: 1700°, 1470°, 1370°, and 1270°C. Analyses for carbon, nitrogen, and oxygen will be obtained for this material.

4.2.5. New Compatibility Tests at 1800°C (Run D_2-4)

Another series of specimens was used to determine whether the incompatibility of 98 wt-% W–2 wt-% Mo alloy with uranium carbide would extend to uranium carbide fuel materials stabilized with ZrC. To accomplish this evaluation, 90 UC–10 ZrC and 30 UC–70 ZrC were placed in contact with 98 wt-% W–2 wt-% Mo alloy at 1800° ±20°C for 24 hr in the following array:

W	W	30 UC– 70 ZrC	W	W– 2 Mo	30 UC– 70 ZrC	W– 2 Mo	90 UC– 10 ZrC	W– 2 Mo	W

The diffusion furnace and sample holders have been described in Ref. 1.

A 30 UC–70 ZrC with tungsten sample was included as a comparison standard; this combination is considered to be compatible for the test conditions. Figure 40 shows the microstructure of the pretest 30 UC–70 ZrC with a carbon content of 7.63% to 7.72% C (stoichiometric carbon content = 8.17%). The test results are described below.

90 UC–10 ZrC with 98 wt-% W–2 wt-% Mo. The microstructure of 90 UC–10 ZrC in contact with 98 wt-% W–2 wt-% Mo showing one edge of the tungsten alloy is shown in Fig. 41. It is apparent that an extensive liquid phase was formed which surrounded the 90 UC–10 ZrC grains in amounts much greater than could be generated by precipitation heat treatment of the 90 UC–10 ZrC not in contact with the alloy. Radical grain growth occurred in the 90 UC–10 ZrC. Visual estimates of the amount of liquid phase present showed less than the amount present with pure uranium carbide in contact with 98 wt-% W–2 wt-% Mo under the same test conditions.

A liquid phase, determined by electron-microprobe analysis to be a U-Mo alloy, was found throughout the 98 wt-% W–2 wt-% Mo alloy at triple and quadruple grain-boundary intersections; Fig. 42 shows an example of this phase. This liquid phase extended through the 1/8-in.-thick alloy and completely filled the interface between the tungsten and the 98 wt-% W–2 wt-% Mo, as shown in Fig. 43. In addition, the interface was obscured by grain growth.

30 UC–70 ZrC with 98 wt-% W–2 wt-% Mo. The 30 UC–70 ZrC showed essentially a single-phase structure. No large amounts of liquid phase were observed (see Fig. 44).

The 98 wt-% W–2 wt-% Mo revealed very small amounts of a liquid phase at triple grain-boundary intersections throughout its volume (see Fig. 45). Some liquid was seen at the 98 wt-% W–2 wt-% Mo to tungsten interface, as shown in Fig. 46.

30 UC–70 ZrC with Tungsten. No liquid-phase formation was observed either in the carbide or in the tungsten (see Fig. 47).

Conclusions. As a cladding material, 98 wt-% W–2 wt-% Mo alloy does not appear to be as attractive as pure tungsten for uranium carbide fuels, even when diluted with as much as 70 ZrC, because of a probable degradation of the alloy strength due to the presence of a grain-boundary liquid phase and because fissioning would occur in this liquid phase; as electron-beam microprobe analysis indicates, it does contain uranium.

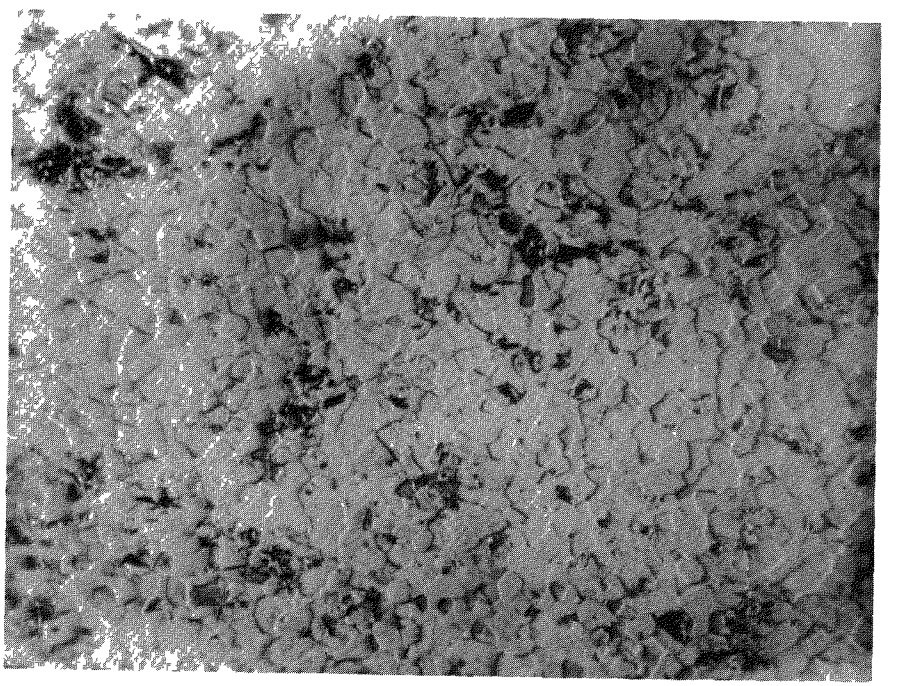

3390-1-1 ×500

Fig. 40--Pretest 30 UC–70 ZrC (hot-pressed), dark areas are etchant stain (oblique light)

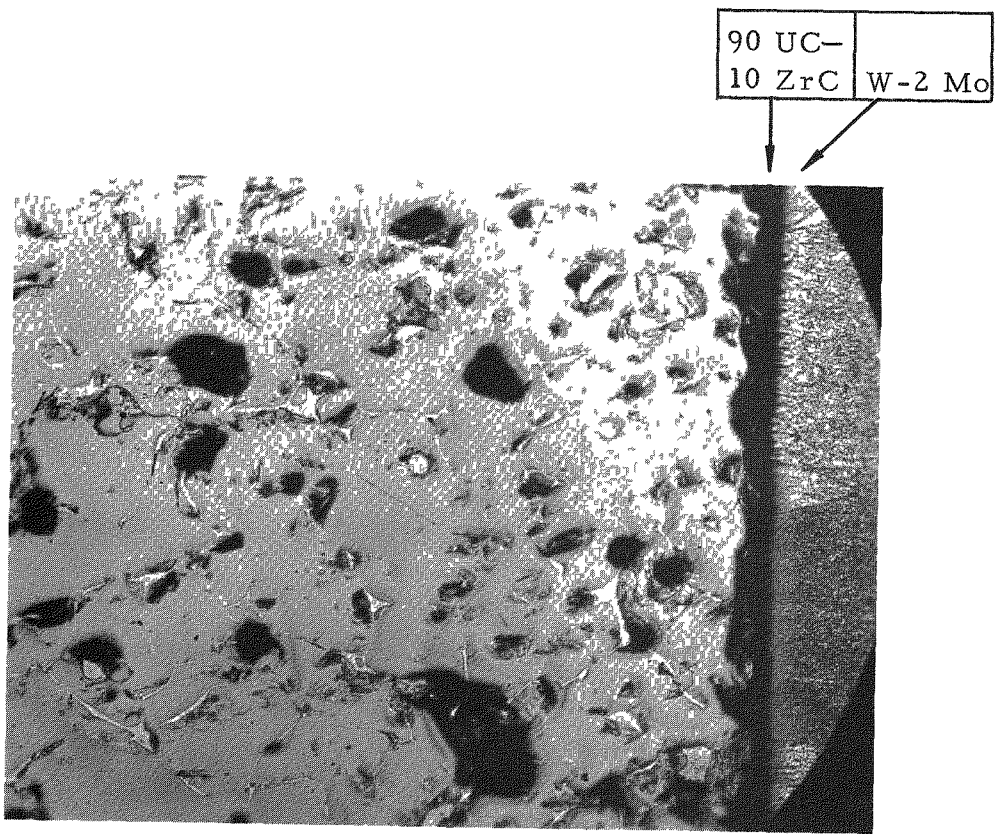

Fig. 41--Microstructure of 90 UC–10 ZrC in contact with 98 wt-% W–2 wt-% Mo at 1800°C for 24 hr, showing 98 wt-% W–2 wt-% Mo edge

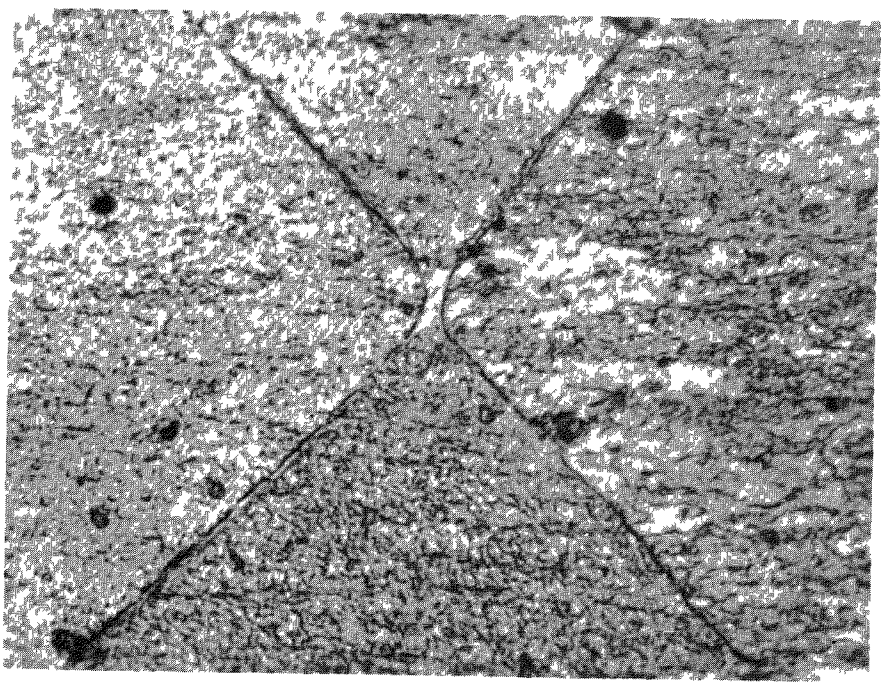

3496-2-1 ×500

Fig. 42--98 wt-% W–2 wt-% Mo in contact with 90 UC–10 ZrC for 24 hr at 1800°C; note liquid phase at quadruple grain-boundary intersections

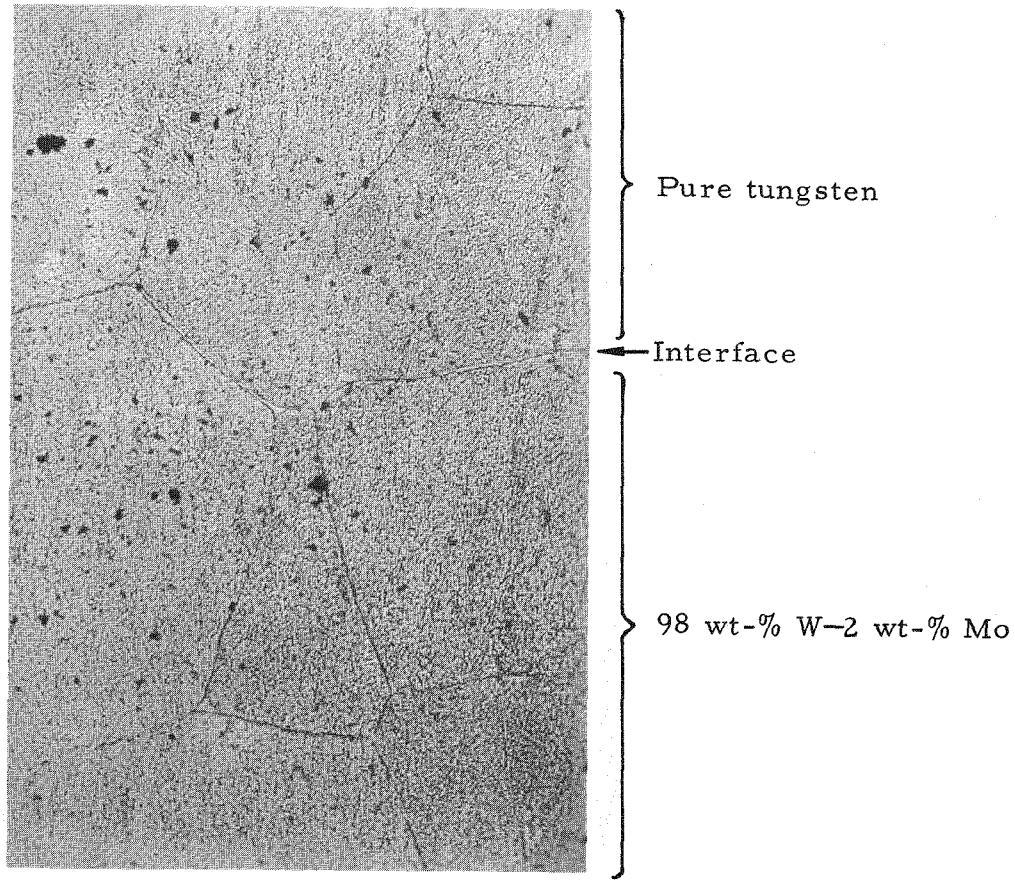

Fig. 43--Interface of pure arc-cast tungsten versus 98 wt-% W–2 wt-% Mo in contact with 90 UC–10 ZrC for 24 hr at 1800°C; note liquid phase at interface and at 98 wt-% W–2 wt-% Mo grain-boundary intersections

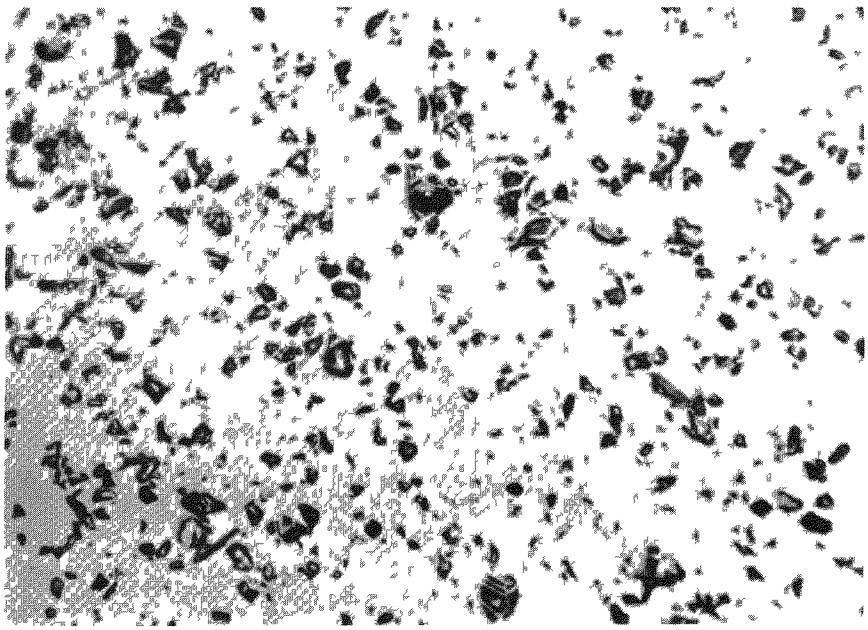

3496-5-1 ×500

Fig. 44--Microstructure of 30 UC–70 ZrC in contact with 98 wt-% W–2 wt-% Mo for 24 hr at 1800°C

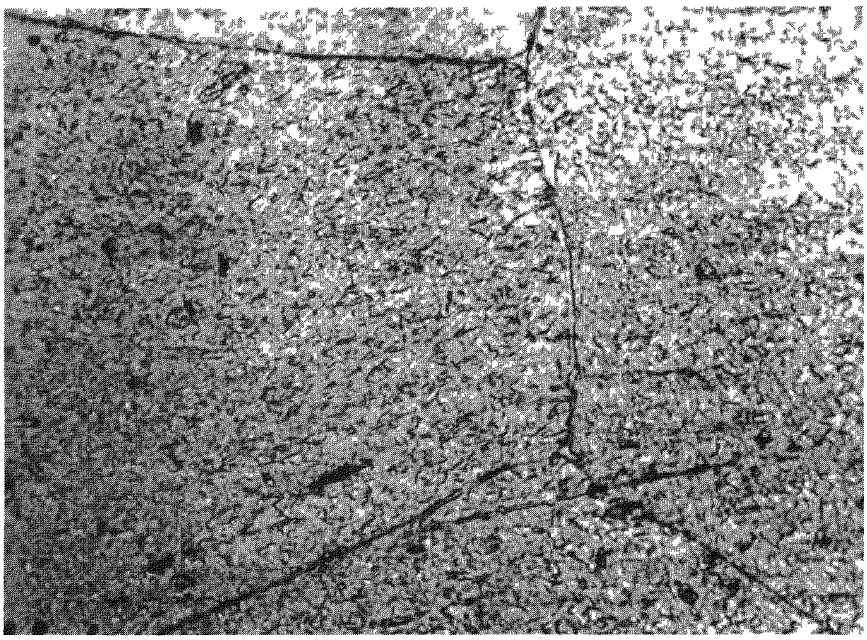

3496-1-1 ×500

Fig. 45--98 wt-% W–2 wt-% Mo in contact with 30 UC–70 ZrC for 24 hr at 1800°C; note liquid at multiple grain-boundary intersections

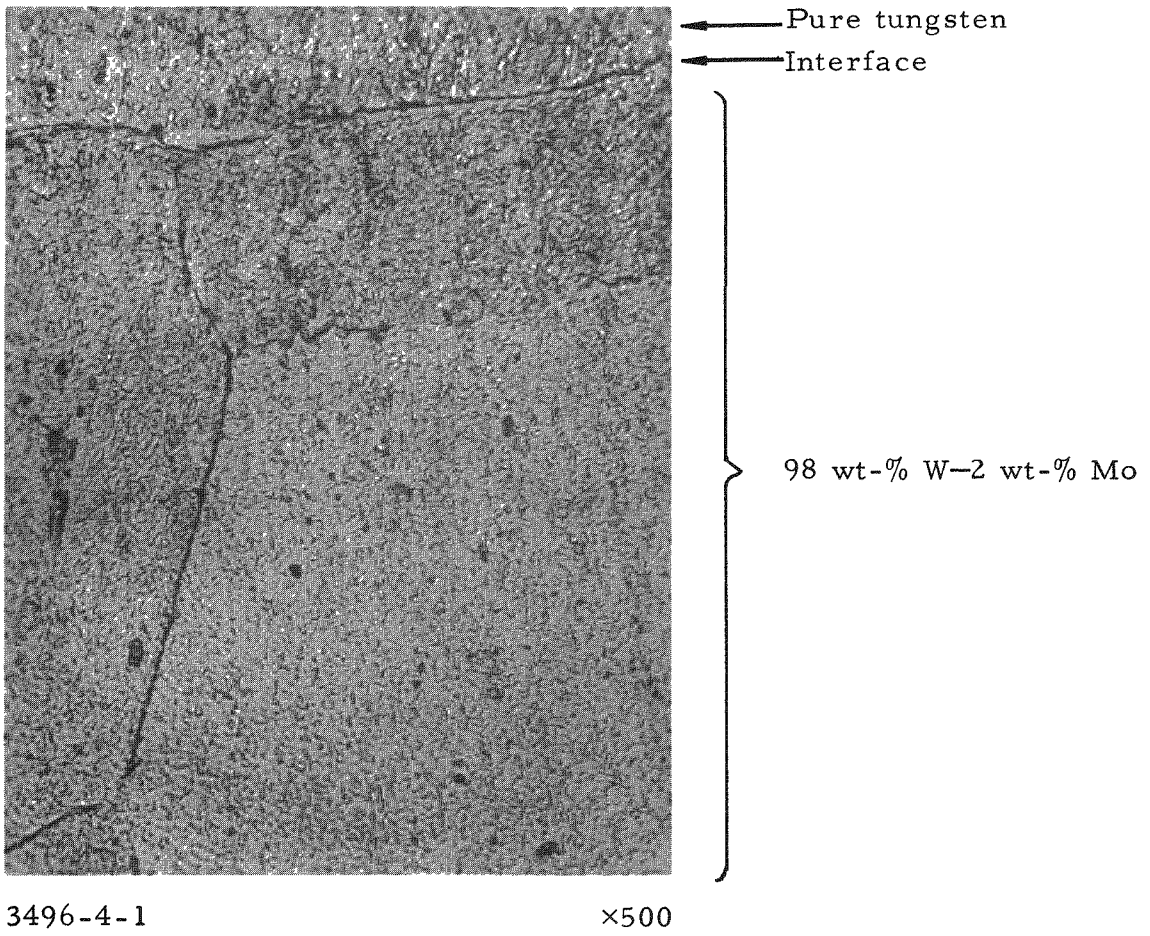

Fig. 46--Interface of arc-cast tungsten versus 98 wt-% W—2 wt-% Mo in contact with 30 UC—70 ZrC for 24 hr at 1800°C; note interfacial liquid phase

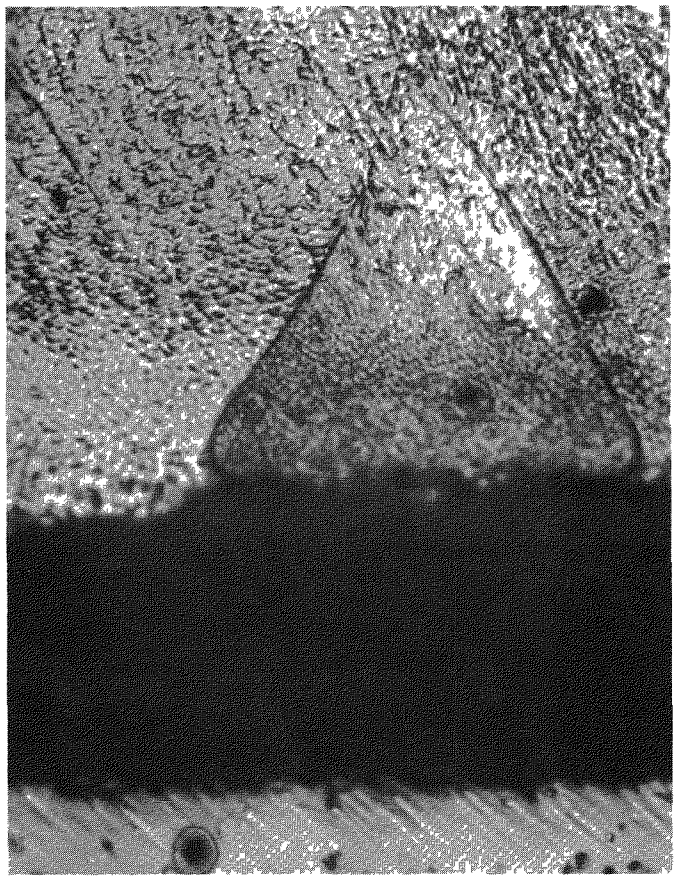

Fig. 47--30 UC–70 ZrC versus tungsten at 1800°C, showing no liquid at the tungsten boundaries

In addition, several truisms can be stated about the compatibility of these W-Mo alloys with UC and with the UZrC compositions studied:

1. The incompatibility of W-Mo alloys with UC and UZrC increases with the excess metal content and the U/Zr ratio of the carbide because liquid uranium is more easily formed by gettering of carbon by the alloys.
2. Increased amounts of Mo in the W-Mo-alloy system create larger quantities of liquid phase in the alloy, indicating a greater susceptibility to attack by liquid uranium.
3. Pure tungsten was not attacked by liquid uranium but shows grain-growth inhibition in contact with uranium carbide. The inhibition of grain growth is most probably a result of grain-boundary pinning by impurities introduced from uranium carbide.

4.3. Diffusion-Emission

In diffusion-emission studies, the vacuum emission from the surface of the metal emitter cladding around a uranium-containing fuel is monitored as a function of time at the operating temperature of the emitter. Since the vacuum emission is sensitive to the presence of small amounts of impurities, emission monitoring is a sensitive method for detecting trace diffusion of fuel ingredients through the cladding to the emitter surface. Any emitter-fuel combination, qualified in gross diffusion studies, should be subjected to further trace diffusion studies for two reasons: First, any small amount of impurity, if accumulated on the emitter surface, changes its work function and therefore the cesium adsorption property; second, the presence of uranium, even in trace amounts in the emitter (especially along the grain boundaries), leads to fissioning and fission-product accumulation in the emitter and a reduction in its mechanical integrity.

Gross diffusion studies carried out previously[1] showed that tungsten was compatible with UC (5.02 wt-% C) and 90 UC–10 ZrC at 1800°C. During the first quarter of this contract, it was shown that tungsten deposition by the thermochemical reaction between WF_6 and H_2 represented one of the most convenient methods for cladding the fuel. Diffusion-emission studies were therefore carried out during the second quarter on a vapor-deposited tungsten-clad hyperstoichiometric uranium carbide (5.02 wt-% C) sample (D_3-1) at 1800°C. The results indicated that the vacuum emission of the tungsten surface decreased gradually during the first 700 hr at 1800°C. Examination of a section of the sample after 838 hr at 1800°C showed that the diffusion of carbon from the hyper-stoichiometric uranium carbide through the tungsten cladding to its surface was probably the reason for the change of the emission characteristics.

During this quarter, sample D_3-1 was examined by the electron-microprobe technique to detect if there was any uranium diffusion into the tungsten cladding. The results indicated that within the limit of the sensitivity of the instrument used (a few hundred ppm) no uranium penetration into the tungsten cladding was detected. Samples similar to D_3-1 (vapor-deposited tungsten-clad hyperstoichiometric uranium carbide) are being prepared to study its performance in cesium vapor as outlined in Section 1.2.

To cover a wider range of uranium carbide stoichiometry and to study the effect of the addition of ZrC to UC, two more samples have been prepared for diffusion-emission studies. One is a vapor-deposited tungsten-clad hypostoichiometric uranium carbide (4.70 wt-% C) sample (D_3-2), and the other is a vapor-deposited tungsten-clad 30 UC–70 ZrC sample (D_3-3). The carbide samples were first coated with a thin layer (~0.002 in.) of tungsten under conditions such that the attack on the carbide by the ambient gas mixture was minimized. The coated carbide samples were laid on cast tungsten bases (Fig. 27, Ref. 3) and the cladding thickness was built up to about 50 mils. The coating process was interrupted a few times during the deposition in order to break down the columnar grain structures of the deposit. The clad samples are being machined by the electrical-discharge machine to the dimensions required. They will be installed in the emission-diffusion cells early in June for 1000-hr tests.

5. FABRICATION DEVELOPMENT

The fabrication effort during this quarter has been devoted to the preparation of samples of the clad capsule.

FUTURE PLANS

1. LONG-TERM TESTS ON THE VAPORIZATION AND EMISSION OF UC-ZrC AND W-CLAD UC AND UC-ZrC IN Cs VAPOR

The 1000-hr vaporization runs of 90 UC–10ZrC and 30 UC–70 ZrC samples in cesium vapor will be initiated.

The operating conditions of the emission life-test control cell containing a solid tungsten emitter will be optimized in order to establish the conditions for achieving an output of 5 w/cm^2. The assembling of the four emission life-test cells will be pursued. The emitters for these cells are tungsten-clad hyperstoichiometric UC, tungsten-clad 30 UC–70 ZrC, unclad 90 UC–10 ZrC, and unclad 30 UC–70 ZrC.

2. STUDIES OF HIGH–TEMPERATURE PROPERTIES OF UC-ZrC

Studies will be continued on the effect of porosity on the rate of vaporization and electron emission of UC-ZrC in vacuum, using the following samples: (1) 30 UC–70 ZrC, density ~95%; (2) 30 UC–70 ZrC, density 85% to 90%; (3) 90 UC–10 ZrC. density 85% to 90%.

Anode condensate from the previous physical redeposition runs will be analyzed. Physical redeposition studies of uranium carbide will be extended to an anode temperature higher than 983 ^{o}K prior to the introduction of cesium and Cs + CsF into the test cell.

Correlation between the emission pattern and the microstructures of uranium carbide will be pursued. Activation, poisoning, and regeneration of emission from 30 UC–70 ZrC and 90 UC–10 ZrC will be studied.

The modified bearing arrangement for the loading rod of the high-temperature mechanical property furnace will be tested and measurements will be initiated on 10 UC–90 ZrC.

3. IRRADIATION STUDIES

Hot-cell examinations of the contents of the unclad-carbide capsule will be carried out.

Irradiation of the clad capsule in the GETR will be initiated and the behavior of the capsule followed.

4. STUDIES OF NEW CATHODE MATERIALS

The vacuum emission of sample D_1-3 (cold-pressed and sintered, 30 UC–70 NbC, density 74.5%) will be measured. The vacuum vaporization rates of 30 UC–70 NbC of higher densities and 30 UC–70 TaC will be studied.

Diffusion between 30 UC–70 ZrC and Ir, Re, and W–26Re will be studied. The use of ZrC as a diffusion barrier between tungsten and uranium carbide at 2000°C and between tantalum and uranium carbide at 1800°C will be tested.

Diffusion-emission studies of sample D_3-2 (vapor-deposited tungsten-clad hypostoichiometric UC, 4.70 wt-% C) and D_3-3 (vapor-deposited tungsten-clad 30 UC–70 ZrC) at 1800°C will be initiated and continued for 1000 hr.

5. FABRICATION DEVELOPMENT

Studies on the preparation of submicron UC-ZrC powder will be resumed.

REFERENCES

1. Weinberg, A. F., et al., "Investigations of Carbides as Cathodes for Thermionic Space Reactors," General Atomic Report GA-3523 (Final Report on Contract NAS 5-1253).

2. Yang, L., et al., "Carbide Cathode Studies. Physical and Chemical Redeposition," General Atomic Report GA-3642 (Final Report on Contract NAS 3-2301), January 30, 1963.

3. Yang, L., et al., "Investigations of Carbides as Cathodes for Thermionic Space Reactors, Quarterly Progress Report for the Period Ending November 30, 1962," General Atomic Report GA-3866.

4. Yang, L., et al., "Investigations of Carbides as Cathodes for Thermionic Space Reactors, Quarterly Progress Report for the Period Ending February 28, 1963," General Atomic Report GA-4173, May 15, 1963.

5. Haas, G. A., "Thermionic Electron Sources," U. S. Naval Research Laboratory Report NRL-5657, October, 1961.

6. Vozzella, P. A., A. D. Miller, and M. A. De Crescente, "The Thermal Decomposition of Uranium Monocarbide," United Aircraft Corporation Report PWAC-378, January 15, 1962.

7. Brownlee, L. D., "The Pseudo-binary Systems of Uranium Carbide with Zirconium Carbide, Tantalum, and Niobium Carbide," J. Inst. Metals, 87, 58 (1958-59).

8. Accary, A., "Uranium-Carbon Alloys--Some Recent Research and Development Studies at the Commisoriat a L'Energie Atomique," presented at the Fourth Uranium Carbide Meeting, United Aircraft Research Laboratory, East Hartford, Connecticut, May 20-21, 1963.

9. Walter Hayes, Atomics International, Canoga Park, California, private communication.

DISTRIBUTION LIST

	No. Copies
National Aeronautics and Space Administration Lewis Research Center 21000 Brookpark Road Cleveland 35, Ohio Attention: J. W. R. Creagh	3
National Aeronautics and Space Administration Western Operations Office 150 Pico Boulevard Santa Monica, California Attention: Donald Keaveney, Patent Counsel	1
National Aeronautics and Space Administration Lewis Research Center 21000 Brookpark Road Cleveland 35, Ohio Attention: John J. Fackler, Contracting Officer Space Electric Power Procurement Office	1
National Aeronautics and Space Administration Lewis Research Center 21000 Brookpark Road Cleveland 35, Ohio Attention: Office of Reliability and Quality Assurance	1
National Aeronautics and Space Administration Western Operations Office 150 Pico Boulevard Santa Monica, California Attention: John Keeler	1
National Aeronautics and Space Administration 801 Nineteenth Street, N. W. Washington 25, D. C. Attention: Fred Schulman	2
National Aeronautics and Space Administration 1512 H Street, N. W. Washington 25, D. C. Attention: George Deutsch	1

National Aeronautics and Space Administration — 2
Lewis Research Center
21000 Brookpark Road
Cleveland 35, Ohio
Attention: Daniel Bernatowicz

National Aeronautics and Space Administration — 1
Lewis Research Center
21000 Brookpark Road
Cleveland 35, Ohio
Attention: Bernard Lubarsky

National Aeronautics and Space Administration — 2
Lewis Research Center
21000 Brookpark Road
Cleveland 35, Ohio
Attention: Library

National Aeronautics and Space Administration — 2
Lewis Research Center
21000 Brookpark Road
Cleveland 35, Ohio
Attention: Roland Breitwieser

National Aeronautics and Space Administration — 2
Jet Propulsion Laboratory
Pasadena, California
Attention: Library

Aerojet-General Nucleonics — 1
San Ramon, California
Attention: Kenneth Johnson

Thompson-Ramo-Wooldridge, Inc. — 1
New Devices Laboratories
7209 Platt Avenue
Cleveland 4, Ohio
Attention: J. E. Taylor

Electro-Optical Systems, Inc. — 1
125 North Vinedo Avenue
Pasadena, California
Attention: Joseph Neustein

UAC-Research Laboratories — 1
East Hartford, Connecticut
Attention: Library

U. S. Atomic Energy Commission — 3
Technical Reports Library
Washington 25, D. C.

The Martin Company — 1
Nuclear Division
P. O. Box 5042
Baltimore 20, Maryland
Attention: Peter J. Poletti

Advanced Research Projects Agency — 1
Office of General Research
Room 3D148, Pentagon
Washington 25, D. C.
Attention: John Huth

National Aeronautics and Space Administration — 1
1512 H Street, N. W.
Washington 25, D. C.
Attention: Harold Finger

U. S. Atomic Energy Commission — 3
Technical Information Service Extension
P. O. Box 62
Oak Ridge, Tennessee

General Electric Company — 1
Missile and Space Vehicle Department
3198 Chestnut Street
Philadelphia 4, Pennsylvania
Attention: Edward Ray

Air Force Cambridge Research Laboratories — 1
Bedford, Massachusetts
Attention: Albert W. Diniak

General Motors Corporation — 1
Research Laboratories
Warren, Michigan
Attention: Frank E. Jamerson

Thermo Electron Engineering Corporation — 1
127 Smith Place
Cambridge, Massachusetts
Attention: George N. Hatsopoulos

Atomics International 1
Canoga Park, California
Attention: R. C. Allen

Los Alamos Scientific Laboratory 1
Los Alamos, New Mexico
Attention: R. Lee Aamodt

Ford Instrument Company 1
Long Island City, New York
Attention: Michael Silverberg

Westinghouse Electric Corporation 1
Electronic Tube Division
Elmira, New York
Attention: Gene R. Feaster

Westinghouse Electric Corporation 1
Research Laboratories
Pittsburgh, Pennsylvania
Attention: Robert J. Zollweg

General Electric Company 1
Schenectady, New York
Attention: John M. Houston

Allied Research Associates, Inc. 1
Boston, Massachusetts
Attention: Philip Goodman

International Telephone and Telegraph Laboratories 1
Fort Wayne, Indiana
Attention: Donald K. Coles

Republic Aviation Corporation 1
Farmingdale, Long Island, New York
Attention: Alfred Schock

Air Force Systems Command 1
Aeronautical Systems Division
Flight Accessories Laboratory
Wright-Patterson Air Force Base, Ohio
Attention: Captain Eugene F. Redden

Office of Naval Research 1
Washington, D. C.
Attention: Lt. Cdr. John J. Connelly

National Aeronautics and Space Administration 1
1512 H Street, N. W.
Washington, D. C.
Attention: Walter Scott

Naval Research Laboratory 1
Washington, D. C.
Attention: George A. Haas

National Aeronautics and Space Administration 1
Jet Propulsion Laboratory
Pasadena, California
Attention: Owen S. Merrill

National Bureau of Standards 1
Washington, D. C.
Attention: G. F. Rouse

Massachusetts Institute of Technology 1
Cambridge, Massachusetts
Attention: Wayne B. Nottingham

North Carolina State College 1
Raleigh, North Carolina
Attention: A. C. Menius

National Aeronautics and Space Administration 1
1512 H Street, N. W.
Washington 25, D. C.
Attention: W. H. Woodward

Atomic Energy Commission 1
Germantown, Maryland
Attention: Lt. Colonel G. M. Anderson

Radiation Effects Information Center 1
Battelle Memorial Institute
505 King Avenue
Columbus 1, Ohio
Attention: Mr. R. E. Bowman

Bureau of Weapons 1
Research and Engineering Material Division
Washington 25, D. C.
Attention: W. H. Gilbert

RCA Laboratories, Inc. 1
Princeton, New Jersey
Attention: K. G. Hernqrist

Union Carbide Corporation 1
Parma Research Center
12900 Snow Road
Parma, Ohio
Attention: Librarian

United Nuclear Corporation 1
5 New Street
White Plains, New York
Attention: Al Strasser

Metals and Ceramics Research 1
Armour Research Foundation of Illinois
Institute of Technology
10 West 35th Street
Chicago 16, Illinois
Attention: David W. Levinson,
Metallurgical Advisor

Pratt and Whitney Aircraft Company 1
East Hartford 8, Connecticut
Attention: W. Lueckel

Department of the Navy 1
Bureau of Ships
Washington 25, D. C.
Attention: B. B. Rosenbaum

General Electric Company 1
Nuclear Materials and Propulsion Operation
P. O. Box 15132
Cincinnati 15, Ohio
Attention: J. A. McGurty

Chief, Reactor Engineering Branch 1
U. S. Atomic Energy Commission
San Francisco Operations Office
2111 Bancroft Way
Berkeley 4, California

U.S. Atomic Energy Commission 1
San Francisco Operations Office
2111 Bancroft Way
Berkeley 4, California
Attention: Director, Reactor Division

NASA-Scientific and Technical Information 2
Facility
Box 5700,
Bethesda 14, Maryland
Attention: NASA Representative